Utrecht University

Subaqueous and Subaerial Debris-flow deposits

Physical experiments of debris-flow lake interactions, and controls on subaqueous flow deposits

Nikoleta Santa

Final version

Utrecht, April 2019

MSc. Thesis Earth Sciences

Student number: 6182984

Email: n.santa@students.uu.nl

First supervisor: Tjalling de Haas

Second supervisor: Maarten G. Kleinhans

Preface

The current master thesis is managed as a part of the final year of the master entitled Earth Structure and Dynamics, in Utrecht University. The main aim of this master thesis project is to broadly discuss the combined knowledge I learnt through this master program, and finally get involved in the scientific world. This thesis is a complementary project of Tjalling de Haas, who analyzed the effect of mass, composition, and slope variations on subaerials debris flows deposits in a small-scale experimental setup. In that regard, I analyzed the effect of mass, composition, and outflow channel slope in the terrestrial, and expanded also to the subaqueous environment. My laboratory partner Sjoukje I. de Lange has studied the proportional impulse waves resulting from the subaerial debris flow when it hits the water basin.

Foremost, I would like to express my sincere gratitude to my first supervisor dr. Tjalling de Haas. Without his help, guidance, motivation words, faithful attitude and belief in me, this research would not have been fulfilled. Not to mention the effort and patience to revise my enormous huge manuscripts. Thankfulness for my second supervisor Maarten Kleinhans. Additionally, I would like to thank my partner Sjoukje I. de Lange for her help, the positive attitude, and the entire collaboration in the laboratory. My deep appreciations for Shivas Pudasaini from Bohn University for his brief observations and comments on the experiments. Next, Arjan van Eijk is greatly thanked for building and maintaining the experimental setup, Bas van Dam for providing the technical support, and Mark Eijkelboom for providing the sediments for the experiments.

My gratitude goes also to my parents who gave me a childhood full of knowledge, experiences, respectfulness, and the unlimited support during my entire life. Without their support, confidence on my skills, motivating words, and their imperative love, I would never be able to achieve what I have done until now. Additionally, my appreciation goes to my brother Dimitris who helps, supports and gives me courage every single day of my life to continue my long walk in the scientific community.

I would like also to thank all my private English course teachers I had in my life. Specifically, my gratitude goes to my childhood friend and teacher Dimitra Orfanou for preparing me to study abroad the last year I spent in Greece. Additionally, my second English teacher Adriana Nearchou, who also prepared me and stayed by my side in this difficult walk of studying abroad.

Next, I would like to thank my partner Dimitris Petrocheilos for giving me courage, motivation words, and love during my master program in Utrecht University. Additionally, Andrea Cuesta is thanked for being my friend and partner during master courses, where I have learned a lot working with her the last 2 years. Eliza Antonopoulou, Joel Koupermann, and Michael Delagas are thanked for being such good friends and partners during master courses. I also thank Floris van Rees who was sharing part of the laboratory during our experiments, and bringing positive mood every day. Lastly, I thank all the Greek and international friends who helped me and supported me during my studies.

Abstract

Subaerial debris flows occur when masses of poorly sorted and water saturated-sediments surge down slopes due to gravity force. Subaqueous debris flow arises when subaerial sliding material mixes with water and becomes a debris flow. Both flows either in subaerial or in subaqueous environment can cause major and secondary hazards. Subaqueous and subaerial debris flows are difficult to be observed in nature. Additionally, the effect of composition on subaqueous and subaerial debris flow deposit dimensions is poorly understood due to the lack of observations. Here we develop a multi-phase subaqueous and subaerial debris flow, and we focus on the effect of mass (3.5-18.0 kg), composition (e.g., water 40-60%, gravel 0-64%, and clay 0-29%), and outflow channel slope ($20\text{-}40^0$) on subaqueous and subaerial debris flow deposit dimensions and grain size sorting. The experimental setup consists of a 2.0 m outflow channel slope with a varied angle such as $20\text{-}40^0$, a 0.90 m wide and 1.85 m long basin, and a 10^0 inclined outflow plain bed. The basin is either filled with water for the subaqueous runs with a water depth of 0.33 m, or empty for the subaerial runs. Debris flow deposit dimensions are highly dependent on flow momentum and velocity. Therefore, debris flow deposit runout distance, width, and thickness are controlled by the flow mass, composition, and slope variations.

I found that debris flow runout distance and width are mainly determined by flow velocity and composition. Subaqueous debris flow deposit runout distance is controlled by the mass and clay variations, while subaerial flow deposits are determined by mass and gravel. Subaqueous deposit width is affected by mass, gravel, and clay variations, whereas subaerial deposit width is influenced by mass, water, and clay content variations. Deposit thickness is mainly determined by the subaqueous clay and by the subaerial gravel variations. Flow velocity and runout distance are controlled by the subaqueous mass and clay, and by the subaerial mass, water, and gravel content. Flow velocity and deposit width are controlled by the subaqueous mass, clay, and slope variations, and by the subaerial gravel. Grain size sorting varies between relatively well to poorly sorted along the subaqueous and subaerials deposits. Coarse-grained sand and gravel particles are distributed in the margins and the front, while the interior consists of fine and medium grained sand in most of subaqueous experiments like the mass, water, and slope variations. However, in clay (<21%) rich subaqueous and subaerial flows grain size sorting is absent due to high flow viscosity. Increasing gravel content causes a uniform accumulation of the coarse-grained sand, and gravel particles along the subaqueous and subaerial debris flow deposits. My results demonstrate the significance of debris flow mass, composition, and slope variations on the deposit runout distance, width, thickness, and grain size sorting.

1. Introduction

Landslides, debris flows, mud-flows, rockfalls, snow, ice and rock avalanches are common geophysical mass flow events in mountainous and coastal regions (Pudasaini and Hutter, 2007). Debris flows are common phenomena in mountainous regions. They differ from rock avalanches and sediment-laden water floods because both solid and fluid forces influence their motion and govern their rheological properties (Costa, 1988; Iverson, 1997). Subaerial debris flows occur mainly in steep areas where the sediments are purely sorted and water-saturated, where the inclination of the slope is high and in places with high precipitation rates. The velocity and volume of debris flows make them very dangerous. As a result, these physical phenomena are capable of baring slopes, drastically changing stream channels, endangering human life and causing damages in structures. Even small debris flows can cause damages in a mountainous area. Iverson, (2004) explained that their deposits can cause damages such as damming rivers or sudden river supply to a river system. Additionally, impulse waves such as tsunamis are generated by debris flow.

Johnson et al., (2012) as well as De Haas et al., (2015) have created physical and experimental models of subaerial debris flow to predict the relationships between debris flow, flow runout distance, flow composition and deposition, deposit morphology, sediment sorting and flow behavior. Kafle et al., (2016), modeled submarine landslides, particle transport and tsunamis by taking into consideration deformable and two-phase debris, in a fully-coupled solid–fluid mixture resistance and viscous model with 3-D landslide fluid body interactions, a simulation strategy that includes one framework for the landslide and fluid body, impact and future dynamics of landslide, debris flow, turbidity currents and tsunami.

One significant property of debris flow is the deposit geometry, such as the height and width of leeves and lobes, which is strongly influenced by debris flow composition (Coussot et al.,1998; Major and Inversion, 1999). Debris-flow deposition may be the result of various processes, including:

- Decay of excess pore fluid pressure (Terzaghi, 1956; Hutchinson, 1986),
- Viscoplastic yield strength (Johnson, 1970; Coussot and Proust 1996),
- Decay of grain collision stresses (Lowe, 1976; Takahashi, 1978, 1991),
- Increasing grain contact friction and friction targeted at flow margins (Major, 1997, Major and Iverson, 1999).

According to Major and Inversion, (1999), increasing grain contact friction and friction targeted at flow margins relies on in-situ measurements from replicable, large-scale flume experiments. However, the varied hypothesis such as decay of excess pore fluid pressure as well as decay of grain collision stresses, and viscoplastic yield stress are unreliable. This means that the exact mechanism that causes debris-flow deposition is still unknown.

Debris flows are notorious hazards in both terrestrial and submarine environments. They can be triggered by earthquakes, volcanic eruptions, after intense rainfalls (only the subaerials), and other

reasons. A recent example of a subaerial debris flow occurred on 13 September 2013 due to intense rainfalls which triggered at least 1,138 debris flows in a 3430 km^2 area of the Colorado Front Range (Coe et al., 2014). An even larger hazard is when a subaerial debris flow hits a water reservoir such as a lake, dam, or the sea. When subaerial landslides enter a water body, impulsive water waves are formed together with (subaqueous) landslides (Ataie-Ashtiani and Shobeyri, 2008). Submarine debris flows are commonly considered as laminar flows transferring downslope, an agglomeration of particles held together by a thick sediment matrix composed mainly of silt, clay, and water (cohesive material).

Subaqueous debris flows are of major interest for many reasons. They play a significant role in producing turbidity currents (Hampton, 1972; Mulder and Cochonat, 1996) and also are of importance due to the sand-rich deposits which are expected to create important hydrocarbon reservoirs (Shanmugam, 1996). In addition, great secondary hazards occur, such as damages of submarine cables like the case of cable damage in the Grand Banks slide of 1929 (Masson et al. 2006). Most importantly, when a mass slides down a slope into a body of water to become a subaqueous debris flow (Pudasaini, 2014), it creates a tsunami wave (Ataie-Ashtiani and Shobeyri, 2008). More specifically, as the debris instantaneously hits the water reservoir, a tsunami wave is generated, potentially causing damage in many coast areas. Several studies have discussed subaerial landslide impact-generated tsunamis and extreme runup heights at Tafjord (1934) and Lake Loen (1936) in Norway (Jørstad, 1968; Harbitz et al., 1993), Lituya Bay, Alaska, in 1958 (Fritz et al., 2001, 2009), Vajont dam in Italy in 1963 (Müller, 1964), Sulawesi-Indonesia (European Commission, Joint Research Centre; report; 2018).

A recent example is the terrible event of 28 September 2018 in Sulawesi Province, Indonesia, which was damaged by an earthquake (magnitude 7.5R), and caused many casualties. Subaerial debris flows and landslides occur due to the earthquake, and a debris-flow generation tsunami (height 3-10 m) occured in the coast area of Sulawesi. Last but not least, another tsunami event hit this area the same year on December, 2018, where a debris-flow generated tsunami in Indonesia was triggered by eruption of the Anak Krakatau volcano. Tsunami waves occurred with run-up heights around 1-3 meters.

Subaqueous debris flow present similarities with subaerial debris flow, although they may also vary in striking ways. In particular, the deposit morphology and geometry, runout distance and grain size sorting, likely differ between subaerial and subaqueous debris flows. One of the questions which remains unanswered, is how morphology, sedimentology, and runout distance differ between subaqueous and subaerial debris flows. Another research question is how runout distance, deposit dimensions and grain size sorting, are affected by debris flow composition, both in a subaqueous and subaerial setting.

This master thesis project aims at answering these questions. I will perform a series of small-scale subaqueous and subaerial debris flow experiments in otherwise similar conditions, to answer these questions. The structure of the master thesis project will be as follows. A literature review is introduced in the next chapter, where subaerial and subaqueous debris-flow morphology, flow

dynamics as well as their hazardous effect, is described. Furthermore, subaerial and subaqueous debris-flow dynamics based on experimental and field observations are discussed. Additionally, the knowledge gaps and uncertainties are identified. Based on the literature review, the research questions and hypotheses are then presented. The methodology is also discussed afterwards. Subsequently, I present the main results. Discussion and Conclusions are the last parts of this master thesis report, focusing on the interpretation of the data analysis and on the comparison of the results with between other studies.

2. Literature review

2.1 Subaerial debris flows
2.2.1 Definition and occurrence.

Debris flows occur when masses of poorly sorted and water saturated-sediments surge down slopes due to gravity force. Debris flows are multi-phase, gravity-driven flows, containing randomly interacting phases of water and sediments (O'Brien et al., 1993; Hutter et al., 1996; Iverson, 1997; Iverson and Denlinger, 2001; Pudasaini et al., 2005; Takahashi, 2007; Hutter and Schneider, 2010a, 2010b). Both solid and fluid forces affect the motion, which is what distinguishes debris flows from related phenomena, such as rock avalanches. Whereas solid grain forces dominate the physics of avalanches, and fluid forces dominate the physics of floods, solid and fluid forces must act in concert to produce a debris flow.

Broad distribution of grain size mixed with fluid, characterize a debris-flow. Sediment composition and percentage of solid and fluid phases, determine the rheology and flow behavior. According to Hungr et al. (2001), debris flows are ''a very rapid to extremely rapid flow of saturated non plastic debris in a steep channel. Plasticity index is less than 5% in sand and finer fractions". Several studies, in the past few decades, have focused on a single-phase, dry granular avalanches (Savage and Hutter, 1989; Hungr, 1995; Pudasaini and Hutter, 2003; Zahibo et al., 2010), single-phase debris flows (Bagnold, 1954; Chen, 1988; O'Brien et al., 1993; Takahashi, 2007; Pudasaini, 2011), flows composed of solid-fluid mixtures (Iverson, 1997; Iverson and Denlinger, 2001; Pudasaini et al., 2005), and two-layer flows (Fernandez-Nieto et al., 2008).

According to Iverson, (1997), large debris flows in terms of volume can exceed 10^9 m^3, and the release of energy is more than 10^{16} J, which can cause a lot of damage or generate tsunami waves. Still, debris flows with small volumes of 10^3 m^3, can also cause damage structures. Takahashi, (2014) cited that, debris flow velocities vary from 0.5 – 20 m/s and runout distances differ from 0.2 up to 10 km. Costa, (1984), mentioned that cohesive strength, buoyant forces, grain interactions, structural support, and maybe turbulence, is what enables sediments transportation in debris flows. However, all definitions of the various studies end up with the same conclusion. The fact that, debris flow consists of sediments with distinct composition and fluids which imbues the mixture. Because of that, debris flows can occur on both shallower and steeper slopes. Debris flows are usually initiated in poorly sorted colluvium on sparsely or unvegetated hillslopes above tree line (Costa and Jarrett 1981) or as shallow landslides in hillslope hollows without channels (Iverson et al. 1997).

2.2.2 Debris flow materials

In the well-established North American landslide classification system of Varnes (1978), which has been modified by Cruben and Varnes (1996), only two different materials have been recognized: *debris*, a soil consisting of more than 20% of gravel and coarse grain sizes and *earth,* a soil with less than 20% in coarser sizes. Five years later, Hungr et al., (2001) suggested that, these definitions should be replaced by new ones, derived from geomorphology.

Jakob & Oldrich (2005), suggested that, the term *earth* should refer to unsorted clayey colluvium derived from clays or weathered clay-rich rocks, with a consistency closer to the plastic limit than the liquid limit. This low-sensitivity clay-rich material of intermediate consistency can produce a slow to rapid sliding movement along shear surfaces. Hungr et al. (2001), defined debris as a loose unsorted material of low plasticity, such as that produced by mass wasting processes (colluvium), weathering (residual soil), glacier transport (tilt or ice contact deposits), and explosive volcanism of human activity (e.g mine spoil).

Rate of movement	Bedrock	Debris (<80% sand and finer)	Earth (>80% sand and finer)
Rapid and higher (>1.5 m/day)	Rock flow (creep, slope sagging)	Debris flow Debris avalanche	Wet sand and silt flow Rapid earth flow Loess flow Dry sand flow
Less than rapid (<1.5 m/day)		Solifluction Soil creep Block stream	Earth flow

Figure 2.1: Mass movement categories according to Varnes (1978).

2.2.3 Flow behavior, deposit morphology and sediment sorting of debris flow.

Flow behavior affects the deposited morphology and sediments sorting of debris flow. De Haas et. al. (2015), observed multiple flows surges in the debris flows, in their laboratory experiments. More specifically, coarse particles were detected to be concentrated at the flow front in most of experimental debris flows. Elongated debris flow deposits were formed by the leeves, where laterally confined at the flow. De Haas et. al. (2015), observed that the flow front in these debris flow, had more gravel, while their tail consisted of finer-grained particles. However, only in debris flow with high clay enrichment composition, the coarse particles did not accumulate at the front. Inverson et. al. (1997), explained that, deposition occurs when all kinetic energy attenuates to irrecoverable forms. Complete energy degradation occurs first, when granular temperature falls to zero in the coarse-grained debris that collects at debris flow snouts and lateral margins, where levees may form. This coarse grained material, consequently composes the perimeter of most debris flow deposits.

Debris flow often moves as noticeable *surges* or slugs of material, separated by watery *intersurge flow* (Jakob & Oldrich, 2005). One surge, or multiple of successive waves characterize the debris flow event. Takahashi (1991) suggested that the mechanics of surge growth may vary. During the flow, the largest grains (boulders) are finer matrix supported (coarse sand and clay). Jakob & Oldrich, (2005), suggested that longitudinal sorting of debris flow material can cause flow instability, which is resulted in some surges. Such surges are characterized by boulder fronts that are relatively free of matrix (Pierson,1990).

Finer mass of liquefied debris characterizes the main body of debris flow. Jakob & Oldrich, (2005) mentioned that, similar to debris flood, there is a dilute turbulent flow of sediment-charged water, which is called the tail of the afterflow. A rise in the level of flow behind which is caused by the growth of the boulder, leads to a proportional increase of the peak discharge (Inverson, 1997; Hungr, 2000). Fine-grained debris floods or flows that lack significant boulder content, is another type of surging. The main flow peak discharge can be of a laminar nature, but it is retained behind the turbulent front (Davies, 1986, Takahashi, 1991).
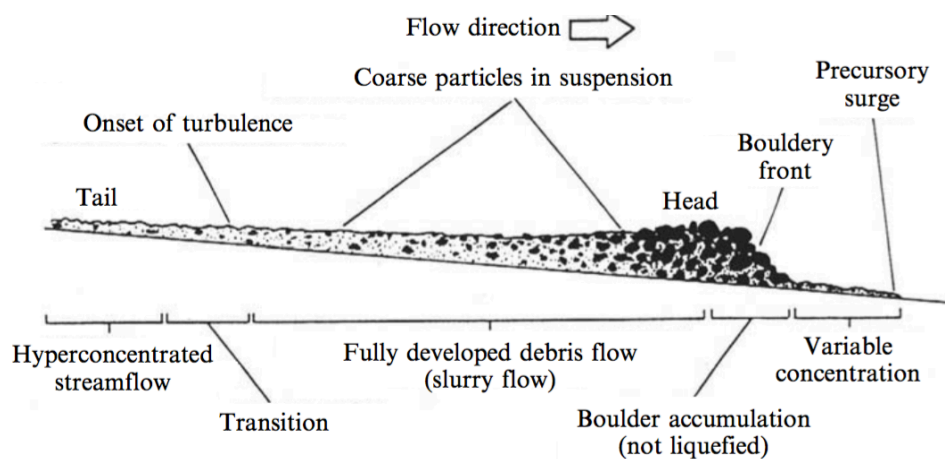
Figure 2.2: Diagram of a debris-flow surge with a boulder front (Pierson 1986, Jakob & Hangr,2005)

The deposition usually occurs as a result of combination of slope reduction and a loss of confinement, where a part of the surge behind the front collapses. Preferential transport of the large coarse-grained and gravel particles is a process occurring during deposition. Large accumulation of the coarse particles in the flow head, leads to a natural dam for the debris. Therefore, debris flow loose energy, and due to the presence of the coarse-grained particles, it slows down and deposit. The front is deprived of the hydraulic thrust, propelling it forward, where it slows down, steepens and may be partly expelled to the margins of the channel, where it builds elongated ridges or levees of coarser material. Fine-grained particles are kept suspended by the viscous forces, and are deposited slightly later. Iverson, (1997), determined that larger grains are dependent on grain-to-grain interactions to keep them suspended, and that grain size distribution affects the pore pressure.

Coarse grained levees, scoured channels and coarse grained linear debris flow lobes with a snout, describe a typical debris flow deposits (e.g. Beaty, 1990; Suwa et al. 2009). Apart from the debris flow snout lobes, can also occur depositional lobes (Suwa & Okuda, 1983; Suwa et al., 2009; De Haas et al., 2015). According to De Haas et al. (2015), debris flows with very high clay fraction (>0.22), miss the internal particle segregation process. This leads on producing the coarse grained blunt snout, resulting in the increase of lateral spreading a less defined debris flow deposit. De Haas et. al. (2015), also reached to the conclusion that, because of the increasing spreading and the runout distance of a more clay rich debris flow and a water with higher viscosity, the lower parts of the fan, consist of a low-relief and smoother surface.

De Haas et. al. (2015), used a wide range of conditions where debris flows formed deposits that consisted of a channel bordered by self-formed lateral levees. These ended in a well-defined depositional lobe with coarse gravel particles concentrated in lateral levees and at lobe margins. The interior deposits consisted of much finer particles. Additionally, they observed that debris flow with high clay fraction presented similar sorting trends. However, in debris flows for which the clay fraction exceeded 0.22, distinct particle size sorting was absent and this is possible due to the high viscosity of this debris flow (De Haas et. al., 2015).

In addition, a clue based on the good formation of the grain size sorting, proves that numerous procedures, such as kinematic sorting, squeeze expulsion and preferential transport of coarse particles to the flow front, are interrelated with the way natural debris flows behave, highlighted clearly by Vallance and Savage, (2000); as well as Gray and Kokelaar, (2010); and Johnson et al, (2012). This also implies that, frictional forces dominated the flow in the majority of De Haas et al. (2015), experimental debris flows (Vallance and Savage, 2000), as they generally also do in natural debris flows (e.g., Zhou and Ng, 2010).

2.2.4 Effects of debris flow composition on runout distance and deposit morphology.

Debris flow composition strongly affects runout distance and deposit morphology. Debris flow composition may vary according to, the wider variance of different sediment composition. De Haas et. al. (2015), experimentally tested the effects of debris flow composition on runout distance and deposit morphology. In their study, the runout distance varied between 0.2 and 1.2 m, and greatly depended on the composition and water concentration. In experimentally flumes of D'Agostino et al. (2010) and Hürlimann et al. (2015) has also been observed that runout distances and areas become larger for increasing water fractions.

Additionally, De Haas et. al. (2015), observed that the longest runout distance occurred for intermediate gravel fractions between 0.25 and 0.5 however, few percentages lower or higher of gravel fraction decreased the runout distance. Large accumulation of coarse particles at the front of the deposits was also been observed in their experiments, which affects the runout distance. This has also been indicated by Major and Iverson, (1999), in large experimental debris flows at the USGS flume.

Runout distance has also been affected by the flow momentum (De Haas et al., 2015). Rickenmann, (1999), evaluated empirical relations for natural debris flows and also proved that runout distance strongly depends on flow momentum. The highest flow velocities identified at the optimal gravel fraction, while for both lower and higher gravel fraction the velocities decreased. It has been discussed that, high frictional resistance in the coarse-grained flow front maybe occurred, by the increased pore fluid loss due to higher diffusivity, which is the possible explanation for the lower flow velocities when the gravel fraction is high. Furthermore, low flow velocities exist when the gravel fraction is low and this is due to low driving collisional forces between the grains.

Debris flows composition affects the deposited morphology. Experiments of De Haas et al., (2015) have shown that debris flow deposit geometry is strongly affected by the coarse-grained sand, clay, and water fractions which had also a big impact on lobe height, lobe width, and leeve height, whereas the effects of topography and volume are imperceptible. Depositional lobe thickness was mainly enhanced by the height of the frontal accumulation of coarse particles, behind which the more fluidal debris flow body additionally raised up to the height of the frontal coarse-particle accumulation in experiments of De Haas et. al (2015). Furthermore, Pierson, (1984), stated that there is similar dependence between lobe height and frontal coarse-particle accumulation which have been identified in natural debris flows. De Haas et. al. (2015), indicated that the reply of deposit morphology, runout distance, and depositional mechanisms to topographic forcing (i.e., channel slope and outflow plain slope) and internal characteristics (i.e., composition) in their experiments of debris flows was similar to the reply of natural debris flows to this forcing (e.g., Major and Iverson, 1999; Rickenmann, 2005)

2.3 Subaqueous Debris flows.

2.3.1 Definition and occurrence.

When a subaerial debris flow hits a water body, e.g., a lake or sea impulsive waves, are formed together with submarine (subaqueous) landslides (Ataie-Ashtiani and Shobeyri, 2008) Submarine landslides initiate when sliding material mixes with the water and becomes debris flow. In several areas, such as across the continental margins, submarine landslides and debris flows are formed in unconsolidated and compacted clays, which often occur on a geological timescale. Finely comminuted mixtures of clay and water with properties of a non-Newtonian liquid are the transformation of the unconsolidated and compacted clays. This mixture of water and clay gradually develops to a turbidity current, which is characterized by turbulent flow. Both subaqueous landslides and debris flows are highly mobile and can travel distances of hundreds of kilometers down gentle slopes (Locat, 2002; De Blasio et al., 2004).

The most effective process of sediment transport from the shallow continental margin into the deep ocean, are the turbidity currents, submarine slides and debris flow, (Blasio et al., 2003). These mass flows can demonstrate very long run-out distances of more than 150 km, even on very gentle slopes, i.e., less than 1° (Embley, 1976; McAdoo et al., 2000; Vorren et al., 1998; Hampton, 1972).

Submarine debris flows can occur in slope with every inclination meaning that, the slope inclination is not an important trigger mechanism. However, the water concentration and the gravitational force, play a major role in generating subaqueous debris flow. Jakob and Hungr, (2005), mentioned that submarine movements are triggered either by an increase in gravitational (driving) stress, a decrease in resisting forces (strength) or a combination of both of them.

Subaqueous debris flow can be triggered by earthquakes Earthquakes-induced shear stresses, are quite large relative to shear strength in fully saturated sediments, due to the impact of acceleration of all sediment column along with the included water (Jakob & Hungr, 2005). Additionally, pore pressure is increased due to cyclic loading, so this can make the strength lower or even induce a state of liquefaction (Piper et. al., 1988).

Interpretation of submarine debris-flow deposits resulting from slope failures, is hampered by the lack of information in terms of their dynamics. Norem et al. (1990), indicated the fact that, it is impossible to measure the events themselves directly in the field, and until recently, there have been very few relevant studies under controlled laboratory conditions (Hampton, 1972). This lack of information makes the development and evaluation of the physically based on predictive numerical models, necessary to understand submarine debris-flow deposits.

2.3.2 Submarine debris flow, runout distance and hydroplaning

Submarine debris flow, arising in both compacted and unconsolidated clays, respectively, are relatively common events in many areas around (Embley, 1976; McAdoo et al., 2000; Hampton, 1972). According to Hampton et. al. (1972), submarine debris flows have mostly been described as Bingham fluids. In simple shear, no deformation until a specified yield stress is involved to the material, as it is implied by the stress-strain relation for a Bingham fluid in laminar flow. Deformation is driven by the excess of the stress beyond this yield stress. However, this viscoplastic concept seems that exists in clay-rich subaqueous debris flows. Elverhoi et. al (2000), mentioned that, the very long runout distances on gentle slopes require low coefficients of friction or a low viscosity.

Laboratory experiments at St. Anthony Falls Laboratory, University of Minnesota (SAFL) have, however, shown that hydroplaning can cause the mobility of subaqueous debris flows (Mohrig et al., 1998, 1999). Explained by Elverhoi et. al. (2000), the bed friction can be reduced by the presence of a basal layer of water and this is the answer for the long travel distances and high velocities of many submarine flows on very gentle slopes. Moreover, hydroplaning strongly affects the rheology of debris and usually causes the head to run out ahead of the body. Consequently, the thickness of deposit is much lower than what would be expected according to the yield strength of the flowing mass.

Hydroplaning also inhibits the remobilization of a preexisting debris flow by an over passing debris flow (Elverhoi et. al.,2000). The lubricating layer inhibits the transmission of shear stress between the two debris layers. However, hydroplaning does not provide a full-proof mechanism, it merely offers a rheology-independent mechanism for greater runout distance, higher velocity and elimination of remobilization in the subaqueous environment, which is both physically well discovered and appealing in its simplicity (Elverhoi et. al.,2000). When hydroplaning is entrenched, the moving debris flow head is substantially decoupled from its bed, as shown in the experiments of Elverhoi et. al (2000). Runout distance and head velocity become independent of debris flow rheology (Mohrig et al., 1999).

More specifically, once hydroplaning is set up, the water film under the head, associated with hydroplaning, offers great resistance to being squeezed out and remains as the lubricating layer between the two surfaces (Elverhoi et. al., 2000). Because the thickness of the water film is too small, the rate of strain and the stress due to viscosity are very large. Large pressure to support the hydroplaning above can be generated by this large stress (Elverhoi et. al., 2000). The following figure illustrates the dominant transport processes along different parts of the continental slope as it is characterized by hydroplaning debris flow. In several studies such as, De Blasio et. al., (2004), Mohrig et. al., (1998), Mohrig et. al., (1999), Elverloi et. al., (2000), Acosta e. al., (2016), the effect of hydroplaning in submarine debris flow has been examined.
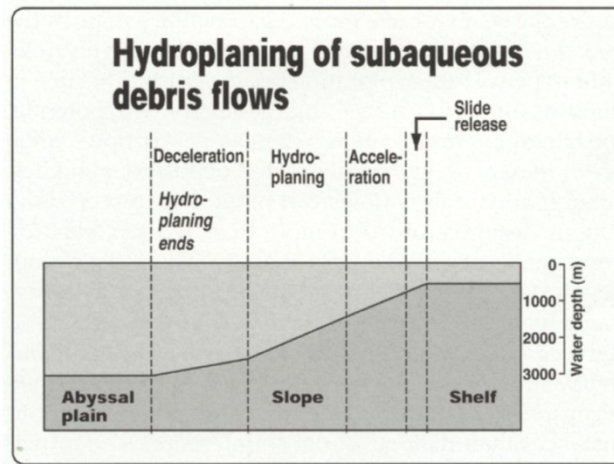
Figure 2.2.3:Dominant transport processes along different parts of continental slope characterized by hydroplaning debris flow, (Elverhoi et. al (2000).

De Blasio et. al., (2004) stated that data for subaerial debris flows show that, the run-out distances are much smaller than of their subaqueous counterpart, while simple arguments would lead to the opposite conclusion. Indeed, initiating on steeper slopes subaerial debris flow can experience mush less drag forces compared to their subaqueous counterparts. Additionally, subaerial debris flow is depended on full gravity force, whereas in the submarine environment the buoyancy effect, approximately halves the effective gravity.

However, subaerial flows do not experience hydroplaning due to basal friction. Specifically, the density of air relative to debris is very small (<1:1000) as explained by Mohrig et al., (1998). Therefore, the stresses applied to the flow surface by the fluid are negligible compared to the basal friction in the terrestrial setting. Although, when a subaerial debris flow hits a water reservoir, such as a lake or a sea, the possibility of hydroplaning to occur, is huge. Considering the fact that subaerial debris is initiated by steep slopes, it is flowing with high flow front velocity, and entering in the ambient water with high momentum. I hypothesize that this may exhibit to higher frontal velocities and to a slight small elevation of flow front, and thus a thin water layer may penetrate underneath of the debris. This enhances the flow front to hydroplane and therefore, longer runout distances occur. It is important to highlight that, this is likely to happen only in clay-rich debris flows, where the permeability is low and the water can be trapped easily with less escapes.

2.3.3 Deposit morphology and sedimentology.

Subaqueous debris flow deposition is affected under different conditions compared to subaerial debris flows. To be more specific, in subaerial debris flows, deposition is mainly controlled by gravity, whereas in subaqueous environment the effect of gravity is half diminished due to Archimedean buoyancy. Debris flow deposition in subaqueous setting is often determined by processes called dense flows, turbidity current, and suspension flow. Marked differences are noticed between these processes specifically when the debris flow is dense and has enough clay, so the coarse grained material can be carried as the flow moves (Middleton and Hampton, 1976). Although, turbidity currents are an intense, rapid, and dilute process which carries clay and other grain sizes in a water solution and dispersed sediments. The dispersed sediments are kept in suspension by turbulence (Middleton and Hampton, 1976), and have been resulted from eroded material from the surface of the debris (Hamton, 1972). Pratson et al., (2000), cited that this difference explains why debris flows are massive unsorted deposits, while turbidity currents result in a normally graded deposit which fines upward.

Norem et. al. (1990), suggested that subaqeous debris flow has more similarities with snow avalanches in which the interstitial fluid is air. Jakob & Hungr, (2005), illustrated the point that, debris flow can also generate turbiditic current, which is the cloud for snow avalanche, that will travel over long distances around 1000 km such as, in the case of Grand Banks slide (Piper et. al. 1988). This is also in agreement with Elverloi et. al (2000), who also alleges that, submarine debris flows can usually display very long runout distances of up to more than 150 km, even on very smooth slopes, such as less than 1^0. This has led to the proposal of numerous deep sea fan models built around the transportation of mud, sand, and gravel, from shelf areas downwards the basin plain, through passages, subaqueous gorges and other routes. Deep-sea deposits from submarine landslides, debris flows, and turbidity currents have been recovered hundreds of kilometers from inland, even along very gentle seabed slopes (Bugge et al. 1988).
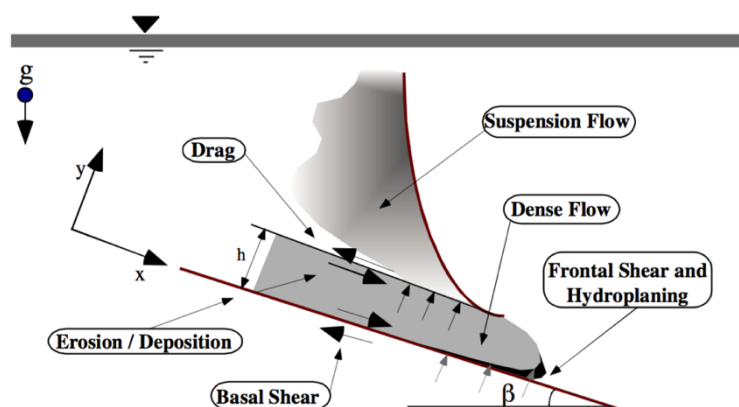

Figure 2.3: Boundary conditions during a subaqueous mass flow event. The suspension flow is created by the drag forces acting on the upper surface of the dense flow, Jakob & Hungr, (2005).

2.4 Subaqeous and subaerial debris flow deposits.

This chapter is focused on the process developing on both subaerial and subaqeous debris flow evolution. More specifically, this chapter focuses mainly on the triggering mechanisms, the similarities between subaerial and subaqueous debris flows, experimental and field observations of subaerials and subaqueous debris flows.

2.4.1 Origin and trigger of subaqueous and subaerial debris flow.

In the literature is present, what is in reality the dominant trigger factor in subaerial debris flow. Intense and high rainfall is the dominant trigger mechanism for subaerial debris flows. Suwa et al. (2011) clarified that high rainstorm intensities increase the subsurface perched-water stage in the deposits. These peaks in perched-water stage coincide with the increase in surface runoff afterwards, initiating debris flows (De Haas et. al., 2015). According to Shieh et al. (2009), earthquakes and volcanic eruption trigger landslides, where the amount of sediments material the initiation area. De Haas et. al. (2015), stated that, escaping material is taken up easier and therefore, the rainfall threshold for debris induction drops. As the time is passing, the material reduction is constantly transported downstream, appearing in an increasing threshold (Haas et. al., 2015) (see figures 2.4, 2.5).
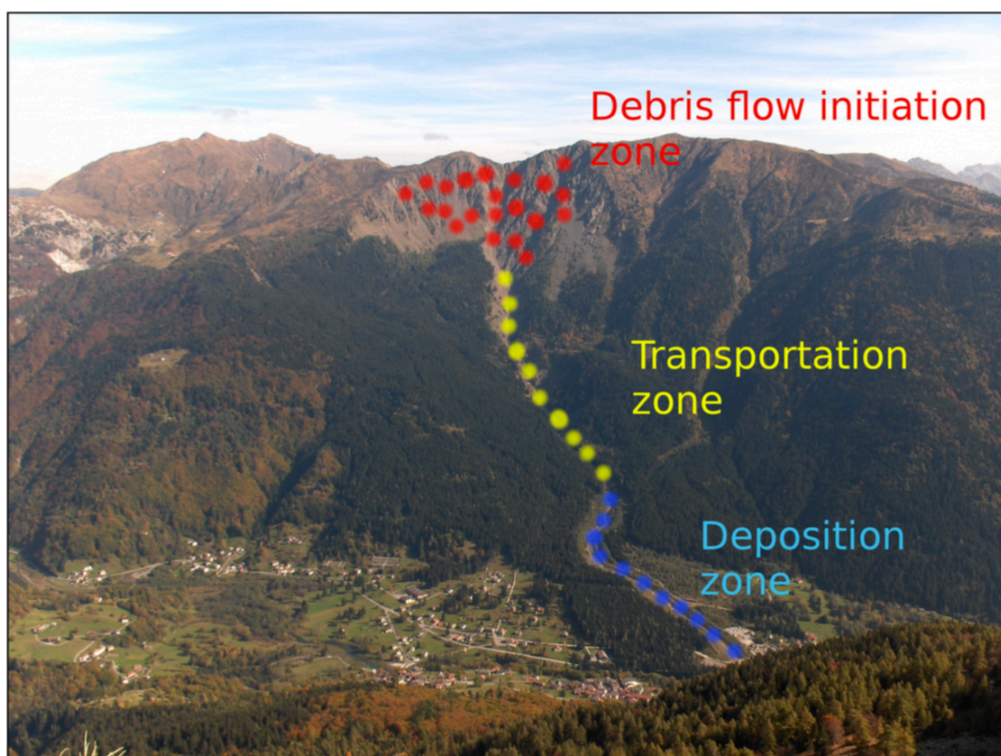

Figure 2.4. Subaerial debris flow initiation, transportation, and deposition zone. The current debris flow is located in Carnic Alps, Northern Italy. (source: S. Crema, 2010)
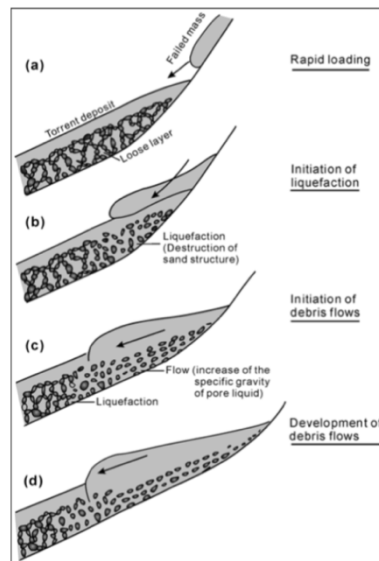
Figure 2.5: Illustration of debris flow initiation (Jakob & Hungr,2005).

Rapid sediments accumulation is a trigger factor of subaqueous debris flows. In general, rapid sediments accumulation leads to any failure due to the increase of pore-water pressure, because of the extra weight. Jakob & Hungr, (2005), mentioned that shear strength increases in some way due to the squeeze of water out, as the weight increases and consequently, there is more load due to the added sediments. Another factor affecting the increase of shear strength is that, more sediments are deposited at the head of the slope than in the bottom (Jakob & Hungr, 2005). All these processes lead to the conclusion that, debris flow or any mass movement may be initiated by the load of extra sediments and thus, by the slope steepness. Similarly, slope steepness is controlled by slope stability.

According to Jakob & Hungr, (2005), localized erosion is a common event which takes place in the deep submarine environment. To be more precise, localized erosion takes place in deep-sea channels, submarine canyons and other active sediment transport systems. Slope stability can be decreased when slopes are undercut, by increasing the shear strength. Green et. al., (2002), illustrated many examples of erosion-induced slope failures in Monterey Canyon offshore California.

Another significant trigger factor for subaqueous debris flow is, the volcanoes where many volcanic islands such as Hawaii, have been built up over pre-existing pelagic sediments bodies. Dietrich, (1988), claimed that this could produce a weak basal layer that might contain surplus pore pressure. According to Iverson, (1995), magma pressure in the rift zones has been suggested as trigger, which has evaluated that the zones of enhanced magma pressure are too small to trigger mass movements wider than a few kilometers.

Another point of major importance is that, human activity is a further subaqueous debris flow trigger factor. Humans construct facilities either in coastline areas or on the seafloor where they change the stress distribution in the bottom sediment, increasing the downslope component (Jakob & Hungr, 2005).

2.4.2 Comparison between subaerial and subaqueous debris flows and deposits.

Subaerial and subaqueous debris flow present similarities, while they are different in striking ways. One way in which subaerial and subaqueous debris flow are slightly similar in terms of topography. Specifically, this means that the subaqueous environment (ocean bottom) where subaqueous debris flow occur, is also morphological unstable as it happens in the land. For instance, steep slopes occur in the land where are also present in the ocean bottom (topographic effect due to midoceanic ridges, old landslides, faults. An earthquake may trigger both subaerial and subaqueous debris flow due to topographic effect on both subaerial and subaqueous environments.

Another similarity is the composition. Subaerial and subaqueous debris flow is mainly consisted of poorly sorted sediment and water saturated sediments. The water ingredient is also similar between subaerial and subaqueous debris flow. However, it is obvious that subaqueous debris flow contains more water than the subaerial. De Blasio et al. (2006) stressed that the comparison with subaerial landslides becomes even more striking, considering that the effective gravity is diminished in water due to Archimedean buoyancy, and that the drag resistance in water is about one thousand times larger than in air.

Subaerial and submarine debris flow deposits refer to the deposited fans. Their deposits are mainly alluvian fans, where leeves and lobes are formed. This is also confirmed by Bernhardt, (2011), who stated that both flows can form depositional lobes and levees. Bernhardt, (2011), also mentioned an example of marginal levees up to 100 m, transiting into an enormous frontal lobe that has been observed in Alika 2 landslide offshore in Hawaii (Lipman et al., 1988). The runout distance of the debris flow fan deposits can be reached at hundrend of kilometers. Bugge et al. (1988), indicated that deep-sea deposits from submarine landslides, debris flows, and turbidity currents have been recovered hundreds of kilometres from inland, even along very gentle seabed slopes. The sediments transportation of the subaqueous debris flow includes mud, sand, and gravel from shelf areas downwards the basin, whereas, from the subaerial it includes mud, sand, gravel, clay and water. This results from the steep slopes in mountainous areas.

In contrast, subaerial debris flow runout distance is much longer than the subaqueous runout distance. This is due to the water interaction from the subaqueous environment. This exerts higher resistance force to the mass as it slides. However, this force is missing from the subaerial environment and thus, the runout distances are longer. Another point in which subaerial and subaqueous debris flow also differ is, their mobility. The explanation for the mobility must rely on the interaction of debris flow with water (De Blasio et al. 2006). De Blasio et al. (2006), also stated that large landslides usually reach longer horizontal runout than the small ones (the "volume effect"), it seems natural that subaqueous landslides should be more mobile. However, subaqueous landslides appear to be more mobile even when compared to subaerial landslides of the same volume.

Subaqeous debris flow may also be initiated by a couple of different mechanisms such as earthquakes, sediment accumulation, erosion, volcanoes, and human activity, (Jakob & Hungr, 2005).

However, the main trigger mechanism for subaerial debris flow is the high rainfall during cloudbursts as it has been mentioned in several studies (Suwa et al., 2011). Intense high rainfall, along with earthquake and volcanic eruptions are the major trigger factors of debris flow.

2.4.4 Experimental observations

According to several studies, debris flow is capable of being separated into both large and small scale experiments, paying attention on properties and behavior of single debris flows (c.f. Iverson, 1997; Iverson et al., 2010; De Haas et al., 2015), and experiments focusing on debris-flow fan spatio-temporal dynamics (c.f. Hooke, 1967; De Haas et al., 2016, in review). Both small and large-scale experiments have been performed to analyse debris-flow behavior and debris-flow fan dynamics (e.g. Hooke, 1967; Iverson, 1997; Major, 1997; D'agostino et al., 2010; Iverson et al., 2010; Johnson, 2012; De Haas et al., 2015, 2016, in review).

According to several studies, debris flow is capable of being separated into both large and small scale experiments, paying attention on properties and behavior of single debris flows (e.g., Iverson, 1997; Iverson et al., 2010; De Haas et al., 2015), and experiments focusing on debris-flow fan spatio-temporal dynamics (e.g., Hooke, 1967; De Haas et al., 2016, in review). Both small and large-scale experiments have been performed to analyse debris-flow behavior and debris-flow fan dynamics (e.g. Hooke, 1967; Iverson, 1997; Major, 1997; D'agostino et al., 2010; Iverson et al., 2010; Johnson, 2012; De Haas et al., 2015, 2016, in review).

On the one hand, large scale experiments on single debris-flow behavior occured in the United States Geological Survey (USGS) debris-flow flume (e.g. Major, 1997; Iverson, 2010). On the other hand, smaller scale experiments on both single debris-flow behavior and debris-flow fan dynamics were carried out at the University of Utrecht (respectively De Haas et al., 2015 & De Haas et al., 2016; In review). Nevertheless, Iverson et al. (2010) stated that dynamic similarity between natural and small-scale experiments is unattainable due to disproportionally large yield strengths, viscous flow resistance and grain inertia.

Several authors have used laboratory flumes to simulate debris flow (Van Steijn and Coutard, 1989; Liu, 1996; Major and Iverson, 1999; D'Agostino et al., 2010; Hürlimann et al., 2015). De Haas et al. (2015), performing small-scale laboratory experiments to simulate the effects of debris flow composition on runout, depositional mechanisms, and deposit morphology. More specifically, they used debris flow experiments to investigate the effects of subaerial debris flow composition on runout distances and deposit geometry.

Field observation on subaqeous debris flow has been examined by Elveroi et. al. (2000), where their study is based on field data from the continental margin west of Svalbard and the Barents Sea, combined with experimental studies at SAFL and analytical/numerical modelling. Listad et. al. (2004), also simulated laboratory studies of subaqeous debris flow by measurements of pore-fluid pressure and total stress. De Blasio et. al. (2004), produced experimentally subaqeous debris flow, where typically one third of material drops down. Mohrig et al. (1998) performed a series of experiments of

muddy subaqueous and subaerial debris flows to demonstrate hydroplaning, showing that a thin layer of water intrudes into the front underneath of subaqueous debris flows. Marr et al. (2001) investigated the role of clay and water content in flow dynamics and depositional structures.

Based on several studies, an important knowledge gad is identified until now, where subaerial and subaqueous debris flow have not been combined yet, to study what happens when a subaerial debris flow becomes a subaqueous debris flow. The current master thesis study will fill this knowledge gap by combining both subaerial and subaqueous debris flows, and comparing the effect of different debris flows composition on the deposit morphology, runout distance, width, and thickness.

2.5 Subaqeous and subaerial debris flow as hazard for human life.

Based on Downling & Santi, (2014), significant damages and fatalities worldwide are caused because of the destructive tendency of fast-moving debris flow. Migration of humans in mountainous areas have increased during the last decades meaning that, people have been enforced to live close to debris fans resulting in increasing risks, (Dowling & Santi, 2014; Pederson et al., 2015). The studies concerning the hazards of debris flow, have focused on structural damage (Jakob et al., 2012) and actual amount of fatalities (e.g. Dowling & Santi, 2014). Structural damage is based on hazard probability, spatial and temporal probability of the element at risk (Jakob et al., 2012). Dowling & Santi, (2014) however, assumed that the fatalities have been assessed for example, by relating to socio-economic factors. Debris flow hazards mainly affect directly, the mountainous and coastline areas and indirectly areas located in midland.

Submarine debris flows are believed to be one of the most serious geo-hazards in offshore and coastal areas. Hazards correlated with their occurrence including tsunamis and destruction of underwater infrastructure (Jiang and LeBlond, 1992; Hampton and Locat, 1996). Unfortunately, natural debris flows are difficult to study directly because they are relatively unpredictable, infrequent, and short-lived (Mohring, 1998). These difficulties can be overcome by observing flows in a controlled laboratory environment. Laboratory facilities are often used to study subaerial debris flows (Johnson, 1970; Phillips and Davies, 1991; Major and Pierson, 1992; Inverson and Mejor 1999), but too rarely to study subaqueous flows (Hampton, 1972; Elverhoi, 2000). With this in mind, a new facility was built for the parallel study of subaerial and subaqueous debris flows.

Numerous subaqueous mass movements and their deposits have been mapped all over the world (Locat and Meinert, 2003; Mienert and Weaner,2003; McAdpp et al.,2000), due to the development of improved sea-floor mapping techniques (Locat et al.,1999). One example is of that, on the Atlantic seabord of USA, Booth et al., (1993), which reported more than 120 mass movements signature ranging in aerial extends from 1 km^2 to more than 1000 km^2 with more than 60% on slope inclined at less than 4^0. In many areas, such as in the Gulf of Mexico, they posture a threat to offshore facilities (Silva et al.,2004; Young et al.,2003). What is at risk in coastal population such as, tsunamogenic landslides, coastal infrastructure offshore facilities related to resources development and exploitation,

and transport facilities like pipelines and communication cables (Jakob & Hungr, 2005). An example of submarine cable damage happened in the Grand Banks slide of 1929 where the debris flow and resulting turbidity current, broke a series of submarine cables nearly 600 km away from the debris flow initial zone (Masson et al. 2006). The most recent example describing the debris-flow generated tsunamis occurred in Indonesia. Specifically, on 28 September, 2018, Sulawesi Province, Indonesia, was damaged by an earthquake (magnitude 7.5R) which led to a debris-flow generation tsunami with wave amplitude around 4 to 5 meters. More than 2000 people were killed by the earthquake and the tsunami waves, while there were more than 4000 injured people.

2.6 Knowledge gap, research questions, and hypotheses.

One significant fact is that, subaerial and subaqueous debris flow experiments are not plenty. To understand the different flow conditions and deposits between subaerial and subaqueous debris flow, more future research is needed. This will give future predictions on subaerial and subaqueous debris flow dynamics, deposit dimensions, run-out distance, composition and grain size sorting. Subaerial and subaqueous debris flow deposit experiments are therefore necessary. Some authors have proved that subaqueous debris flow deposits may have long run-out distance due to hydroplaning. Additionally, several authors address the fact that debris flow composition significantly changes run-out and lobe geometry (Iverson, 2010; De Haas et al., 2015). However, the significance of this effect has not yet been tested within an experimental setup. This master thesis study will focus on the comparison between subaerial and subaqueous debris flow deposits, in what extend different debris flow composition will affect the geometry of debris flow deposits, deposited dimensions, and grain size sorting.

The main questions that are addressed in this study are:

1. How does debris-flow composition affect the deposit dimensions and grain-size sorting?

2. What is the importance of grain size sorting in debris flows and to what extent does this affect the flow deposits?

3. To what extend does debris flow run-out distance differ above and below water?

4. Does hydroplaning exist in coarse-grained debris flows that are formed when a subaerial debris flow enters a water body?

5. How does the morphology and sedimentology of the subaqueous debris flows, compare to the subaerial debris flows?

The first question arises directly in relation to the studies of De Haas et al. (2015). However, only one part of the question focuses on the studies of De Haas et al. (2015). The part which refers to the subaerial debris flow is present whereas, the subaqueous part is absent. In this part I hypothesize that debris flow composition, such as clay, sand, and gravel, mainly affects the deposit dimensions, and grain size sorting. Specifically, subaqueous debris flow experiments with more gravel will have

shorter run-out distances than subaerials. Additionally, subaerial debris flow dimensions and grain size sorting will be different for the subaqueous debris flow deposits due to different environment (water-air interaction).

The second question is also indirectly reflected in the study of De Haas et. al., (2015), where they tested the effects of flow behavior in deposit morphology and sediment sorting. However, their study is focused only on subaerial debris flow while, experiments on subaqueous debris flow are missing. Although it is yet uncertain how important is the grain size sorting and to what extent does this influence both subaerial and subaqueous debris flow deposits.

The third question arises indirectly in the study of De Haas et. al., (2015), where they measured the run-out distances of subaerial debris flows (above water). However, the effect of run-out distances below water has not yet been tested. I hypothesize that below water, debris flow run-out distance will be shorter than above water. This is due to the water which exerts higher resistance force and thus shorter run-out distances.

The fourth question refers to subaqueous debris flow run-out distance, where some authors such as Mohrig et al. (1998); Elverhoi et al. (2000); Yin et al. (2017), performed subaqueous debris flow experiments based on mud and sand. They showed that subaqueous debris flow may have long run-out distances due to hydroplaning. Their experiments were based on mud and clay. However, they did not perform any experiment with the presence of gravel. At this point, this study will make the difference by adding the gravel component in debris flow composition. I hypothesize that gravel plays a major role on run-out distance of subaqueous debris flow and may change what other authors have claimed until now. To be more specific, the gravel grains are bigger and their total weight is bigger than the total weight of sand or mud. This will give an extra resistance force to the subaqueous debris flow deposit resulting in shorter run-out distances. Thus, hydroplaning is less important due to the presence of gravel.

The last question is indirectly related to Brien et. al. (2007), where they conducted experiments based on both subaerial and subaqueous debris flow estimating the velocity characteristic as a function of the ambient fluid. In this study, they used debris flow composition such as sand, clay, and water, in different concentrations. However, they did not use gravel in their experiments which clearly makes the difference with the current case study. They also concentrated only on velocity profiles between subaqueous and subaerial debris flow. However, on morphology, sedimentology and run-out out distance the focus was absent of both subaerial and subaqueous debris flow. This is the point where the current case study will relate the composition effect to the comparison between subaqueous and subaerial morphology, sedimentology and run-out distance. As far as I am concerned, I hypothesize that morphology, sedimentology and run-out distance will differ a lot between subaerial and subaqueous debris flow deposits. This is due to the water interaction from the subaqueous environment. Hence, this exerts higher resistance force to the mass as it slides in a subaqueous environment and thus, shorter run-out distances occur. Additionally, between the deposited morphology and sedimentology significant differences will be noticed.

3. Methods

3.1 Methodology

A series of small-scale subaqueous and subaerial debris flow experiments were performed, with systematic variations of angular gravel (2 – 5 mm), clay (kaolinite) and water fractions relative to a reference debris flow mixture, consisting of gravel, coarse and fine grained sand, and clay mixed with water, 99 in total. The fraction within the total solid volume was defined by the gravel and clay fractions. The water fraction is characterized as the volume of water relative to the total debris flow volume (solids and water). The topographic effect of channel slope has also been examined. Using an initial unconsolidated ~1 cm thick bed of sand, a fixed rough bed (sand glued to a plate), the effect of outflow plain composition was tested. A reference sediment mixture was selected for all experiments, where gravel, clay, and water fractions were systematically varied relative to this mixture. After this, repeatable experiments with variations in debris flow composition were examined. However, it has been recognized that natural variability, caused remarkable variations in some debris flows. To elucidate the effects of natural variability, each experimental setting was conducted at least 2 times. Using photograph, video, and digital elevation model (DEM) analyses, the resulted debris flow deposit was mapped, in order to analyze the debris flow deposit morphology. This data documented flow velocity and flow depth of the debris flows during motion and the runout distance, lobe width, and levee height of deposits.

Finally, three samples were selected of each debris flow deposit from different locations along the deposits such as, the front, the middle, and the back, thus an extensive grain-size analysis with sieves has been performed. Grain size sorting, mean and median of debris flow have been analyzed by this analysis. Explained by Folk, (1968), grain size sorting is a method of measuring the grain-size variations of a sample by encompassing the largest parts of the size distribution as measured from a cumulative curve. The D50 corresponds to the 50 percentile on a cumulative curve, where half the particles by weight are larger and half are smaller than the median. Lastly, mean is the average grain size which is calculated in order to test the average grain size distribution of each deposit. Grain size analysis, therefore, arranges important information to the sediment allocation and sorting, sediment provenance, transport history and depositional conditions (e.g., Folk and Ward, 1957; Friedman, 1978).

3.2 Experimental setup and Data collection

Focusing on the components that contributed to the fulfillment of the task, a chute including a straight channel of rectangular shape with a length of 2 m and a width of 12 cm (Figure 3.1.B) was joined to an angle outflow plain, free of constraints. Respectively, this chute was attached to an automatic tank releasing the mixture of debris, also including sediment and water, towards an electromagnetically opening entrance. Lasting ~20 s, this mixing process came to an end each time the entrance was opening.

Another point that should be mentioned is, the upward movement of this entrance and the use of tap water of 5.4∘ DH. In order to achieve a more natural harshness on this bed layer, the chute as well as the sidewalls, were covered with sandpaper (grade 80). In contrast, the mixture used to cover the outflow bed plain lacked of specific ingredients such as water, clay and gravel.

Four different lasers were scanning the debris flow as it was flowing, giving back information about pore pressure, flow thickness, flow depth, and water depth (when the basin was filled with water). The first laser is located 76 cm upstream of the intersection point of channel and outflow plain. This is a Baumer CH-8501 Frauenfekd lazer and model OADM 20U2480/S14C, with resolution between 0.015-0.67mm. This is the laser1 which is called OADM_1 and its wavelength takes value such as 650 nm. Above the intersection point of the channel and outflow plain, is positioned the second laser which is different than the first one. This is a Baumer CH-8501 Frauenfekd laser and model FADK 14U4470/S14/IO. This laser is called FADK_01 with resolution 0.1-1mm (lower than the OADM_1). Its wavelength is equal to 660 nm.

Furthermore, in the boundary of the outflow bed plain (which are the boundaries of the basin, when it is filled with water) two more lasers are located with distance difference between each other such as 62 cm. Both sensors are different from the first one and similar to the second one. Both of these lasers are Baumer CH-8501 Frauenfekd and model FADK 14U4470/S14/IO. These lasers are called FADK_02 and FADK_03 with resolution 0.1-1mm and wavelength equal to 660 nm. The last two lasers (FADK_02 and FADK_03) were only used to measure the water depth, the second one (FADK_01) is used to measure the debris flow thickness outlet. The first one (OADM_1), is used to measure the debris flow thickness (middle) in the flow channel.

Three circular sensors (figure 3.2), are presented in the channel floor 76 cm upstream of the intersection point of channel slope and outflow bed plain. The point where these sensors was located below the OADM_01 laser (figure 3.2), is called load cell (Wc) and was used to measure the pore pressure, shear strength, and flow weight during the flow. This point is active only for the first 30 seconds after the release of the material. Debris flow experiments in the USGS flume by Johnson et al. (2012), followed a similar approach. In the end of the channel, there is a basin where the outflow plain is under water located for the subaqueous debris flow experiments while, there is above water for the subaerial experiments.
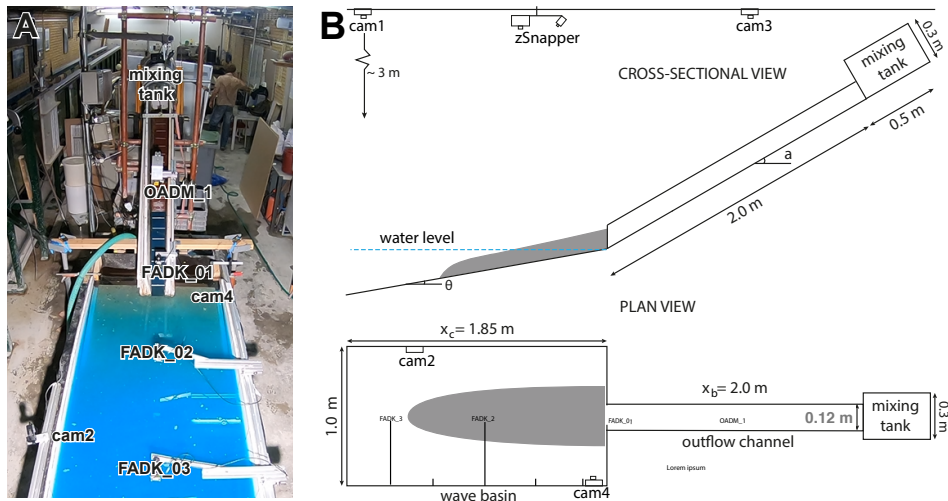
Figure 3.1: overview of the experimental flume. A) photograph. B) schematic overview, adapted from de Haas et al., (2015).
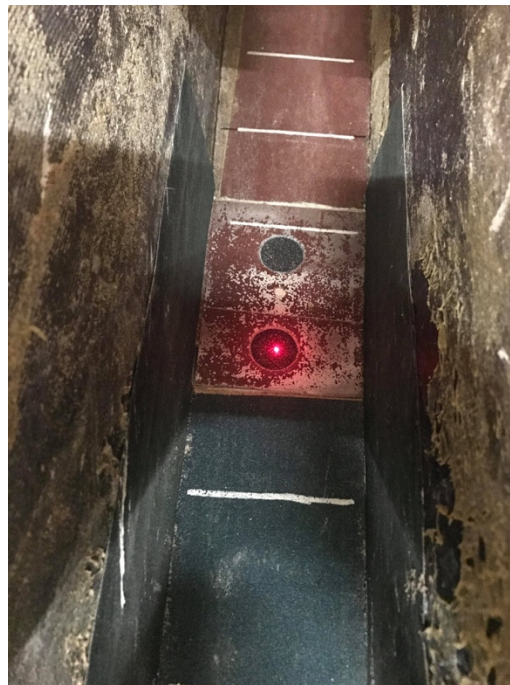

Figure 3.2: Load cell; pore pressure, shear strength, and flow weight sensors along the flume corridor (x_c=1.20 m).

Multiple cameras 4 in total such as, GoPro 6 and GoPro 4 were used to photograph debris flow deposits and capture debris flow motion. A Vialux z-Snapper 3-D scanner that captured a high-accuracy 3-D point cloud from a fringe pattern projector and camera, measured the deposited morphology (submillimeter vertical and horizontal accuracy) (Hoefling, 2004). Point clouds from the 3-D scanner were processed with MATLAB (The MathWorks, R2018b version 9.5.0.944444) using natural neighbor interpolation to a gridded DEM of 1 mm resolution. The DEM was used for visualization and to measure runout distance, lobe width, lobe height. Maximum runout distance was defined as the distance from the apex to the maximum extent of the debris flow, using the DEM. The maximum thickness of the deposit was established by measuring the thickest part of the debris flow deposit. Deposit area was defined as the total area of the debris flow deposit on the outflow bed plain.

Debris flow velocity, weight, and thickness during the flow were measured using devices such as, lasers. The data of these devices were processed using a Matlab script. The input data were taken by the four lasers, OADM_1, FADK_01, FADK_02, FADK_03. The output data of this script give information about the debris flow velocity, thickness (middle and outlet), weight, pore pressure, shear strength, water level, and flow density. However, pore pressure, shear strength, and water level are not used in the current master thesis project.

Table 3.1Intrumentation

Device	Instrument	Wavelength	Resolution	Unit	Measurements
Laser	OADM_01	650 nm	0.015-0.67	mm	Debris flow thickness (middle) x
Laser	FADK_01	660 nm	0.1-1	mm	Debris flow thickness (outlet)
Laser	FADK_02	660 nm	0.1-1	mm	Water level fluctuations (not in this study)
Laser	FADK_03	660 nm	0.1-1	mm	Water level fluctuations (not in this study)
Camera	Cam1	-	-	-	Overview of experiments
Camera	Cam2	-	-	-	Water level fluctuations (not in this study)
Camera	Cam3	-		-	Subaerial debris-flow velocity
Camera	Cam4	-		-	Near-field wave generation (not in this study)
3D Scanner	zSnapper	-	1	mm	Morphology of the deposit
Load cell (Wc)	-	-	± 0.003	kg	Debris flow weight at load cell.

3.3 Debris flow composition

The mixture of debris flow was contained by four types of sediments combined in different ratios. These types were clay (kaolinite), well-sorted fine silica sand, poorly sorted coarse silica sand and basaltic gravel (2–5 mm) (De Haas et al., 2015a). Debris-flow composition of both subaerial and subaqeous flows was varied by systematically changing the amounts of angular gravel (2–5 mm), clay (kaolinite) and water fractions relative to a reference debris-flow mixture (cf. De Haas et al., 2015a) (Table 3.1). The total debris-flow volume was similar in most experiments however, it differed in experiments with water and volume variations.

The reference sediment mixture of 8.0 kg (0.0041 m^3) consists of 13.85 wt% gravel (18.00 vol%), 45.38 wt% of coarse sand (59.00 vol%), 16.15 wt% fine sand (21.00 vol%), 1.54 wt% clay (2.00 vol%), and 23.08 wt% water (0.44 vol%). Keeping a constant grain density of 2,650 kg/m^3 for coarse sand, fine sand and clay, 3,400 kg/m^3 for basaltic gravel, and 1,000 kg/m^3 for water, the mass is converted to volume. The gravel, sand and clay fractions are defined as the fraction within the total solids volume, and the water fraction as the volume of water relative to the total debris-flow volume (solids and water combined).

Parameter	Unit	Reference	Range	nr. of subaqueous Experiments	nr. of subaerial Experiments
Debris-flow composition					
Volume variation (total mass and total volume)	m^3 (g)	0.0042 (8000)	0.0018-0.092 (3500-18000)	22	8
Water variation	g	1846	1600-32900	8	8
	vol %	0.44	39.9-60.1		
	wt%	23.08	20.0-36.3		
Gravel variation	g	1108	0-3921	10	6
	vol %	18.00	0-63.7		
	wt%	13.85	0-49.0		
Clay variation	g	123	0-1784	10	6
	vol %	2	0-29.0		
	wt%	1.54	0-22.3		
Slope variation	$(^0)$	30	$20-40^0$	8	8
Bedrock variation (bed composition)	m^3 g	Reference	Fixed-unconsolidated	2	2

Table 3.2: Varied debris flow composition for submarine and subaerial debris flow

.

3.4 Sieving Analysis.

Blott and Pye, (2001), stated that grain size is the most fundamental property of sediment particles, affecting their entrainment, transport and deposition. Several studies have also confirmed that grain size analysis therefore provides important clues to the sediment provenance, transport history and depositional conditions (e.g. Folk and Ward, 1957; Friedman, 1979). Blott and Pye, (2001), said that for the comparison of different sediments, grain size distributions have most frequently been described by their deviation from a prescribed ideal distribution. Computations performed assuming a normal, or Gaussian, distribution, with an arithmetic grain size scale, are seldom used in sedimentology, since too much emphasis is placed on coarse sediment and too little on fine particles (McManus, 1988). Consequently, geometric scaling is usually used to place equal emphasis on small differences in fine particles and larger differences in coarse particles Blott and Pye, (2001).

Grain size distribution has been described by the following parameters: (a) the average size, (b) sorting of the sizes around the average, (c) the symmetry or preferential spread (skewness) to one side of the average, and (d) the degree of concentration of the grains relative to the average (kurtosis) (Blott and Pye, 2001).

Sieve analysis was performed to all experiments, except for the experiments with very high clay content of both subaerial and subaqueous debris flow. This analysis is initially used to determine the grain size sorting along the deposit, and to compare the differences, due to differences in debris flow composition, between the varied debris flow deposits. Three small samples were selected from each deposit, that varied in dried weight between 10 and 93 g. In most experiments the middle samples weighted less than the samples derived from the front and the back of each deposit. This is due to the fine-grained deposit interior, while the deposit margins and front are contained by coarse-grained and gravel particles. Consequently, the samples which derived from the middle are fine and medium-grained. These samples were located in different positions along the deposits, such as the front, the middle, and the back. These locations had a cyclic shape with diameter around 5 cm, and the sample thickness varied according to the thickness of each independent deposit (see figure 3.5).

Sieve analysis consists of shaking the soil sample through a set of sieves that have progressively smaller openings. First the soil is oven dried for 24 hours in 125 ^{0}C and then all lumps are broken into small particle before they are passed through the sieves (figure 3.4).

Figure 3.3. Samples after 24 hours in 125 ^{0}C.

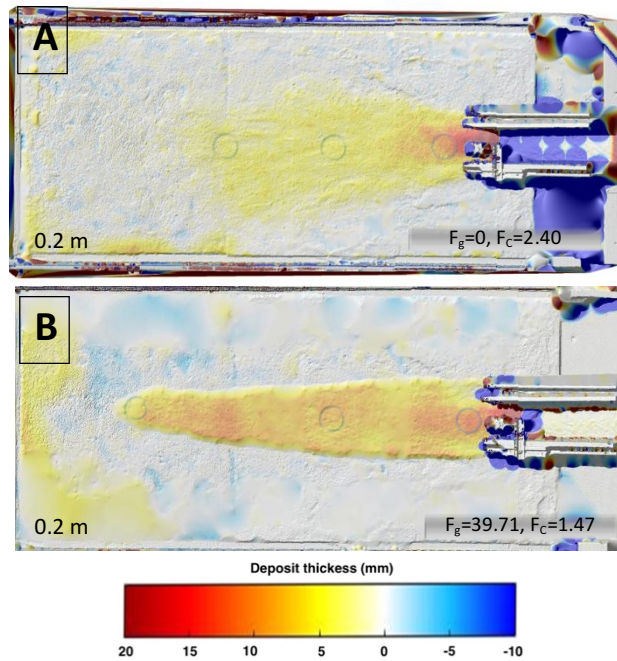*Figure 3.4: Complete order of sieves, performing sieve analysis.*

Figure 3.5 Digital elevation model (DEM) illustrating the locations where the samples were taken along the deposits. A) Subaqueous debris flow deposit with gravel content 0%, B) Subaerial debris flow deposit with gravel content 39,71 %

After the completion of the shaking period (2-5 minutes), the mass of soil retained on each sieve is determined by weighting each sieve and subtract this value from the initial weight of each sieve. The results of sieve analysis are generally expressed in terms of the percentage of the total weight of soil that passed through different sieves. Based on Blott and Pye, (2001), the geometric percentiles were calculated such as, D10, D50, and D90. In a later stage, the D10, D50, and D90 were described by scatter plots indicating the D10, D50, and D90 against the volume of the variable composition.

3.5 Data Analysis

This section describes the way the data analysis was performed. In order to analyze the data resulting from the experiments, these data were processed in Matlab using different scripts. The input data were different between the scripts and thus, variable scripts giving information about different results were created for all experiments. The principal aim of the first script was first to subtract the final digital elevation of the deposit (t1) from the initial digital elevation model before the deposit (t0), and second to measure the runout distance, width, and the length of the thick deposit and maximum thickness (Z). The input data of the current script were digital elevation models (DEM point clouds) resulting from the Vialux z-Snapper 3-D scanner that captured a high-accuracy 3-D point cloud from a fringe pattern projector and camera, measured the deposited morphology (submillimeter vertical and horizontal accuracy) (Hoefling, 2004). Specifically, the point clouds from the 3-D scanner were processed with MATLAB (The MathWorks, R2018b version 9.5.0.944444) using natural neighbor interpolation to a gridded DEM of 1 mm resolution. The DEM was used for visualization and to measure runout distance, maximum width, runout of the thick deposit, maximum thickness (figure 3.4). These DEM were two in total for each deposit, the first (t0) was scanned before the deposit, and the second (t1) was the final debris flow deposit.

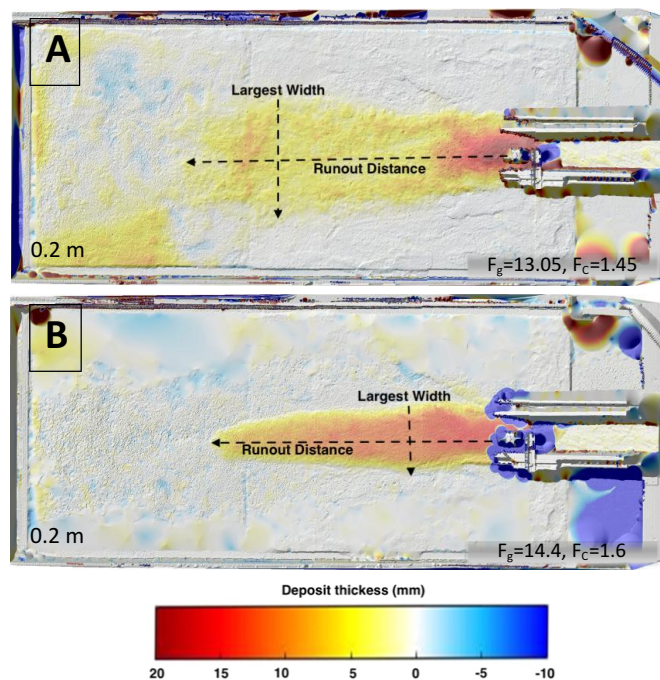*Figure 3.6: Digital elevation model (DEM) of A) subaqueous debris flow (water fraction 0.50), and B) subaerial debris flow deposit (water fraction 0.40), illustration of runout distance, and deposit width measurements.*

Debris flow velocity has been measured during the flow in the outflow channel slope, using the above located goPro (cam3) camera. A video was recorded during the flow where afterwards,

analyzing each image from the video, the exact velocity of the flow front was calculated. This was done by measuring the exact time of arriving the flow front at locations along the channel, such as x= 0, 50, 100, 150, 200 cm. The average velocity is calculated by the velocity values of the flow front in every location, and was used to plot the results in the report. Debris flow middle and outlet thickness have been measured by the lasers in the channel flow. Debris flow weight was measured in the load cell (Wc, see also section 3.2). Debris flow momentum is an expression of flow velocity multiplied by the flow mass. Therefore, by multiplying each flow velocity with the resulted flow mass, the debris flow momentum is determined.

3.5.1 Quantification of scaling

Dimensional characterizations have been used by several authors and scientists to compare experiments with different sizes and dimensions with each other. The following equations are used in this study to compare its experimental results with other studies. However, equations in table 3.3 have been analysed and studied in depth by Iverson, (1997), and De Haas et al., (2015). Ratios between collisional to frictional forces, are described by Savage number, collisional to viscous by Bagnold number, and frictional to viscous by the friction number. The tendency for pore fluid pressure to buffer grain interactions were demonstrated by the Darcy number, and the ratio between the solid to fluid inertia by the mass number. Lastly, Reynold and grain Reynold number describe the ratio between the solid inertial to fluid viscous shearing stress, and the measure of the influence of viscous effects relative to flow size.

Table 3.3. Dimensional equations describing different force ratios applied within the debris flow. Variable values derived by Iverson, (1997), and Haas et at al., (2015).

Dimensionless parameter	Equation	symbols
Savage number	$$v = \frac{\rho_s \delta^2 \gamma^2}{(\rho_s - \rho_f) g H \tan(\varphi)}$$	δ=mean grain size of debris flow (m)
Bagnold number	$$Bg = \frac{v_s \rho_s \delta^2 \gamma}{(1-v_s)\mu}$$ $$\gamma = \frac{u}{h_s}$$	μ= fluid viscosity (Pa s) (values derived from Haas et al., 2015) \n\n γ= flow shear rate (1/s)
Darcy number	$$D_n = \frac{\mu}{v_s \rho_s \gamma k}$$	ρ_s= solid density (kg/m^3) \n\n L= maximum length of flow mass, which is expected to be equal to the outflow channel slope (m)
friction number	$$F_n = \frac{v_s(\rho_s - \rho_f) g \, h_s \tan(\varphi)}{(1-v_s)\gamma \mu}$$	H= debris flow thickness (m)
mass number	$$M_n = \frac{v_s \rho_s}{(1-v_s)\rho_f}$$	u= flow velocity (m/s)
grain Reynolds number	$$Re_g = \frac{Bg}{Mn} = \frac{\rho_f \gamma \, \delta^2}{\mu}$$	P$_f$= fluid density (kg/m^3) \n\n k= permeability (m^2)(values derived by Haas et al., 2015)
Reynolds number	$$Re = \frac{\rho_s H \sqrt{gL}}{\mu}$$	ϕ= internal friction angle (^{0}) (assumed 42^0, Parson et al., 2001)

4. Results and interpretation

The raw debris flow and grain size sorting data can be found in supplementary excel files A1, and A2. In this section I will first describe the natural variability achieved in this research (4.1). In the next section, I will develop the subaqueous and subaerial debris flow characteristics (4.2), based on the effect of mass, composition, and outflow channel slope variations. In section (4.3), I will discuss the dimensions of debris flow deposit through a comparison between subaqueous and subaerial. In the last section (4.4), I will identify the effect of debris flow mass, composition, and outflow channel slope, on the grain size distribution along the front, the middle, and the back of both subaerial and subaqueous debris flow deposits.

4.1 Natural variability

To clarify the effect of natural variability, all experiments are done twice. Figure 4.1 illustrates the natural variability of the experiments, by plotting the two similar experiments against each other. It is obvious that all flow characteristics and debris flow deposit dimensions for both subaerial and subaqueous debris, indicate a significant amount of variability. More specifically, outlet and middle thickness for subaqueous debris flow present R^2 values between 0.86 and 0.95 (Figure 4.1.A), respectively. However, for subaerial debris flow the natural variability on outlet and middle thickness is less. Figure 4.1.A, also shows the R^2 values of outlet and middle flow thickness which are varied between 0.91 and 0.94, respectively. Figure 4.1.B defines the natural variability between subaerial and subaqueous maximum debris flow weight. Specifically, R^2 values of maximum debris flow weight for subaerial and subaqueous debris flow are diverged between 0.52 and 0.54, respectively. Figure 4.1.C describes the average velocity of both subaqueous and subaerial debris flows. The variability of the average velocity of subaerial debris flow, where R^2 takes value equal to 0.60, is less than that of the average velocity of subaqueous debris flow, where a lot of randomly allocated scatters are observed. Lastly, figure 4.1.D shows the natural variability of the subaqueous and subaerial debris flow deposit dimensions, occurring in the outflow bed plain. It is clear that the variability on the deposit width of subaerial debris flow deposits is less than the observed variability in subaqueous debris flow deposits (R^2=0.67 and R^2= 0.65, respectively). However, the observed natural variability increases for the deposit runout distance of both subaqueous and subaerial debris flow deposits, meaning that R^2 values for subaerial and subaqueous debris flow deposits vary between 0.57 and 0.58, correspondingly.

Theoretically, the values of debris flow characteristics for both subaerial and subaqueous debris flow should be similar or at least close to each other. This is because all these parameters have been measured in the channel floor during the flow and, theoretically less or none variability is expected. Thus, the R^2 values for all the parameters (e.g., outlet and middle flow thickness, max. flow weight, average flow velocity, runout distance, and deposit width), should be close to 1. However, this

is not happening to all the parameters except for outlet and middle debris flow thickness, where R^2 values are between 0.86 and 0.95 for subaerial and subaqueous debris flow, respectively. It is therefore clear that, between flows with varied mass, composition, and outflow channel slope a significant amount of natural variability exists in both debris flow characteristics and deposit dimensions.
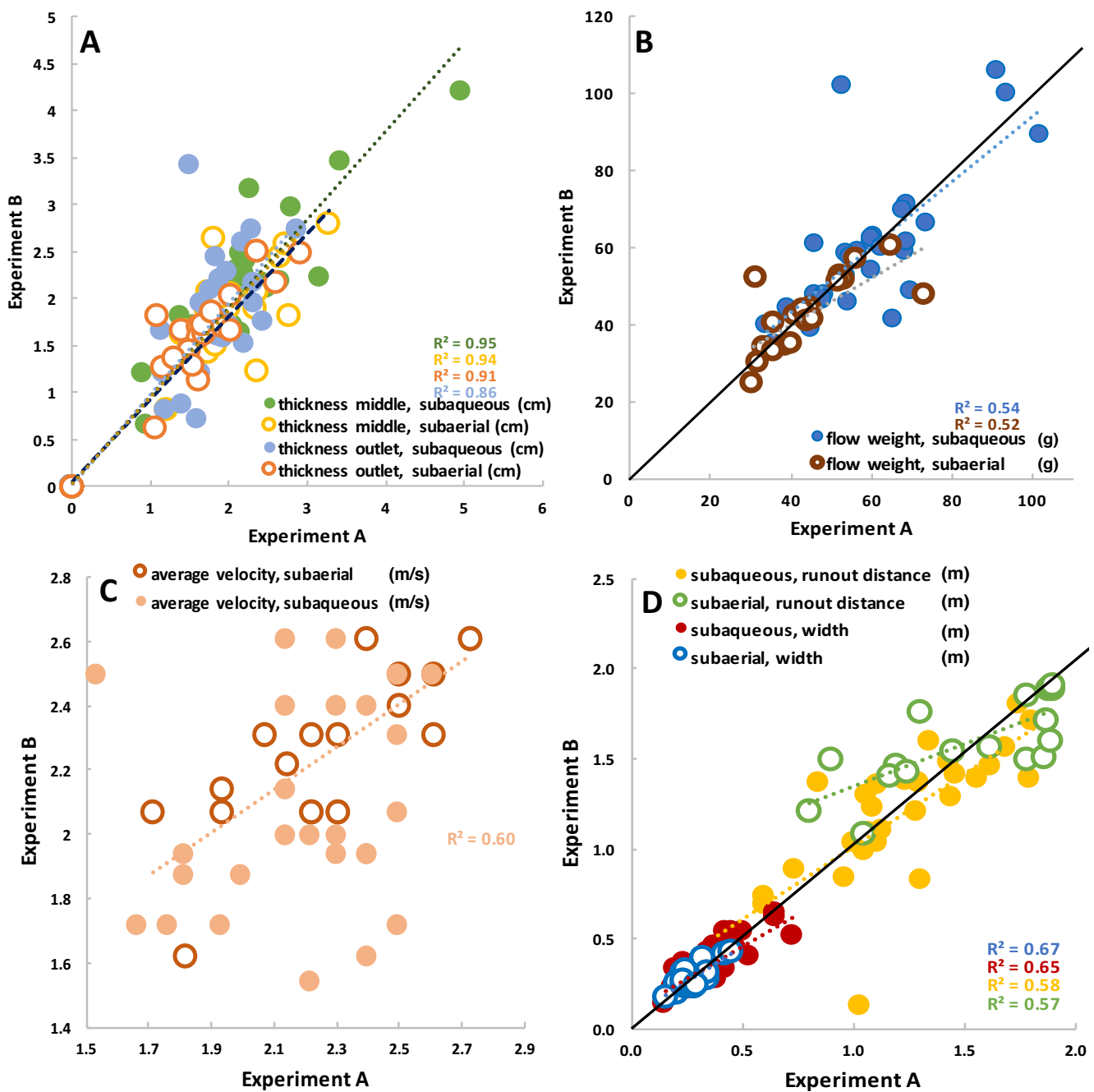

Figure 4.1. Natural variability of A) Average velocity B) Runout distance and width, C) Flow weight, D) Outlet and middle flow thickness, of subaerial and subaqueous debris flow.

4.2 Subaqueous and subaerial debris-flow

Subaqueous and subaerial debris flow have been influenced by the variations of mass, composition, and outflow channel slope. Figure 4.2.A, B, C, D, represent an example of middle and outlet subaqueous and subaerial debris flow thickness, and weight, profiles respectively. It is observed that both subaqueous and subaerial debris flow middle and outlet thickness, and weight as well, present a peak at around 1.3 seconds. This means that the whole debris flow has crossed the point where thickness and weight are measured is during the 2 first seconds. The tail of the plot shows that material stayed behind in the channel slope. These are examples of the subaqueous and subaerial experimental runs with flow mass 14,0 kg, and water content 55%, correspondingly.

The average of subaqueous and subaerial debris flow velocity along the outflow channel slope (2.0 m) is qualified to 2.12 m/s, and to 2.26 m/s, with a standard deviation (std) of 0.32 and 0.27, respectively. In the first 50 cm (0-50 cm) subaqueous debris flow has a faster velocity than the average which varies significantly (std 0.71), while subaerial debris flow has lower although, comparable to the average, 2.16 m/s (std 0.41). In the next 50 cm (50-100 cm) of the outflow channel subaqueous and subaerial debris flow velocities are even lower than the average (1.6 m/s, std 0.44, and 1.9 m/s, std 0.33, respectively). Subaqueous and subaerial debris flow velocities of the last 100 cm (150 and 200 cm of channel slope) are faster and more comparable to the average (average 2.3, and 2.7, respectively) however, there is large variability (std 0.64, and 0.69, correspondingly). Plotting both subaqueous and subaerial debris flow thickness against the maximum flow weight, and average velocity lead to a plot with a lot of scatters. However, subaerial and subaqueous middle flow thickness rely on linear regression with the increase of flow weight. An increase in debris flow thickness, though, is observed with an increase in velocity.
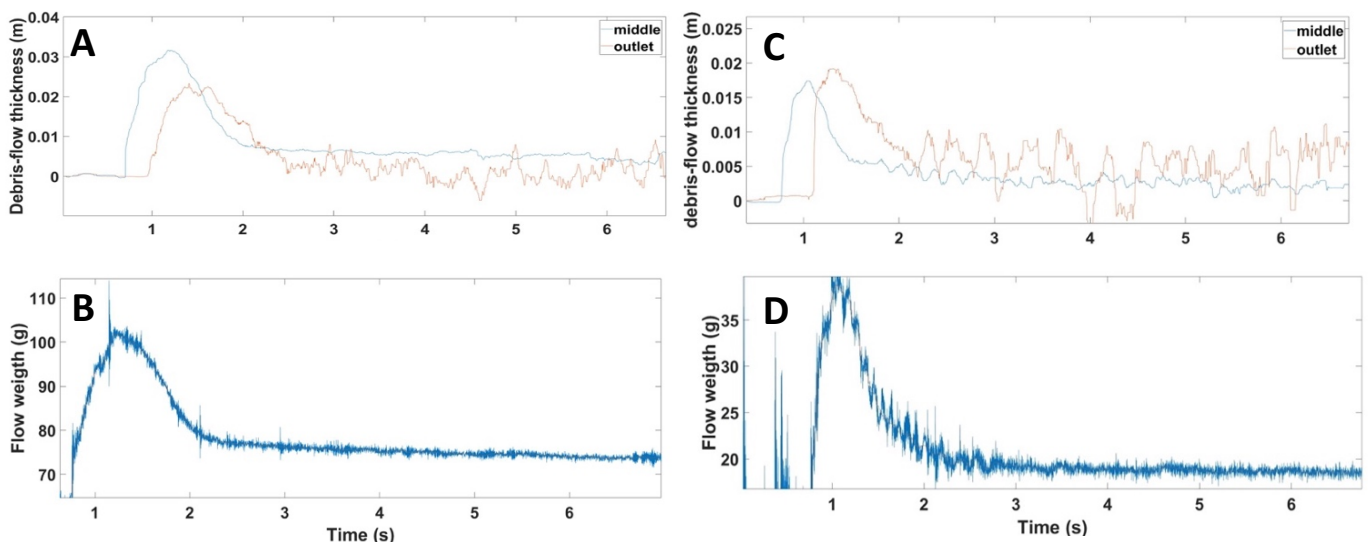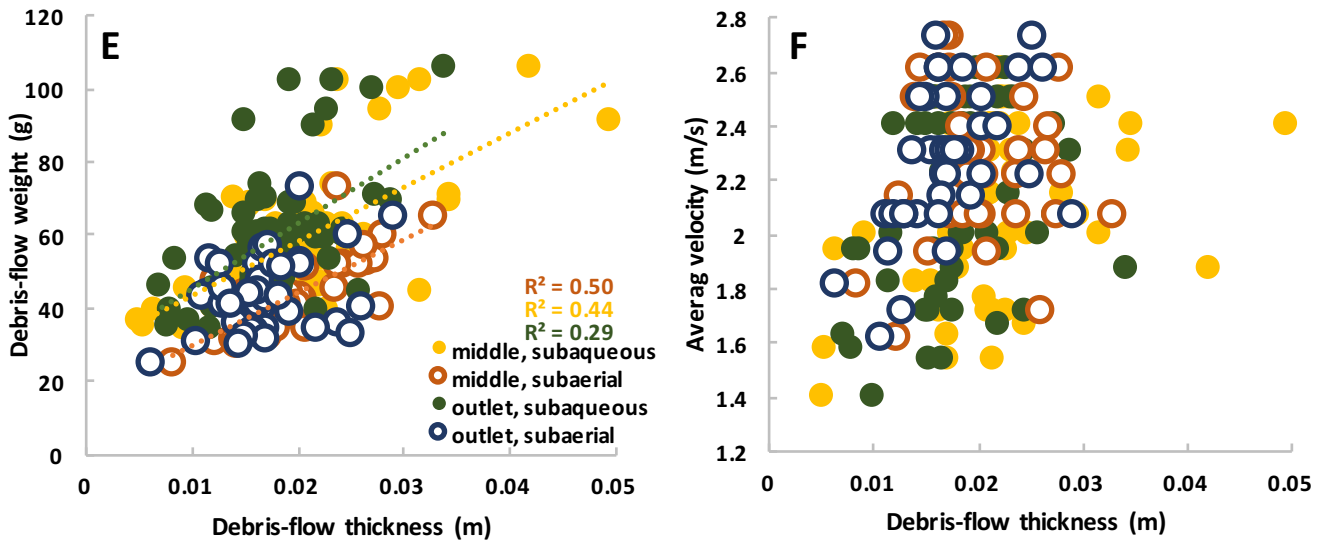
Figure 4.2. A, B) Debris flow outlet and middle thickness, and weight profiles of the subaqueous experiment with flow mass 14.0 kg, C, D) Debris flow outlet and middle thickness profile of the subaerial experiment with water content 55%, E) Subaqueous and subaerial debris-flow thickness against weight F) Average velocity against thickness, of subaqueous and subaerial debris flow.

4.2.1 Debris-flow mass

The original setting of the experiment was that the channel width would remain fixed and this constrains the dimensions of both subaqueous and subaerial debris-flow deposits. Subaqueous and subaerial debris flow maximum thickness and the increase of volume are highly related to each other. This can be noticed especially in the middle, where the debris flow is less extended (R^2= 0.92 and R^2=0.93, respectively). Subaqueous and subaerial outlet thickness also pursues a similar linear regression (R^2=0.68 and R^2=0.87, correspondingly). Therefore, the maximum weight of both subaqueous and subaerial debris flows increase with the increasing mass, following a similar linear relationship (R^2=0.95 and R^2=0.66, respectively). Lastly, average subaqueous and subaerial debris-flows velocity follow a similar pattern, however only average subaerial debris flow velocity shows a linear relation with the increasing mass (R^2=0.88). Although, average subaqueous debris flow velocity does not show any significant linear relationship with increasing mass, resulting in a plot with scatters which are more allocated distributed (R^2=0.35).

Natural variability affects both subaqueous and subaerial debris flows. The parameters: maximum middle and outlet thickness, weight, and average velocity as well, have been measured in the outflow channel slope during the flow and before the effect either by the terrestrial or by the submarine environment. Thus, similar values are expected between the subaqueous and subaerial experimental runs. Although, due to the effect of the natural variability the resulting parameters of the subaqueous flows do not fully coincide with the subaerial debris flows.
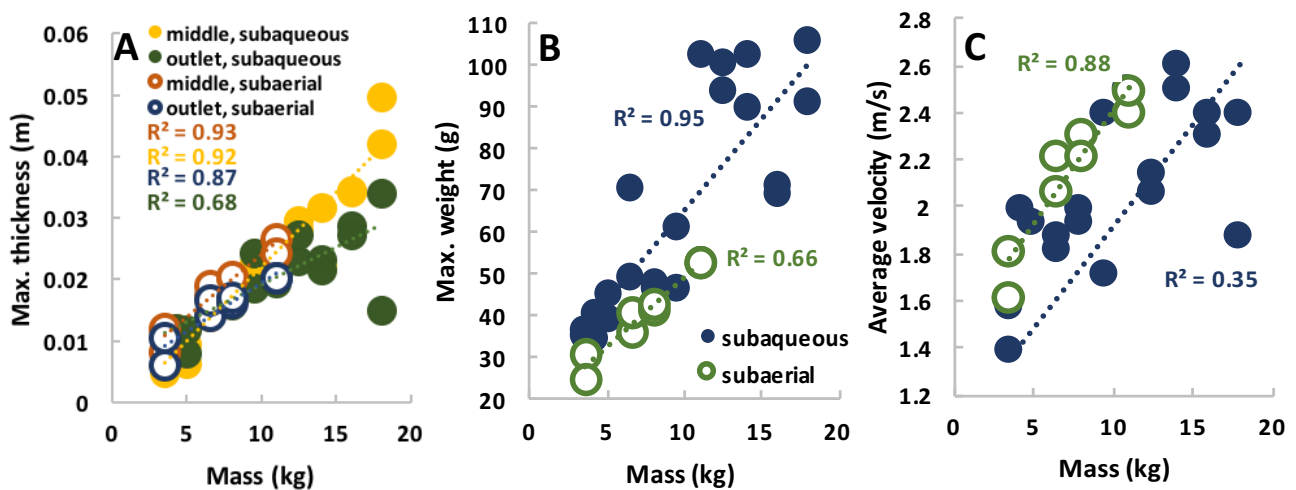

Figure 4.3.Relation between mass, subaqueous and subaerial debris-flow characteristics. A) Maximum thickness in the middle and outlet. B) Maximum weight at load cell. C)Average debris-flow velocity.

4.2.2 Debris-flow composition

Subaqueous and subaerial debris flow composition was varied containing materials such as water (40-60 %), gravel (0-64 %), and clay (0-30 %). All of them affected the debris-flow behavior and characteristics in a different way. However, the subaerial runs differ from the subaqueous on the number of experiments. Specifically, subaqueous experiments with variations in gravel and clay are 10 in total, whereas, the subaerial experiments with the same compositions are 6 in total. Contrastingly, subaqueous and subaerial runs with water variation are 8 in total. In this section, I will analyze the effect of water, gravel, and clay on maximum thickness, weight, and average velocity of both subaqueous and subaerial debris flows.

With an increasing water content (volume: 40-60%), average subaqueous and subaerial debris flow velocity are also increased and present a linear relationship (R^2= 0.87 and R^2= 0.69, respectively). Maximum thickness also follows similar pattern to the average velocity. Especially, the subaqueous outlet debris-flow thickness is related to the water content (R^2=0.57). However, outlet subaqueous flow thickness does not follow any specific pattern, while randomly distributed scatters. In contrast, subaerial debris flow middle and outlet thickness show that, with increasing water content middle subaerial flow thickness is decreased (R^2= 0.56), whereas, outlet subaerial thickness is increased (R^2= 0.90). Maximum subaqueous and subaerial weight does not follow any pattern indicating that there is not clear relationship between debris flow weight and increasing water content.

Gravel content (Figure 4.4 D, E, F) and debris flow characteristics are not related to each other. Specifically, an increasing gravel content does not show or follow any relation with the measured middle and outlet subaqueous and subaerial flow thickness. However, what can be identified is that the middle debris-flow thickness has higher values than the outlet, with the increase of gravel content (volume: 0-63.72%). Maximum subaqueous weight is increased with the increase of gravel content; however, a significant linear relation is not observed (R^2= 0.34). Maximum subaerial weight is not correlated with the increase of gravel. However, average subaqueous flow velocity seems that is well correlated with the gravel, meaning that an increase in gravel relies on a slower average velocity due to the high frictional forces between the gravel particles (R^2= 0.67). The average subaerial flow velocity indicates that, with increasing gravel it decreases (R^2=0.37) due to the large accumulation of the coarse particles in the flow front, thus high frictional forces between the gravel particles exist.

An increase in clay content (Figure 4.4. G, H, I) causes a decrease in both subaqueous and subaerial debris flow weight, while only maximum subaqueous flow weight leads to a linear relation with the increase of clay (R^2=0.80). However, the relation with thickness and average velocity differs. Specifically, an increase in clay content (volume: 0-21%) has a lubricating effect developing an increase in subaqueous debris flow velocity (from 2.31 to 2.5 m/s). In contrast, when the clay content becomes larger than 21%, debris flow becomes very viscous, resulting in a decrease of velocity due to the increase of viscous forces. Additionally, subaqueous debris flow middle thickness is affected by the increase in clay content. Outlet and middle subaerial flow thickness are highly related to the increase of clay (R^2=0.84, R^2=0.92, respectively). Due to the lubricating effect of clay, debris flow thickness increases in the middle of the outflow slope when the clay content increases until 21%. However, when the clay content is higher than 21%, middle subaqueous debris-flow thickness decreases.

However, average subaerial velocity does not show any correlation with the increase of clay content. Therefore, more subaerial experimental runs are needed to finally analyze if the flow average velocity is correlated with the increase of clay.
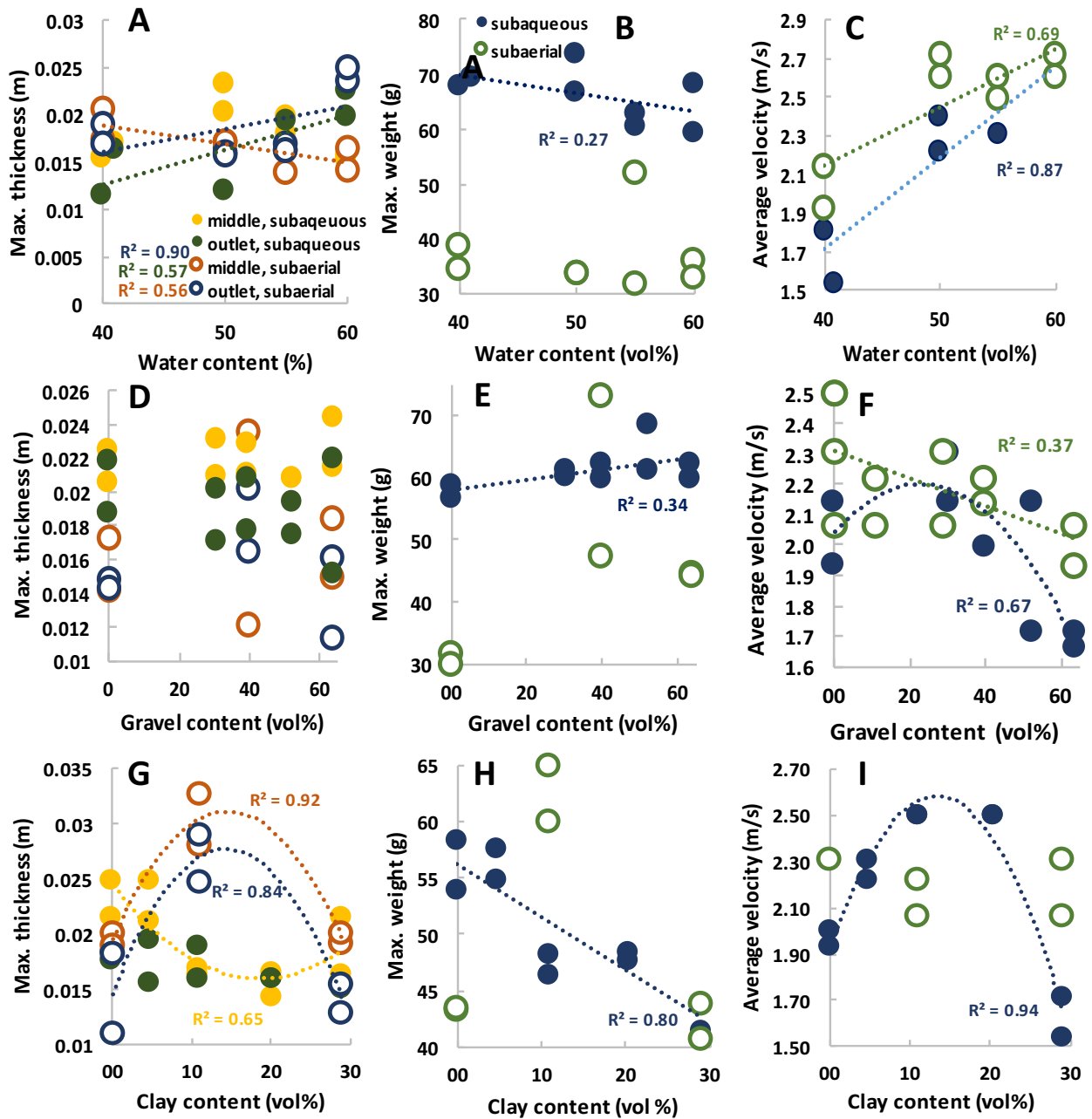

Figure 4.4.Relation between debris-flow composition, subaqueous and subaerial debris flow characteristics. A), B), C) Water content, D), E), F) Gravel content, G), H), I) Clay content.

4.2.3 Outflow slope

With an increase of outflow slope (20 - 40^0), subaqueous and subaerial debris-flow thickness, and average velocity also increase (Figure 4.5.A, C). Values of subaqueous debris middle and outlet flow thickness, and average velocity are varied between 0.020-0.031 m, 0.007-0.025 m, and 1.8-2.5 m/s, respectively, and are linear increased (R^2=0.55, R^2=0.66, and R^2=0.45, respectively). Proportionally, subaerial of debris middle and outlet flow thickness, and average velocity are varied between 0.018-0.027 m, 0.011-0.022 m, and 1.7-2.6 m/s, correspondingly. Only subaerial outlet flow thickness, and average velocity shows a linear relation (R^2=0.81 and R^2=0.63, correspondingly), while subaerial middle flow thickness does not show any correlation with the increase of slope.

However, maximum subaqueous and subaerial flow weight (39.19-54.49 g and 34.78-56.9 g, respectively) are decreased with the increase of outflow slope. This can be explained by the fact that when the slope increases, the water in the mixing tank escapes more easily during the mixing process and thus, less water is still remained until the release of the material. Consequently, with an increase of outflow slope the maximum weight is decreased.
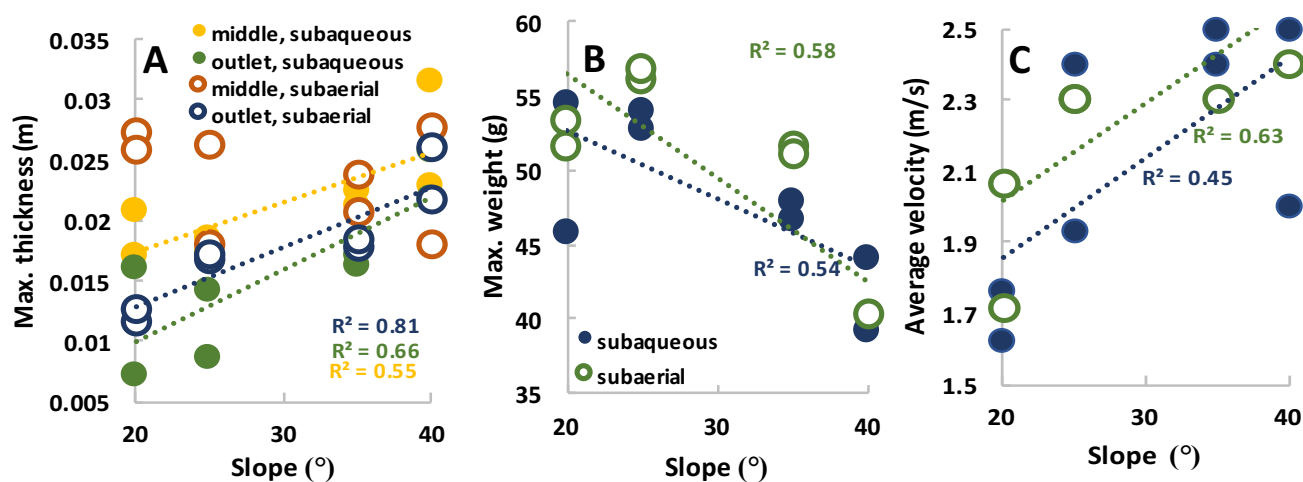

Figure 4.5. Relation between outflow channel slope, subaqueous and subaerial debris flow characteristics. A) Maximum thickness B) Maximum weight, C) Average velocity of debris-flow.

4.2.4 Debris-flow momentum

Debris-flow momentum is a relation of debris-flow mass and velocity. Subaqueous and subaerial debris-flow momentum plotting against the increasing total mass-volume shows a highly linear relation (R^2= 0.92 and R^2= 0.99, respectively). With an increase in water content subaqueous and subaerial flow momentum also increase, resulting in a linear regression (R^2=0.70 and R^2=0.69) (Figure. 4.6.B). In contrast, subaerial and subaqueous debris flow momentum is linear decreased with the increase of gravel content (R^2=0.95 and R^2=0.67). When the gravel content is increased, large accumulation of the coarse particles exists in the flow front and margins. Thus, average flow velocity is decreased with the increase of gravel. Flow momentum is described by the flow mass and velocity. Flow momentum is therefore decreased by the increase of gravel content (39.71 -63.72 %).

With an increase in clay content (Figure 4.6. D), subaqueous flow momentum increases until the clay content becomes 21 %. However, when the clay content becomes larger than 21 %, debris-flow momentum decreases due to viscous flow. Thus, flow momentum is polynomial decreased with the increase of clay. Although, subaerial flow momentum does not show any relation with the increase of clay content.   An increasing outflow channel slope leads to an increase of both subaqueous and subaerial debris-flow momentum (R^2=0.45 and R^2=0.63). Although, more runs are obligated to confirm this trend.
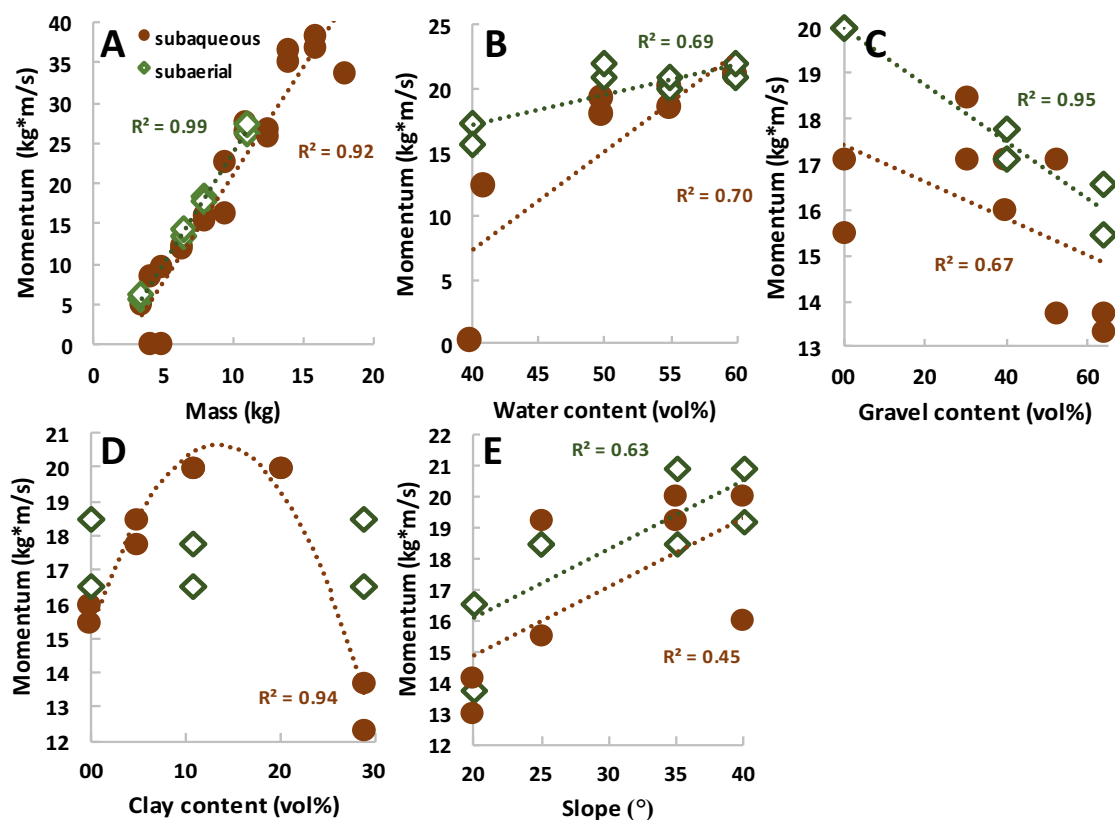

Figure 4.6. Subaqueous and subaerial debris-flow momentum per varied composition, volume, and outflow slope. A) Mass variation, B) Water content, C) Gravel content, D) Clay content, E) Outflow channel slope variation.

4.2.5 Summary of subaqueous and subaerial debris flow characteristics

R^2 values demonstrate the strength between the debris flow characteristics and debris flow mass, composition, and slope variations (table 4.1.A, B). Debris flow mass seems to have the greatest influence on subaqueous debris flow thickness and momentum due to the fixed experimental channel width. Average subaqueous debris flow velocity has been affected by the water and clay due to the lubricating effect. Subaqueous debris flow weight is mainly controlled by the clay, and mass, and is described by the debris flow thickness and density. Subaqueous debris flow momentum is determined by the mass and clay explaining the relation between flow velocity and density.

Strong linear relation is observed between the subaerial mass and momentum, average velocity and weight. Subaerial momentum has also been affected by the gravel where strong frictional forces occur between the particles. Water content seems to have the largest influence on the subaerial debris flow thickness, the higher water the thicker flow. Maximum flow weight is controlled by the slope, and mass, defining the relation between thickness and density. Average subaerial flow velocity is determined by the mass and slightly by the water due to the lubricating effect.

A	Mass	Water content	Gravel content	Clay content	Slope
Thickness (outlet)	0.89	0.57	-	0.65*	0.66
Weight	0.68	0.27	0.34	0.80	0.54
Velocity (average)	0.49	0.87	0.67*	0.94*	0.45
Momentum	0.92	0.70	0.67	0.94*	0.45

B	Mass	Water content	Gravel content	Clay content	Slope
Thickness (outlet)	0.84	0.90	-	0.84*	0.81
Weight	0.87	-	-	-	0.58
Velocity (average)	0.89	0.69	0.37	-	0.63
Momentum	0.99	0.69	0.95	-	0.63

*Table 4.1 A) R^2 values of subaqueous debris flow parameters and the equivalent thickness, weight, velocity, and momentum, B) R^2 values of subaerial debris flow parameters and the equivalent thickness, weight, velocity, and momentum. * indicates polynomial regression, no values indicate unimportant relation.*

4.3 Subaqueous and subaerial debris-flow deposits

This section contains information about the subaqueous and subaerial debris-flow deposits. In the previous sections, subaqueous and subaerial debris-flow parameters have been discussed to have a clearer idea about the relation between flow parameters and characteristics of each flow independent before it leads to the basin, which is either empty or filled with water. In this chapter I will first discuss the subaqueous and subaerial debris-flow deposit dimensions such as runout distance, maximum width, and maximum deposit thickness (4.3.1-4.3.2). Next, I will evaluate the effect of debris-flow velocity on runout distance and width deposit. Lastly, I will explain the grain size distribution and sorting along both subaqueous and subaerial debris-flow deposits.

4.3.1 Deposit dimensions: runout distance and maximum width

4.3.1.1 Debris-flow mass

With an increasing mass, both subaqueous and subaerial deposit runout distance increases (Figure 4.7.A). Subaqueous and subaerial debris-flow mass presents a linear relation with the runout distance (R^2=0.84 and R^2=0.82, respectively). It is clear that, when the subaqueous and subaerial debris-flow mass is increased, the runout distance of the deposits also increases. Nevertheless, runout distance of subaerial debris flow deposits with the same mass, indicate that are longer than the subaqueous. Specifically, between 3.5 and 11.00 kg of mass, subaerial flow deposits (0.7-1.9 m) are longer than the subaqueous (0.3-1.5 m). See also figure 4.8 and 4.10 for the subaqueous, figure 4.9 and 4.11 for the subaerial debris flow deposits.

As the subaqueous and subaerial debris-flow mass is increased, maximum width also increases. Maximum deposit width and debris-flow mass present a linear correlation for both subaqueous and subaerial debris-flow deposits, R^2=0.87 and R^2=0.80, respectively. As discussed above, with an increasing mass subaerial debris flow deposits have longer runout distance than the subaqueous. However, with an increasing mass maximum deposit width is wider on subaqueous than on subaerial debris-flow deposits. It is clear that between 3.5 and 11.00 kg of mass, the deposit width of the subaqueous debris-flow has values between 0.13 and 0.45 m, whereas, for the subaerials is between 0.16 and 0.20 m.
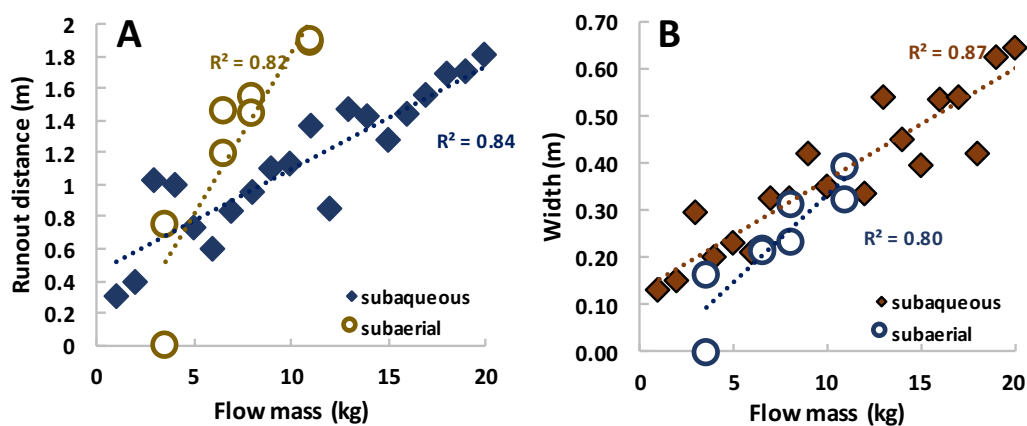
Figure 4.7. Relation between subaqueous and subaerial mass with debris-flow deposit dimensions. A) Runout distance against flo, B) Maximum deposit width.
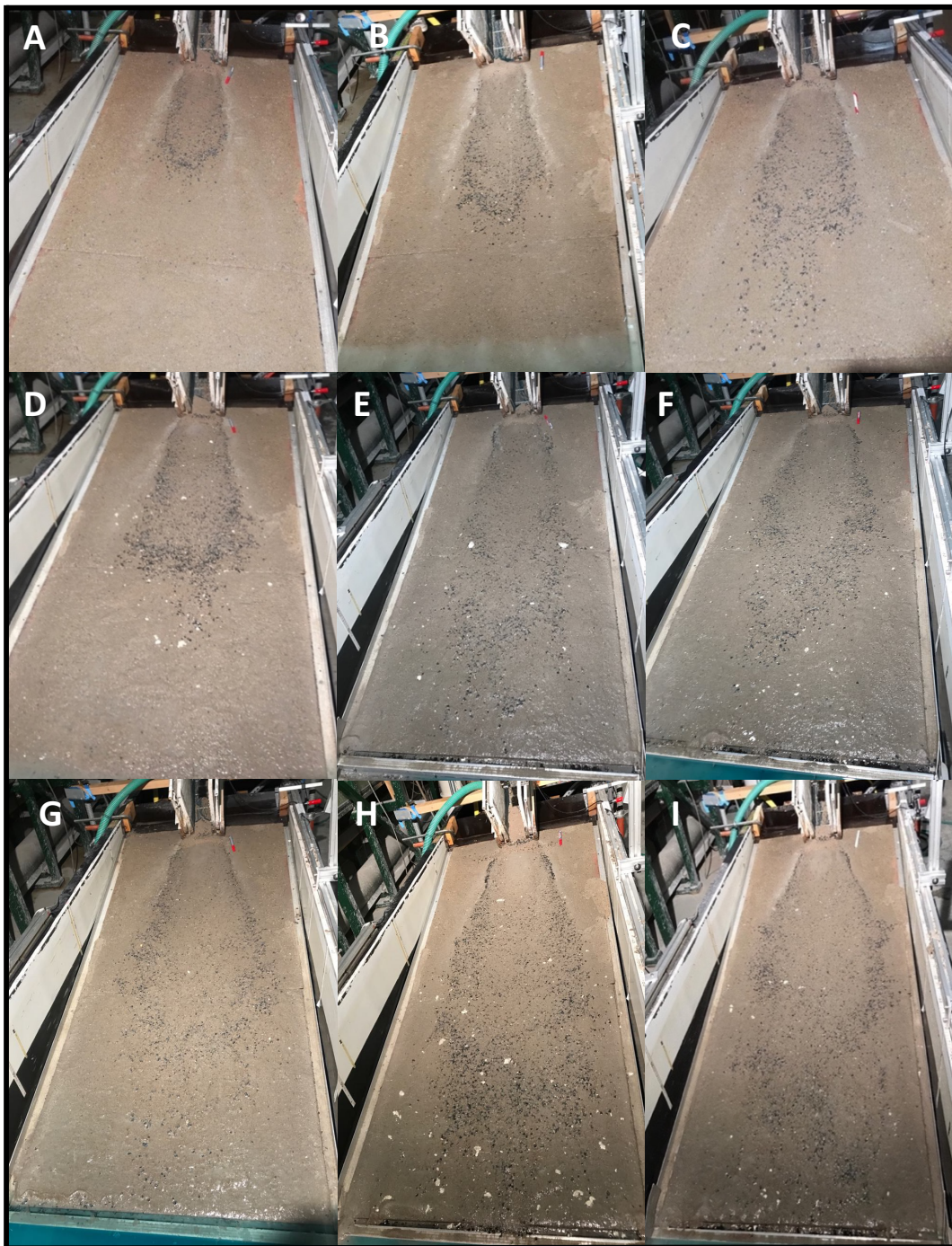
Figure 4.8. Subaqueous debris flow deposits with mass variation A) Flow mass: 3.5 kg, B) Flow mass: 4.25 kg, C) Flow mass 6.5 kg, D) Flow mass: 8.0 kg, E) Flow mass: 9.5 kg, F) Flow mass: 11.0 kg, G) Flow mass: 12.5 kg, H) Flow mass: 14.0 kg, I) Flow mass: 16.0 kg

Figure 4.9. Subaerial debris flow mass deposits a) Flow mass: 3.5 kg, B) Flow mass: 6.5 kg, C) Flow mass 8.0 kg, E) Flow mass: 11.0 kg.

Figure 4.10: DEM Photo-scan of subaqueous debris flow deposit with increasing mass.

Figure 4.11 DEM Photo-scan for subaerial debris flow deposits with increasing mass.

4.3.1.2 Debris-flow composition

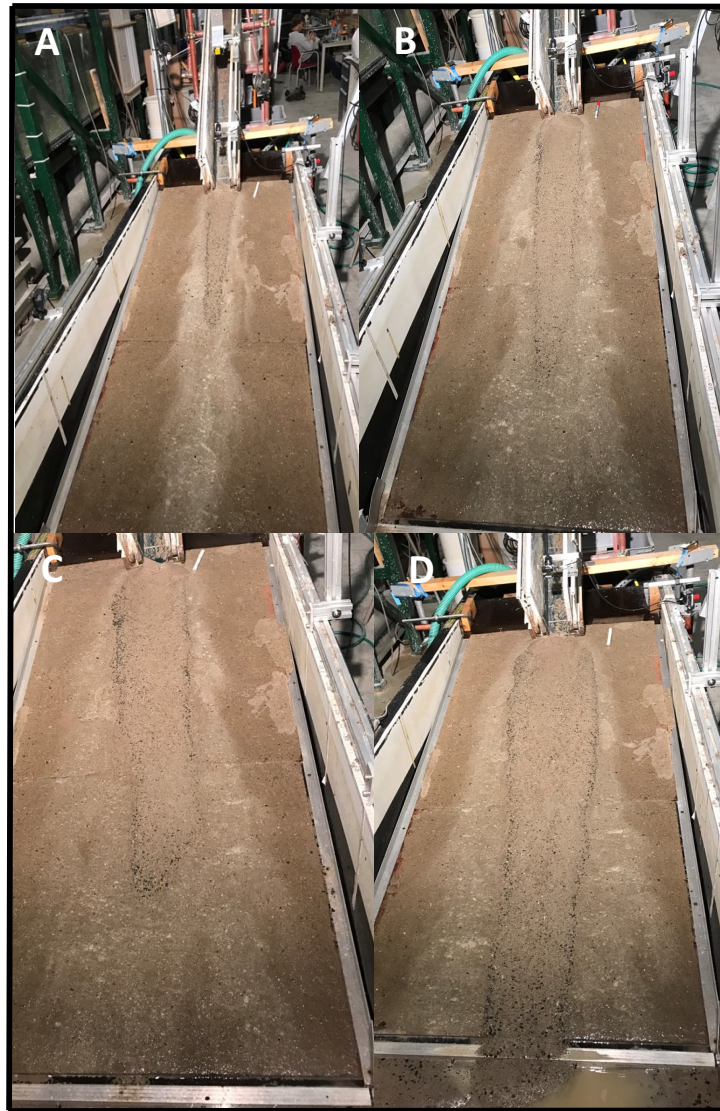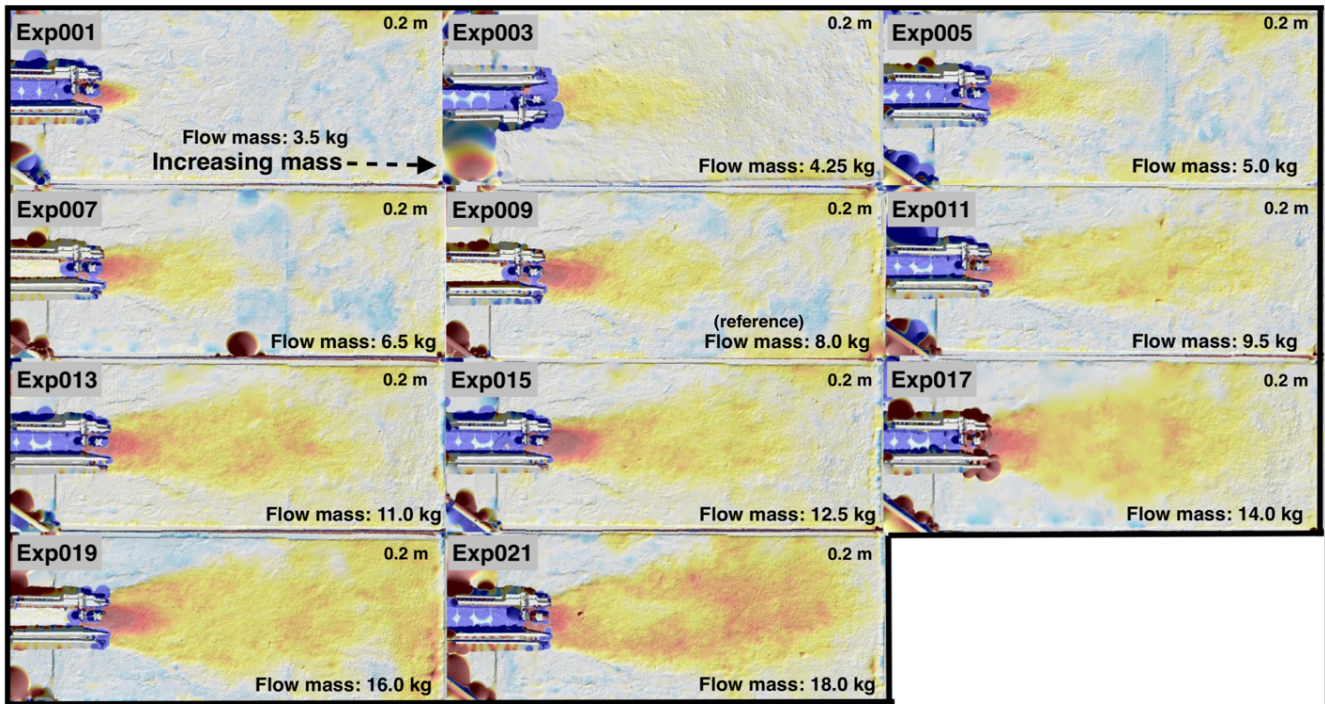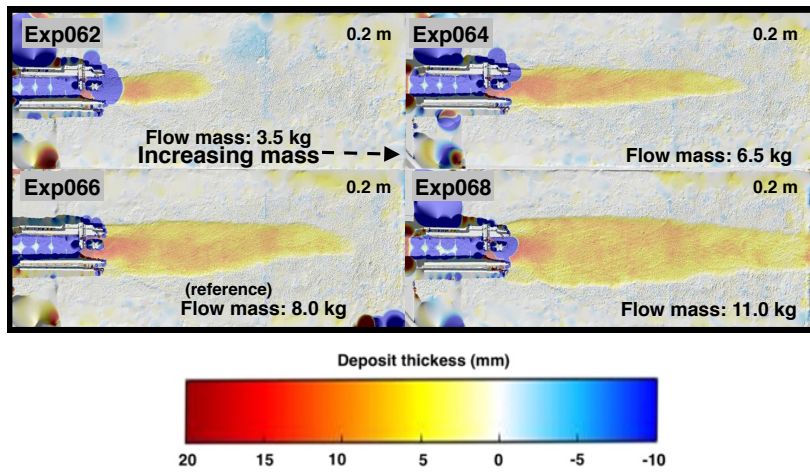When the water content (volume: 40-60%) (Figure 4.12.A) is increased, runout distance of both subaqueous and subaerial debris-flow deposits is increased. Water content and runout distance of both subaqueous and subaerial debris-flow deposits, present linear relation (R^2=0.61 and R^2=0.75, respectively). It is clear that, subaerial debris flow deposits with variations in water content lead to longer runout deposit distance than the subaqueous. Subaerial runout deposit distance varies between 1.16 and 1.9 m, whereas, subaqueous runout deposit distance has values between 0.8 and 1.61 m.

Maximum deposit width is also influenced by the increase of water content (Figure 4.12.B). Specifically, when the water content is increased subaerial debris flow deposit width becomes wider, indicating a significant linear relation (R^2=0.93). However, maximum width of subaqueous flow deposits does not show any correlation with the increase of water content. Water content between 40-50% indicates that maximum width (0.27-0.30 m) is wide in the subaqueous deposits while, is narrow (0.19-0.27 m) for the subaerial runs. However, when the water content becomes larger than 50%, subaerial debris flow deposit width (0.34-0.45 m) is wider than the subaqueous deposit width (0.37-0.39 m).

Figure 4.12. C shows the maximum runout deposit distance for both subaqueous and subaerial debris-flow with a gravel content around 0-63.72 %. Experimental runs with gravel variation on subaqueous debris-flow are 10, whereas, the subaerials are 6 in total. It is very clear that with an increase of gravel content, subaerial runout deposit distances are longer than the subaqueous. However, when increasing the gravel content of the subaerial and subaqueous debris flow, a shorter runout deposit distance is observed. When the gravel content for the subaqueous debris flow becomes 30.5 %, runout deposit distance is increased (0-1.23 m). However, when the gravel content becomes larger than 30.5%, runout deposit distance of subaqueous and subaerial flows is decreased from 1.34 to 0.99 m and from 1.48 to 0.79 m, respectively. Subaerial debris flow runout distance is significant linear decreased with the increase of gravel (R^2=0.83). This is due to excess coarse material and the accumulation at the coarse particles in the flow front where the frontal friction increases and the run-out distance decreases.

The gravel content of both subaqueous and subaerial debris flow influences the maximum width of each deposit. Especially, the subaqueous flow deposits, where there is increase of gravel content, the deposit width becomes significant narrower (Figure 4.12.D). The relation between the increase of gravel and the deposit width of subaqueous debris flow is linear (R^2=0.83). However, the gravel content has less significant effect on subaerial debris flow deposits. Specifically, with an increasing gravel content subaerial debris flow deposit width decreases however, with slightly variations. Because the relation between maximum deposit width and gravel content is not clear thus, more experiments are needed to verify this relation. This can be explained by the fixed width of the outflow channel slope, and due to this, the flow can not spread.

Variations of clay content (Figure 4.12.E, D) on subaqueous and subaerial debris flow have affected the runout deposit distance and width of each flow deposit. Both debris flow dimensions present a complex polynomial trend with the increase of clay content. Maximum runout deposit distance of the subaerial debris flow is longer than the subaqueous deposits. It is clear that in the beginning, the runout deposit distance of the subaqueous is increased with the increasing clay content. This is due to the lubrication of the flow with the increase of clay, resulting in longer runout deposit distance. However, when the clay becomes larger than 11% then the flow becomes viscous and therefore, runout deposit distance of both subaqueous and subaerial debris flow is significant decreased from 1.56 to 0.59 and from 1.8 to 1.2 m, respectively. Multiple outflow surges occur as the clay-rich viscous (29% of clay) flow is deposited.

Maximum deposit width (Figure 4.12.F) is also affected by the increase of clay, resulting in a wider for the subaqueous and narrower width for the subaerial debris flow deposits. It is clear that the relation between maximum width and increasing clay follows the same trend, such as the trend of runout deposit distance and increasing clay. It can be seen that, the maximum width of both subaqueous and subaerial debris flow deposits increases from 0.30 to 0.47 m and from 0.23 to 0.34 m, respectively, until the clay content becomes 11%. Contrary to this, when the clay becomes larger than 11%, the maximum width of both subaqueous and subaerial debris flow decreases from 0.41 to 0.19 m and from 0.34 to 0.23 m, respectively. However, more experimental runs are needed in order to clarify the relation between the increasing clay of subaerial debris flow and the maximum width of the clay-rich deposit. Figures 4.13 and 4.15 illustrate the photo and DEM photo-scans of subaqueous debris flow deposits with varied water, gravel, and clay content. Figures 4.14 and 4.16 represent the photos and DEM photo-scans of the subaerial debris flow deposits with varied composition.
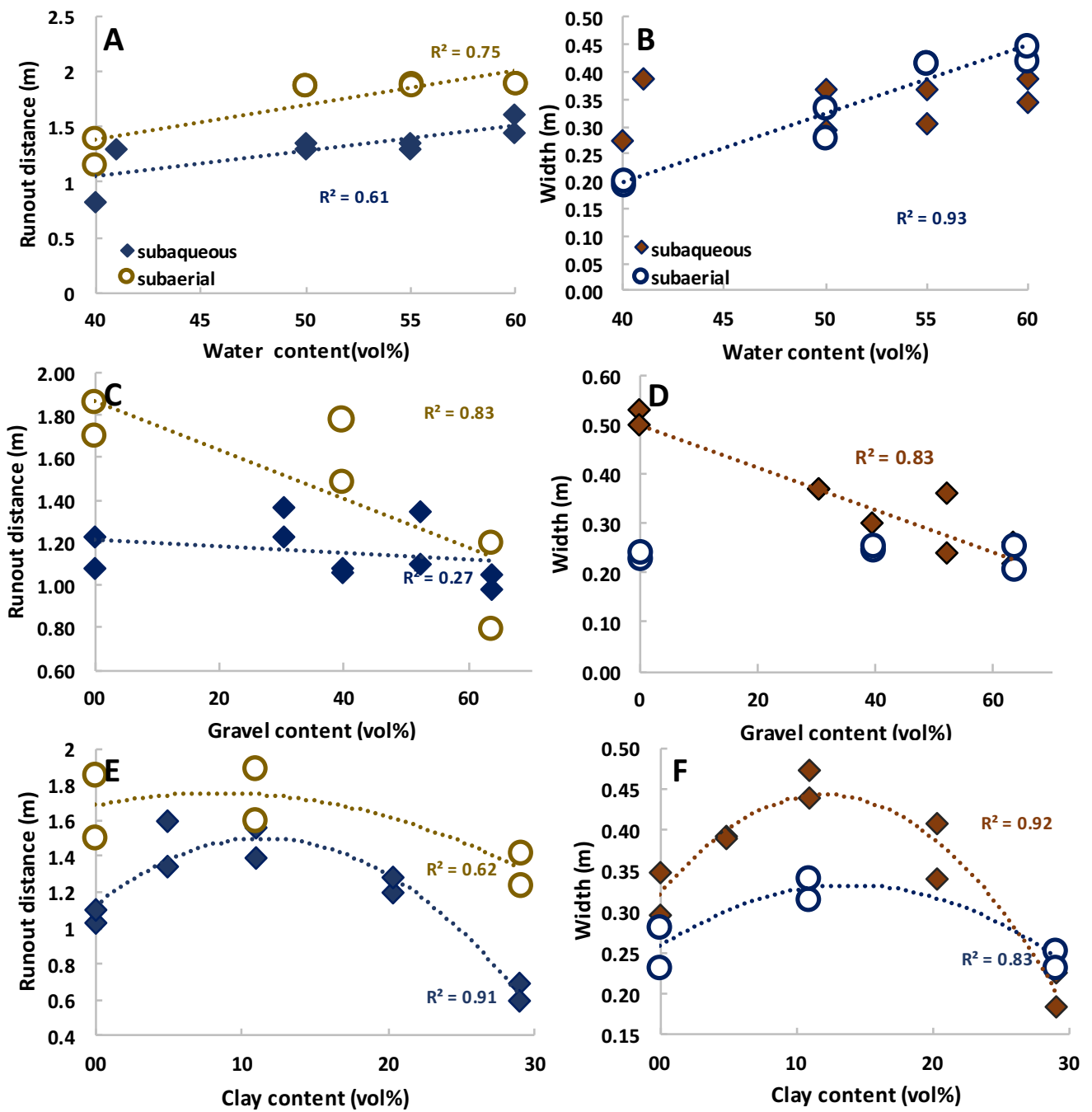
Figure 4.12. Relation between subaqueous and subaerial varied composition with debris-flow deposit dimensions. A) B) Water content, C), D) Gravel content, E), F) Clay content.

Figure 4.13 Subaqueous debris flow deposits with varied composition A) Water 40%, B) Water 50%, C)Water 60%, D) Gravel 0%, E) Gravel 52 %, F) Gravel 64%, G) Clay 0%, H) Clay 0.11, I) Clay 0.29% content.

Figure 4.14 Subaerial debris flow deposits with varied composition A) 40% water B) 55% water, C) 60% water, D)0% gravel, E) 40 % gravel F) 64 % gravel, G) 0% clay, H) 11 % clay, I) 29% clay

Figure 4.15 DEM Photo-scans of subaqueous debris flow deposits of varied composition, Exp023-Exp030) Water content (volume 40-50 %), Exp031-Exp040) Gravel content (volume 0-64%), Exp041-Exp049) Clay content (volume 0-29%).

Figure 4.16. DEM Photo-scans for subaerial debris flow deposits with varied composition Exp070-Exp077) Water content (volume 40-60%), Exp077-Exp082) Gravel content (volume 0-64%), Exp084-Exp089) Clay content (volume 0-29%).

4.3.1.3 Outflow slope

Outflow channel slope variations (20-40^0) have significant impact on both the maximum runout deposit distance and width (Figure 4.17.A, B). Especially the maximum runout distance of the subaerial debris flow deposits is longer than the subaqueous (0.9-1.8 m and 0.12-1.46 m, respectively). It seems that maximum runout distance of both subaqueous and subaerial debris flow deposits increases until the slope becomes 35^0. However, when the outflow channel slope becomes steeper, runout distance of both subaqueous and subaerial debris flow deposits becomes shorter. A steeper slope (>40^0) corresponds to a higher gravitational potential energy and thus a higher vertical momentum component, while a smaller horizontal momentum component. Consequently, there will be greater total momentum loss after the steep transition between the channel slope and the outflow bed slope (10^0), since the vertical momentum component will be diminished due to the stronger collision of the debris with the outflow bled slope. Therefore, subaqueous and subaerial debris flow velocities and runout distances are decreased with a steeper slope.

An increasing slope (20-40^0), has a huge impact on maximum deposit width of both subaqueous and subaerial debris flow. Specifically, with an increasing slope from 20^0 to 35^0 subaqueous maximum deposit width becomes wider (from 0.33 to 0.45 m) (R^2=0.36). Additionally, when the outflow channel slope increases (from 20^0 to 35^0), subaerial maximum deposit width first (between 20^0-25^0) slightly becomes wider from 0.31 to 0.32 m, whereas, when the outflow channel slope is steeper (25^0-35^0), it becomes narrower from 0.32 to 0.24m. Lastly, between 35^0 and 40^0, it seems that subaqueous and subaerial maximum deposit width has opposite trends. To be more specific, subaqueous deposit width becomes narrow (from 0.45 to 0.38 m) while, subaerial deposit width becomes slightly wider (from 0.24 to 0.30 m). The subaqueous deposit width becomes narrower with a steeper slope due to the horizontal momentum component which is attenuated more quickly. To be specific, due to the diminished vertical momentum component, as discussed above, the horizontal momentum component is relatively smaller, thus the deposit is less laterally spread. Consequently, the deposit width becomes narrower with an increase in outflow channel slope. Although, subaerial deposit width seems that is not significant affected by outflow channel slope variations. Figures 4.18 and 4.20 show the subaqueous debris flow deposits photos and DEM photo-scans. Additionally, figures 4.19 and 4.21, depict the photos and DEM photo-scans of the subaerial debris flow deposits
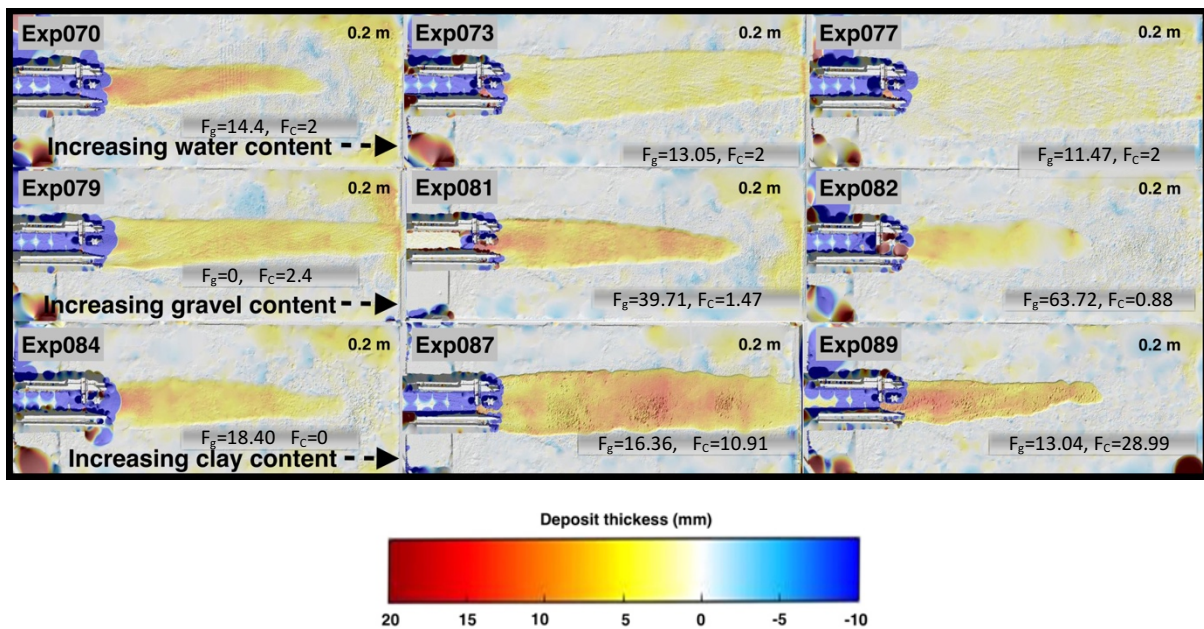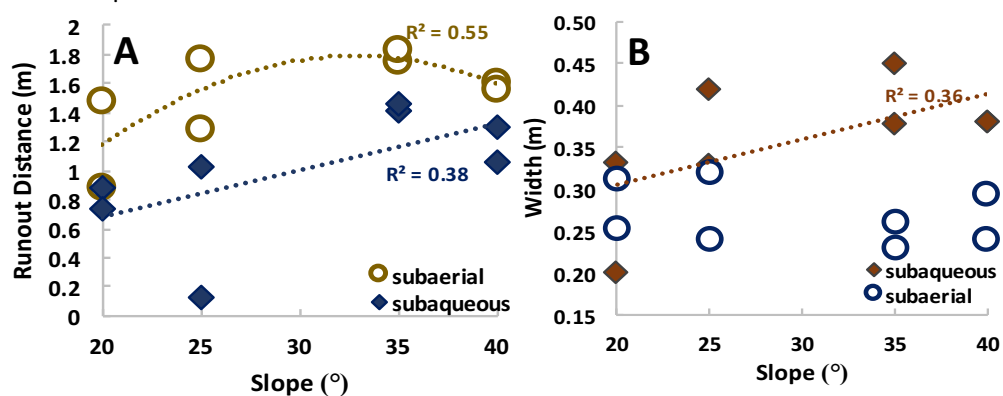

Figure 4.17. Relation between outflow channel slope variations, and A) Maximum runout distance, B) Maximum width.

Figure 4.18. Subaqueous debris flow deposits with varied outflow channel slope A) Slope 20^0, B) Slope 25^0, C) Slope 35^0, D) Slope 40^0.

Figure 4.19: Subaerial debris flow deposits with slope variations A) Slope:20^0 , B) Slope: 25^0, C) Slope: 35^0, D) Slope: 40^0.
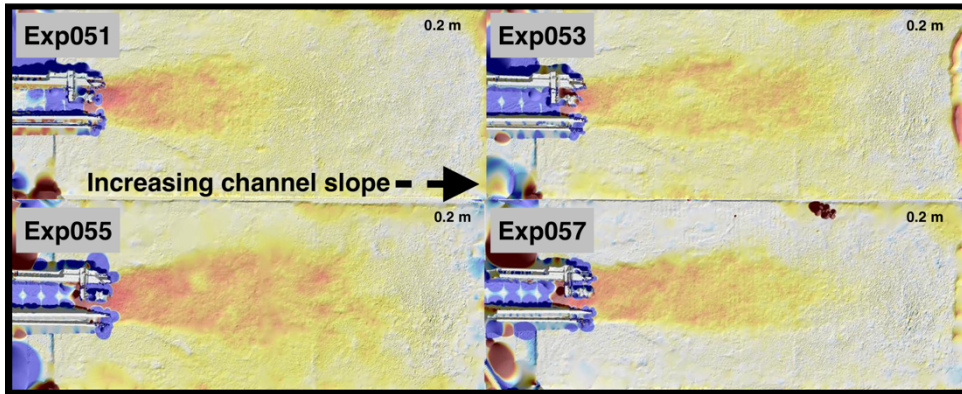
Figure 4.20. DEM Photo-scans of subaqueous debris flow deposits with slope variations Exp051) Channel slope: 20^0, Exp053) Channel slope: 25^0, Exp055) Channel slope: 35^0, Exp057) Channel slope: 40^0.
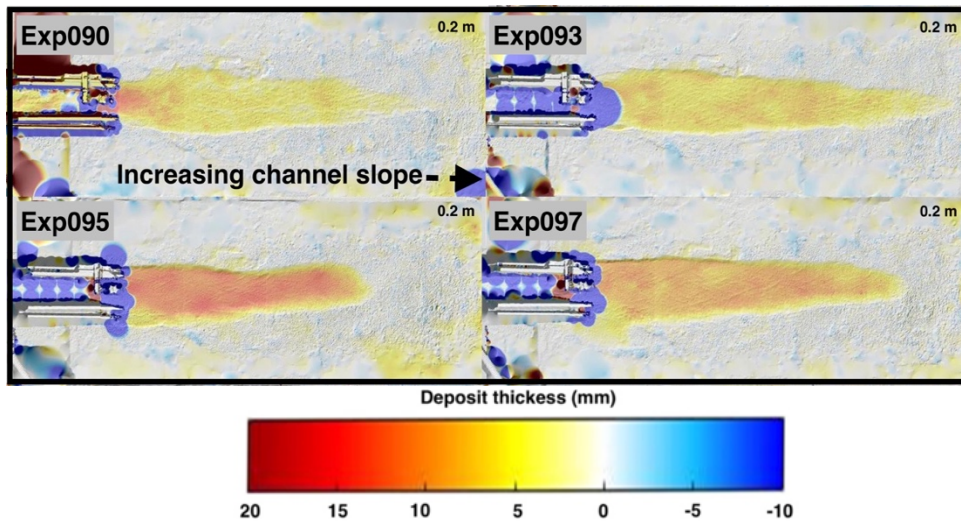
Figure 4.21 DEM Photo-scans for subaerial debris flow deposits with outflow channel slope variations Exp090)Channel slope 20^0, Exp093) Channel slope 25^0, Exp095) Channel slope 35^0, Exp097) Channel slope 40^0.

4.3.2 Debris-flow deposit thickness

Debris flow deposit thickness is another debris-flow dimension which vary between subaqueous and subaerial debris-flow deposits. It can be seen that with increasing mass (Figure 4.22 A), subaqueous debris flow deposits are thicker than the subaerials. An increasing mass (3.5-18.0 kg) for the subaqueous experimental runs, causes an increase in both subaqueous and subaerial flow deposits. However, the relation between subaqueous increasing mass and deposit thickness is not linear and thus, a specific trend cannot be observed. Similarly, the relation with the increase of subaerial debris flow mass and deposit thickness is supposed to be linear (R^2=0.44). With an increase of subaerial debris-flow mass, subaerial debris-flow thickness also increases although, more experimental runs are obligated to verify this relation.

Variations on both subaqueous and subaerial debris-flow composition have an impact on debris flow deposit thickness. With an increasing water content, subaqueous debris-flow deposit thickness becomes thinner, whereas, subaerial debris-flow deposit thickness becomes thicker, from 0.031 to 0.012 m and from 0.016 to 0.019 m, correspondingly. In contrast, the relation between water content and deposit thickness is not clear and thus, a linear relation cannot be justified.

Maximum deposit thickness of both subaqueous and subaerial debris-flow is also affected by the increase of gravel content (Figure 4.22.C). What is obvious is that, maximum subaqueous deposit thickness does not show any correlation with the increase of gravel content. However, maximum subaerial deposit thickness seems that becomes thicker (from 0.01 to 0.11 m) with the increasing gravel, resulting in a linear relation (R^2=0.83).

Significant impact on debris-flow deposit thickness has the clay content. Especially, the increasing clay content affects both subaqueous and subaerial debris flow deposit however, in a different way. Figure 4.22.D shows that for subaerial debris flow the maximum deposit thickness becomes thicker with an increase in clay content while, in subaqueous exist exactly the opposite. Maximum deposit thickness of subaqueous flow becomes thinner with the increasing clay content. Specifically, the relation between maximum subaqueous deposit thickness and increasing clay is polynomial (R^2= 0.70). Although, the relation between maximum deposit thickness of subaerial debris-flow and increasing clay is linear (R^2=0.63).

Outflow channel slope variations (20- 40^0) change the deposit thickness of both subaqueous and subaerial debris flow. It seems that, slope variations and deposit thickness are not related to each other. It is observed though, that subaqueous debris flow deposits are thicker (0.013-0.022 m) with an increasing slope while, subaerial debris flow deposits are thinner (0.009-0.015 m).
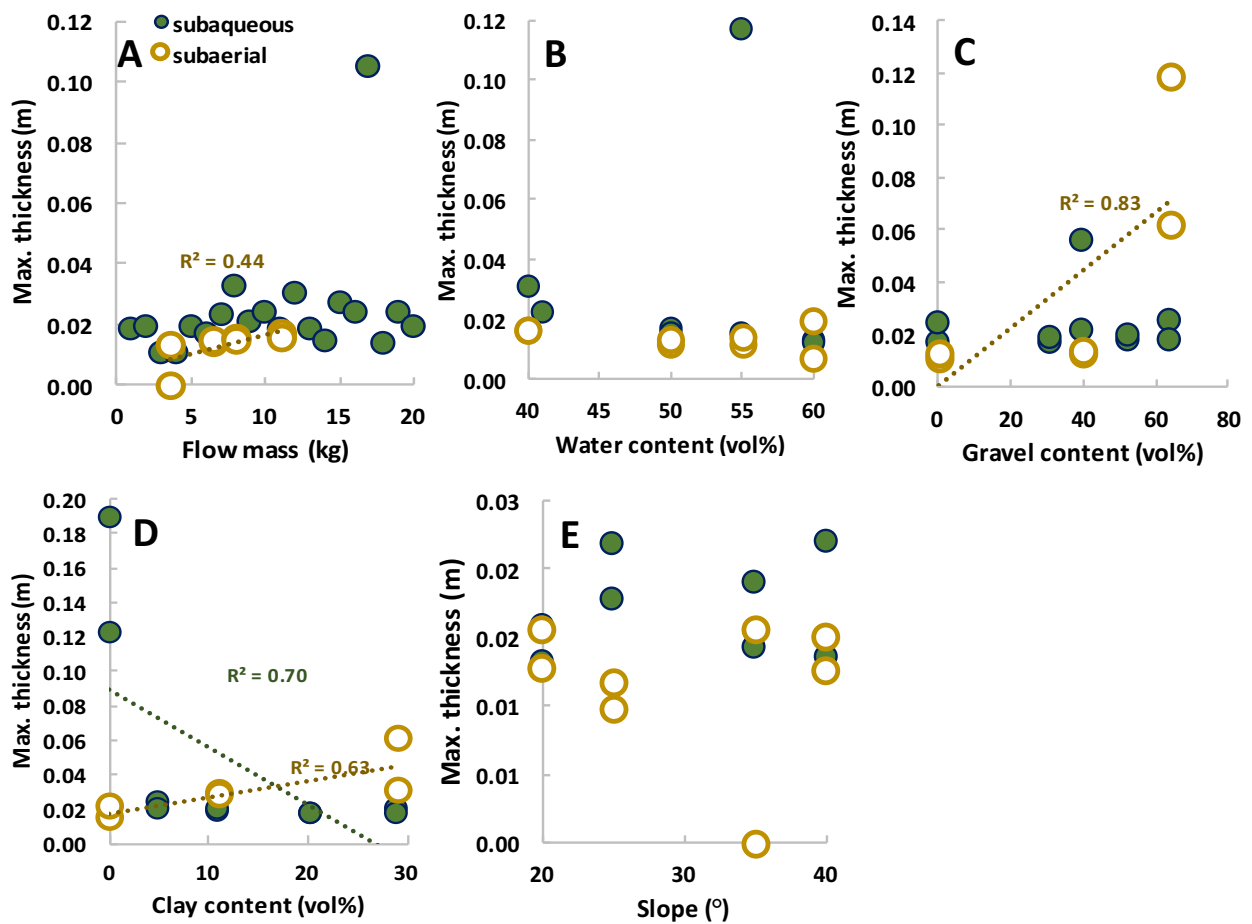
Figure 4.22. Relation between subaqueous and subaerial deposit thickness and debris flow varied A) Mass, B, C, D) Composition, E) Outflow channel slope.

4.3.3 Effect of debris-flow velocity on runout distance and width

Variations in composition, as well as, in mass and outflow channel slope of subaqueous and subaerial debris flow have caused significant impact on the dimensions of the deposits. Maximum runout distance and width of subaqueous and subaerial debris flow deposits have been influenced by the previous stated variations.

4.3.3.1 Debris-flow mass

Debris flow average velocity has a huge impact on runout distance and is affected by the increase of mass (figure 4.23.A). As the debris flow mass of both subaerial and subaqueous flows increase, average velocity and runout distance also increases, resulting in a linear relation (R^2=0.68 and R^2= 0.70, respectively). Another significant observation is that; runout distance of subaerial debris flow deposits is longer than the runout distance of subaqueous debris flow deposits as the average velocity increases.

Deposit width, is also affected by the average velocity of both subaqueous and subaerial debris flow with mass variations. More precisely, with an increase in debris flow mass, average velocity increases as well as the deposit width becomes wider. Particularly, the deposit width of subaqueous debris flow becomes significant wider than the deposit width of subaerial, with an increase in average velocity. Deposit width and increase of average velocity due to the increase of mass are highly related to each other, resulting in linear regression for both subaqueous and subaerial debris flow deposits (R^2=0.46 and R^2=0.64, respectively).
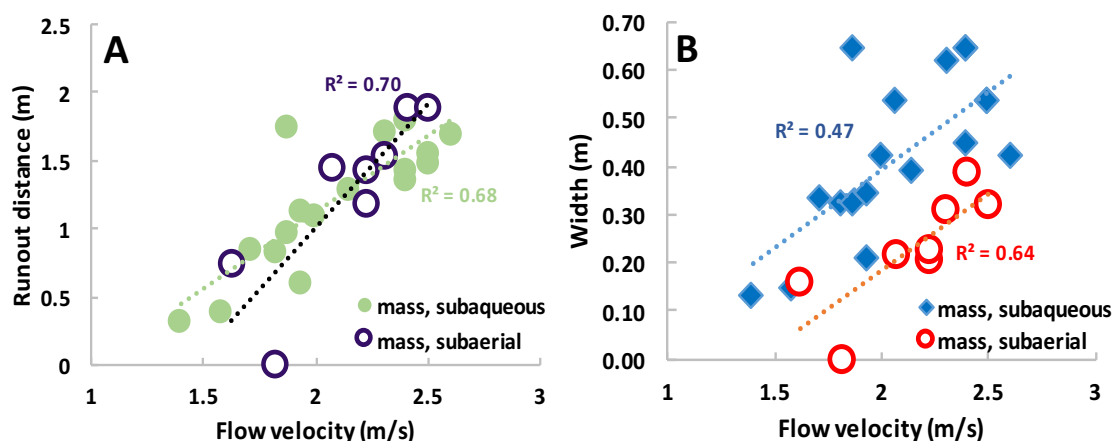

Figure 4.23 Relation between debris flow velocity and a) Runout distance, B) Width, mass.

Debris flow composition has clearly determined the relation between deposit runout distance and the average velocity of both subaqueous and subaerial debris flow. With an increase in water content subaerial debris flow deposit distance is longer than the subaqueous debris flow deposit distance (0.19-0.45 m and 0.27-0.39 m, respectively). Figure 4.24.A, shows the relation between the average debris flow velocity and deposit runout distance with water content variations. It seems that, with an increase in average velocity due to the increase of water content, deposit runout distance of subaerial debris flow also increases, resulting in a significant linear relation (R^2=0.92). Consequently, the relation between the average velocity and runout distance of subaqueous debris flow deposits is linear (R^2=0.37).

The relation between average velocity and deposit width of subaerial debris flow is linear (R^2=0.62). It is obvious that, with an increase in water content subaerial debris flow velocity and deposit width are also increased. Specifically, with an increase in water content (40-60 %) deposit width and average velocity of subaerial debris flow increase from 0.19 to 0.45 m and from 2.1 to 2.7 m/s, respectively, leading to a linear relation. In contrast, the relation between the deposit width of subaqueous debris flow and the average velocity is not linear (R^2= 0.22). Figure 4.24.B illustrates that, with an increase in water content, deposit width of subaqueous debris flow is initially decreased from 0.39 to 0.27 m, with an 10% increase of water content (40-50%). However, when the water content becomes larger than 50%, the deposit width first is increased (from 0.30 to 0.39 m), with small variations.

Flow velocity and runout deposit distance, from subaqueous and subaerial debris flow, have been both affected by the variations of the gravel content. Figure 4.24.C, illustrates the relation between flow velocity and runout distance of both subaqueous and subaerial debris flow. It is clear that, an increase in gravel content of both subaqueous and subaerial debris flow, causes a decrease in both flow velocity and runout distance of flow deposits. This is explained by the increased frictional forces between the gravel particles, which are leading to shorter runout deposit distance when the gravel becomes larger than 31%. The relation between flow velocity and runout distance of both subaqueous and subaerial debris flow deposits is linear, R^2=0.67 and R^2=0.63, respectively.

Maximum deposit width of both subaqueous and subaerial debris flow has also been affected by the coarse gravel particles. The obvious fact is, that the relation between subaerial flow velocity and deposit width of debris flow with gravel variations is not linear for. However, a polynomial relation is observed for both subaqueous and subaerial debris flows, R^2=0.37 and R^2= 0.75, correspondingly. Figure 4.24.D, presents the relation between flow velocity and deposit width. With an increase in gravel concentration maximum deposit, width and flow velocity of subaqueous and subaerial debris flow are decreased. Specifically, flow velocity and deposit width of subaqueous debris flow decreased from 2.14 to 1.67 m/s, and from 0.53 to 0.26 m, respectively. However, maximum deposit width of subaerial debris flow has been influenced by the variations of gravel content in a slightly different way. To be more accurate, when the gravel content was increased from 0 - 40% the deposit width also become wider from 0.23 to 0.25 m while, with larger gravel content, maximum deposit width becomes

narrower from 0.25 to 0.21 m. Flow velocity is decreased from 2.5 to 1.9 m/s with an increase of gravel content, because of high frictional forces between the particles, and due to lack of lateral flow spreading the formed deposit is not wide.

Variations of the finest particles have controlled the relation between flow velocity and deposit dimensions. When the clay content is increased, flow velocity becomes lower, the maximum runout deposit distance is shorter, and the maximum deposit width is narrower of subaqueous and subaerial debris flow deposits. Maximum runout distance of subaqueous debris flow deposits is becoming shorter (from 1.10 to 0.6 m). Flow velocity of subaqueous debris flow is faster (from 1.93 to 2.5 m/s) with an increase of clay content from 0-11%, whereas, is lower (from 2.5 to 1.7 m/s) when the clay become larger than 11%. This is due to lubricating effect of clay between 0 and 11% of clay content, while an increase of clay concentration (>21%), resulting in a too viscous flow and slow velocities.

The response of flow velocity and maximum deposit width on clay content, reflects the behavior of the subaqueous and subaerial debris flow as described, about the relation between runout distance and flow velocity. Maximum width of subaqueous debris flow deposits is affected by the decrease in average subaqueous debris flow velocity due to the increase of clay, and is becoming narrower (R^2=0.77). However, maximum deposit width of subaerial debris flow becomes wider, from 0.23 to 0.34 m, when the clay content increased from 0-11%. In contrast, the clay becomes larger than 11% due to viscous forces between the particles, resulting in a narrower (from 0.34 to 0.23) deposit width and slower velocities.
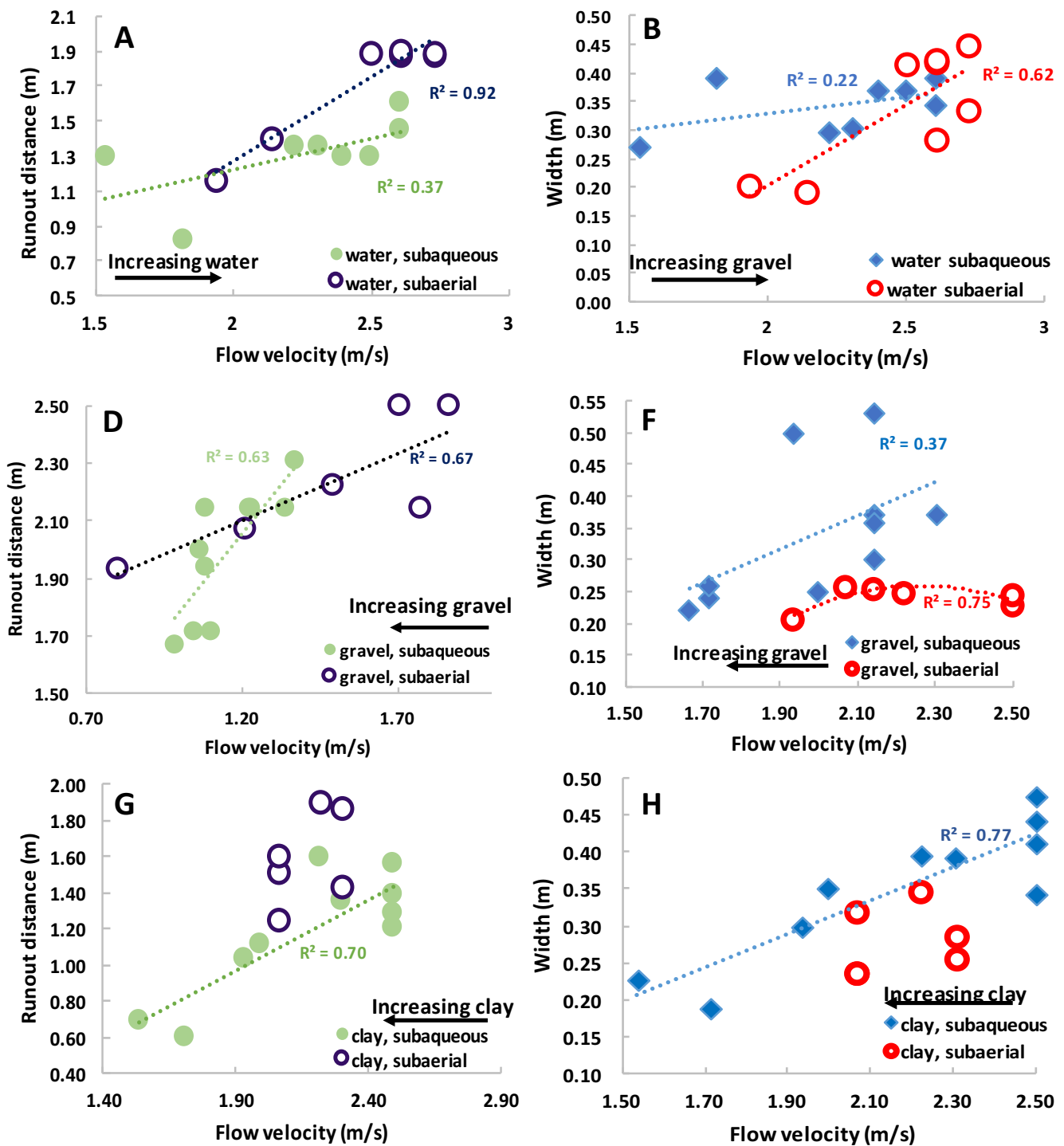
Figure 4.24 Relation between debris flow deposit dimensions and varied composition, A, B) water content, C, D) gravel content, E, F) clay content

4.3.3.3 Outflow slope

Maximum deposit runout distance, width, and flow velocity have all been affected by the outflow channel slope variations (20-40^0). It is observed that, subaerial debris flow has longer deposit runout distances with an increase in flow velocity (0.89 and 1.84 m) due to increasing slope, contrary to the runout distance of the subaqueous debris flow deposits, which is shorter (0.80 to 1.46 m). The relation between deposit runout distance and flow velocity of both subaqueous and subaerial debris flows with increasing slope is not clear. Although, it is observed that with increasing slope (20-40^0) flow subaqueous and subaerial flow velocity become faster (from 1.7 to 2.5 m/s, and from 2.06 to 2.6 m/s, respectively), while both subaqueous and subaerial deposit runout distance are first increased and afterwards are decreased.

Outflow channel slope variations have significant impact on the width of the subaqueous debris flow. Specifically, subaqueous deposit width becomes wider (from 0.33 to 0.45 m) with an increase in outflow channel slope (20- 35^0), and thus, an increase in flow velocity while, when the slope becomes steeper than 35^0, the deposit width is narrower (from 0.45 to 0.38 m). Subaerial deposit width becomes wider from 0.25 to 0.32 m whereas, steeper slope develops a narrower deposit width. However, the relation between flow velocity and both subaqueous and subaerial deposit width is not clear and thus, more experimental runs are needed to verify the correlation between flow velocity and deposit width.
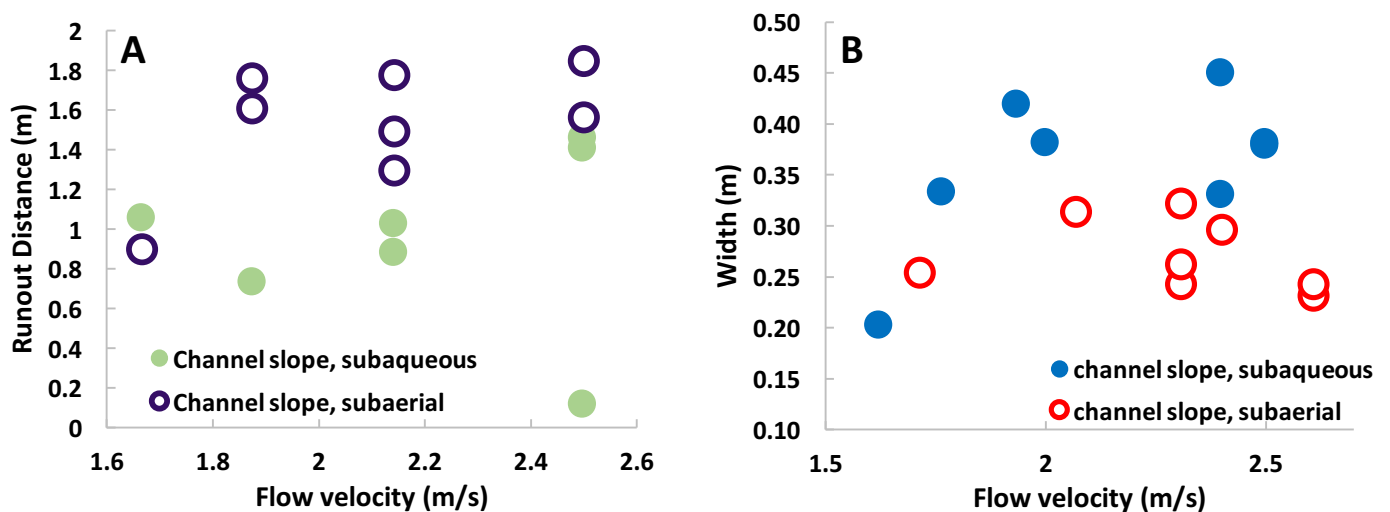

Figure 4.25 Relation between flow velocity and debris flow deposit dimensions with varies outflow channel slope, A) Runout distance, B)Maximum width

4.3.4 Summary of debris flow deposit dimensions

Subaqueous deposit runout distance is mainly affected by the mass and clay variations while, subaerial is also affected by the gravel variations. Additionally, subaerial debris flow deposits are longer and narrower than the subaqueous. The response of the subaqueous deposit width is strong between the mass, gravel, and clay whereas, the subaerial is controlled mainly by the water. Therefore, subaqueous debris flow deposits are wider than the subaqueous, apart from the subaerial experimental runs with water variations which become wider. An increase of water, causes an increase in deposit width and run-out distance of subaerial flow deposits. Deposit thickness is described only by the subaqueous clay and subaerial gravel. The relation between flow velocity and runout distance has an optimum in subaerial debris flow with water variation while, in subaqueous the optimum exists to clay content. Moreover, significant is the correlation between subaerial debris flow velocity and runout distance with mass and gravel variations. Flow velocity plotting against the deposit width seems that is highly affected by subaqueous debris flow deposits with clay variations whereas, the subaerial flow deposits are controlled by the gravel variations.

	Mass	Water	Gravel	Clay	Slope
Deposit run-out distance	0.84	0.61	0.27	0.91*	0.38
Deposit width	0.87	-	0.84	0.92*	0.36
Deposit thickness	-	-	-	0.70	-
Velocity-run-out distance	0.68	0.55	0.63	0.70	-
Velocity- width	0.47	0.22	0.37	0.78	-

*Table 4.2: R^2 values (linear regression) of subaqueous debris flow deposits dimensions with varied mass, composition, and slope . *) indicates polynomial relation.*

	Mass	Water	Gravel	Clay	Slope
Deposit run-out distance	0.82	0.75	0.83	0.62*	0.55
Deposit width	0.80	0.93	-	0.83*	-
Deposit thickness	0.44		0.83	0.63	
Velocity-run-out distance	0.70	0.92	0.67		-
Velocity- width	0.64	0.62	0.75	-	-

*Table 4.3: R^2 values (linear regression) of subaerial debris flow deposits dimensions with varied mass, composition, and slope . *) indicates polynomial relation.*

4.4 Grain size patterns in subaqueous and subaerial debris flow deposits

Grain size analysis distribution has been developed in all experiments, except for the subaqueous runs with clay content larger than 11%. Additionally, in subaerial runs without any clay content grain size analysis has been performed. However, when the clay content was increased at least 11%, grain size analysis was not efficient due to high flow viscosity. In the following sub-chapters, I will first point out the grain size patterns of both subaqueous and subaerial debris flow deposits with mass variations (4.4.1). Next, I will discuss the grain size patterns which have been identified in both flows with varied composition (4.4.2) and varied outflow channel slope (4.4.3). Lastly, in sections (4.4.4), (4.4.5), (4.4.6), I will discuss the effect of mass variations, varied composition, and outflow channel slope on grain size sorting of both subaqueous and subaerial debris flow deposits

4.4.1 Grain size patterns of debris-flow mass

Debris flow mass variations of both subaqueous and subaerial debris flow deposits have determined the cumulative percentile values or D-values, which are the intercepts for 10%, 50% and 90% of the cumulative mass. These D-values are the D10 (Figure 4.26.A) which is also called Effective Size or Diameter (Koukis & Sampatakakis, 2002), the Median or D50 (Figure 4.26.B), and the D90 (Figure 4.26.C). The D10 diameter is the diameter at which 10% of the sample's mass is comprised of smaller particles, and 90% of bigger particles. A small value of D10 indicates that the sample contains significant percentage of fine particles, whereas a high value indicates smaller percentage of fine particles. The D50 is the median, meaning that 50% of particles are larger and 50% are smaller than its value. Large value of D50 shows that the sample is coarser while small values illustrate that the sample is finer. The D90 shows that, 90% of the sample's particles are larger and 10% are smaller. The particle size has been classified based on the USCS system (Unified Soil Classification System).

Figure 4.26.A illustrates the geometric percentile D10 for subaqueous and subaerial debris flow deposits with mass variations. Specifically, the D10 of the front, the middle, and the back of both subaqueous and subaerial debris flow deposits are discussed into details through this scatter plot. It is observed that the D10 front of subaqueous becomes from fine to medium-grained sand with an increasing mass, and varies between 0.19 and 0.44 mm. However, D10 middle and D10 back consists of fine grained sand and varies between 0.18 and 0.23 mm, and between 0.19 and 0.25 mm, respectively. The D10 front of subaerial debris flow deposits is decreased (from 0.34 to 0.24 mm) with an increase in flow mass, resulting in a fine-grained sand front. D10 middle and D10 back are characterized by fine-grained sand and contain almost similar size of fine-grained particles, including values such as between 0.22 to 0.24 mm and between 0.23 to 0.24 mm, correspondingly. However, due to very long runout subaerial deposit distances there is not any D10 front sample for increasing mass higher than 8.0 kg.

Figure 4.26.B depicts the relation between the increasing mass and the median (D50) of the front, the middle and the back of subaqueous and subaerial debris flow. It is clear that, the D50 of the subaqueous front is higher (between 0.6 and 4.92 mm) than the middle (between 0.26 and 0.88 mm) and the back (between 0.4 to 0.9 mm), leading to a coarse-grained sand deposit in the front and a fine-grained sand deposit in the middle and the back. However, the back of subaqueous debris flow

deposits is slightly coarser than the middle. Although, due to very long runout deposit distances there is not any median front sample for increasing mass higher than 8.0 kg. It is observed that, with increasing mass, subaerial debris flow deposits consist of medium-grained sand particles in the middle and the back, and coarse-grained sand in the front. D50 of the middle and the back are decreased from 2.28 to 0.47 mm and from 2.3 to 0.57 mm, leading from a coarse to medium-grained sand in the middle and back with an increasing mass.

D90 front, middle, and back of subaqueous and subaerial debris flow deposits have also been affected by the increasing mass. Figure 4.26.C shows that accumulation of the coarser-grained gravel particles has occurred in the back of the subaerial debris flow deposits (D90 values between 4.97 and 5.9 mm) with an increasing mass. The middle and the front are dominated by coarse-grained sand between 2.67 and 4.61 mm and between 2.71 to 3.1 mm, respectively. Although, due to very long runout deposit distances there is not any subaerial D90 front sample for increasing mass higher than 8.0 kg. Subaqueous debris flow deposits with mass variations also contain coarse-grained sand (2.18 to 4.56 mm) in the back, like the subaerials deposits. With an increase in flow mass (from 9.5 to 18,0 kg), D90 middle becomes coarser (from 3.43 to 4.57 mm). D90 front of subaqueous debris flow deposits is finer than the middle, having values between (2.1 and 4.2 mm). It is also observed that with an increase in flow mass the front of subaqueous debris flow becomes coarse-grained sand.
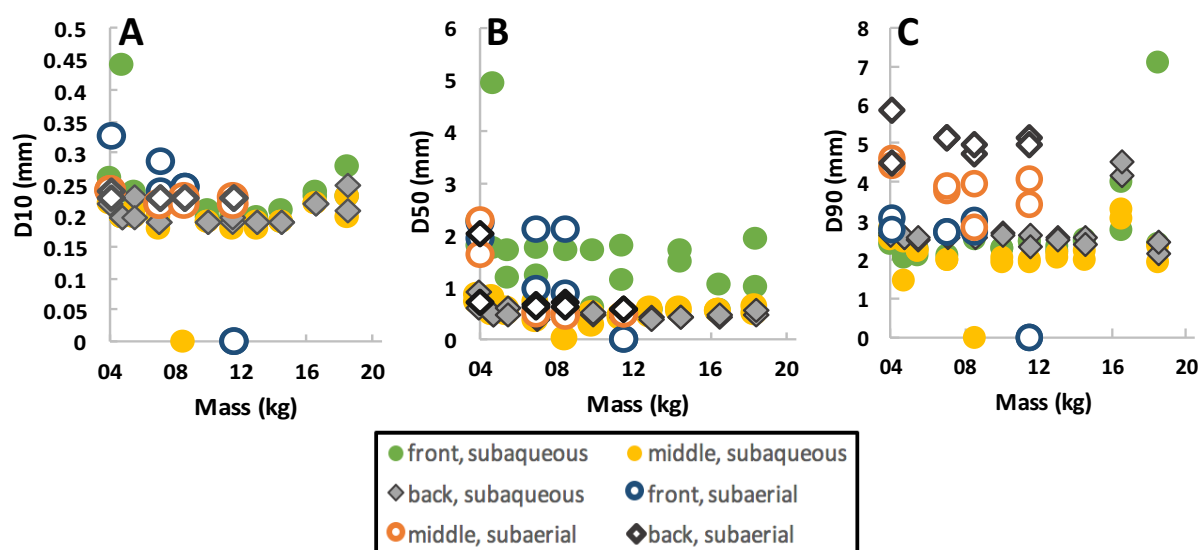

Figure 4.26. Grain size patterns expressed by the geometric percentiles for subaqueous and subaerial debris flow with mass variations A) D10, B) D50, C) D90, from locations along the deposit such as, the front, the middle, and the back.

4.4.2 Debris-flow composition

Variations in flow composition have affected the grain size distribution along subaqueous and subaerial debris flow deposits. Especially, D-values of the front, the middle, and the back of debris flow with varied composition present significant variations between subaqueous and subaerial debris flow deposits. Figure 4.27.A shows the D10 front, middle, and back for subaqueous and subaerial debris flow deposits with varied water content (40-60%). It seems that with an increase in water content the subaqueous front, middle, and back are characterized by fine-grained sand, from 0.20 to 0.28 mm, from 0.19 and 0.24 mm, and from 0.2 to 0.25, respectively. Subaerial debris flow deposits with water variations consist of fine-grained sand to all locations. D10 subaerial deposit front, middle, and back, range in values between 0.17 to 0.19 mm, between 0.18 to 0.19 mm, and 0.18 mm, respectively. Although, due to very long runout deposit distances there is not any D10 front sample for subaerial debris flow with water content larger than 50%. It is observed that the effective particles size (D10) of subaerial debris flows with water variations lead to finer-grained deposits than the subaqueous.

Figure 4.27.B illustrates the D50 of subaqueous and subaerial debris flow deposits with variations in water content. The D50 of the subaerial debris flow deposits seems to present a coarse-grained sand character with water variations. Specifically, subaerial debris flow deposits show that their middle is a medium to coarse-grained sand (0.48 to 2.23 mm), and that their median front and back are characterized by medium-grained sand, (0.73 to 0.77 mm and 0.54 to 1.44 mm, respectively). However, due to very long runout deposit distances there is not any D50 front sample for subaerial debris flow with water content larger than 50%. It can be seen that the subaqueous debris flow deposits are coarser (1.08 to 1.87 mm) in the front, whereas are medium-grained sand in the middle (0.47 to 0.6 mm) and the back (0.48 to 0.69). D50 seems to be increased from the back to the middle and the front, explaining the coarse-grained of subaqueous flow deposits.

Water variations of subaqueous and subaerial debris flow deposits have influenced the D90 size from all locations along the deposits. Subaerial debris flow deposits are contained at their back by coarse-grained sand or gravel (4.44 to 5.47 mm), in their middle by coarse-grained sand (2.68 to 4.57 mm), and in their front (until the water becomes 50%) coarse grained sand (2.68-2.74 mm). However, due to long runout deposit distance with the increase of water higher than 50%, there is not any D90 for the front of subaerial debris flow. An increase in water content higher than 50% classifies the D90 back from gravel to coarse-grained sand. D90 of subaqueous debris flow deposits defines that all locations are characterized by medium to coarse-grained sand, such as the front (1.92 to 2.77 mm), the middle (1.92 to 2.45 mm), and the back (1.87 to 2.59 mm). D90 of the subaerial debris flow deposits explains that their back consists of gravel, whereas the backs of subaqueous deposits are contained by coarse-grained sand.

With an increasing gravel content, the geometric percentiles of subaqueous and subaerial debris flow deposits vary significant between the deposits. The effective size (D10) front of subaqueous and subaerial debris flow deposits seems to lead to a linear regression with the increase of gravel. Specifically, it is observed that D10 front of subaqueous vary between 0.1 and 1.43 mm, resulting from fine-grained sand to medium-grained sand. The same trend follows the subaerial D10 front, which is becoming from fine-grained to coarse grained sand (from 0.19 to 1.73 mm). D10 middle

and back size of both subaqueous and subaerial debris flow deposits are characterized by fine-grained sand, having values between 0.15 and 0.25 mm.

The median (D50) and D90 sizes of both subaqueous and subaerial debris flow deposits follow the same trend. Figures 4.27.E and F show that D50 and D90 of the front (R^2=0.95), middle (R^2=0.98) and back (R^2= 0.97) of subaerial debris flow deposits present a significant linear regression with the increasing gravel content. Specifically, the median (D50) of the middle and the back (0.38 to 2.93 mm) is becoming gradually from fine to medium, and from medium to coarse-grained sand (0.38 to 3.05 mm and from 0.38 to 2.93 mm, respectively). However, the accumulation of the coarse-grained particles has occurred in the front of subaerial debris flow deposits explained by the median (D50) front, which is becoming gradually coarser (1.41 to 3.64 mm) from medium-grained sand. Subaqueous debris flow deposits median (D50) shows that the middle (R^2= 0.79) and the back (R^2=0.88) present a linear regression with the increase of gravel content. Especially, the D50 front and back become coarse-grained sand from 0.31 to 2.12 mm, and from 0.35 to 2.3 mm, respectively, and the D50 middle becomes medium-grained sand from 0.38 to 1.99 mm.

D90 size of subaerial debris flows also show linear relation between increasing gravel content and the accumulation of the coarse-grained particles at the front and the back of each deposit. D90 front (2.63 to 5.98 mm), middle (2.45 to 5.55 mm), and back (2.25 to 5.63 mm) change from coarse-grained sand to gravel with the increase of gravel, leading to a linear regression (R^2= 0.92, R^2=0.96, and R^2= 0.88, respectively). Subaqueous D90 front (1.32 to 4.96 mm), middle (1.89 to 2.74 mm), and back (1.35 to 3.54 mm) change from medium to coarse-grained sand with the increase of gravel content. It is observed that subaerial debris flow deposits consist of coarse-grained and gravel particles to all locations while, the subaqueous are contained by medium to coarse-grained sand.

Clay variations have affected the D10, D50, and D90 sizes of subaqueous and subaerial debris flow deposits as it is seen in Figure 4.27. G, H, and I, respectively. However, the samples of the experimental runs for subaerial debris flow with clay variations contain 0% of clay content, and thus, a comparison between the two flows cannot be discussed. This occurred due to the difficulty of taking samples from too viscous deposits (clay content between 11 and 29 %), (see also Figure 4.14.H, I). However, subaqueous debris flow with clay variations between 0 and 11 % of clay content show that D10 front, middle, and back sizes are characterized by fine-grained sand (0.19 to 0.23 mm to all locations). D50 front, middle, and back sizes are described by medium-grained sand (0.78 to 1.79 mm, 0.4 to 1.71 mm, 0.41 to 0.87 mm, correspondingly). D90 front and back sizes are represented by coarse grained sand with ranging values between 2.2 and 2.76 mm, and between 2.46 and 2.67 mm, respectively. Subaqueous debris flow deposits with clay variations outline a medium to coarse-grained sand D90 middle (1.94 to 2.35 mm).
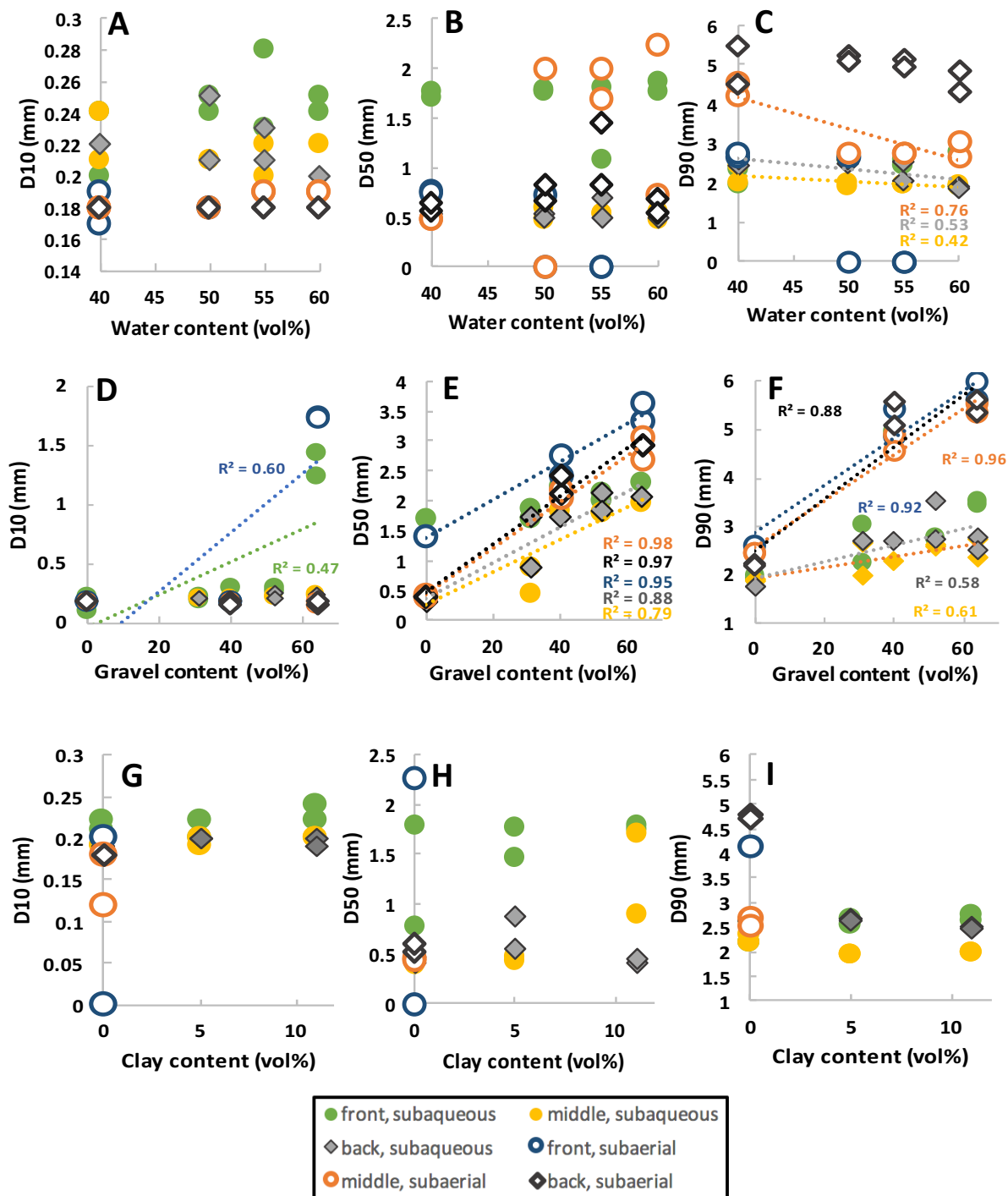
Figure 4.27. Grain size patterns expressed by the geometric percentiles for subaqueous and subaerial debris flow with varied composition A) D10, B) D50, C) D90 of water content, D) D10, E) D50, F) D90 of gravel content, G) D10, H) D50, I) D90 of clay content, derived from locations along the deposit such as, the front, the middle, and the back.

4.4.3 Outflow slope

The D-values of subaqueous and subaerial debris flow deposits have been influenced by the outflow slope variations. Figure 4.28.A, describes the D10 front, middle, and back grain size of subaqueous and subaerial debris flow deposits with channel slope variations (20-40^0). It is observed that D10 size of both subaqueous and subaerial flow deposits is characterized by fine-grained sand in their front, middle, and back with an increase in outflow channel slope. D10 size values of subaqueous and subaerial flow deposits vary between 0.22 and 0.29 mm, and between 0.15 to 0.22 mm, respectively. However, it seems that with an increase in outflow channel slope D10 size of the subaerial front is becoming gradually finer, leading to a slightly linear regression (R^2=0.50)

The evolution of the median (D50) of subaqueous and subaerial debris flow deposits is explained in Figure 4.28.B. The median or D50 size of subaerial and subaqueous flow deposits contained by medium grained sand in the middle and the back (0.45 and 0.99 mm, and between 0.41 to 0.57 mm, correspondingly), while the front consists of medium to coarse grained sand (0.45 to 2.20 mm and 1.08 to 2.17 mm, respectively).

D90 size of subaqueous debris flow deposits shows that with an increase in channel slope, deposit front is coarse grained sand to gravel (2.51 to 5.02 mm), resulting in a linear relation (R^2= 0.55) while, the middle (2.66 to 3.99 mm) and the back (3.76 to 4.74 mm) are characterized by coarse-grained sand without any gravel particles. D90 size of subaerial flow deposits describes that the front, the middle, and the back of the deposits consisted of coarse-grained sand (2.64 to 2.78 mm, 2.61 to 4.3 mm, and 3.58 to 4.81 mm, respectively). It seems that, the relation between increasing outflow slope and D90 back is linear (R^2=0.48) resulting in a slightly decrease of grain size. Specifically, when the outflow channel slope is 20^0 the subaerial back is characterized by a coarse grained sand, whereas with steeper slope (40^0) the grain size is coarse grained sand again but slightly smaller (3.81 mm). In contrast, the D90 of the middle of the subaerial flow deposits is becoming gradually coarser with steeper slope (from 2.61 to 4.3 mm) leading to a linear regression (R^2=0.70), and to the accumulation of the coarser grained particles in the middle of the deposit.
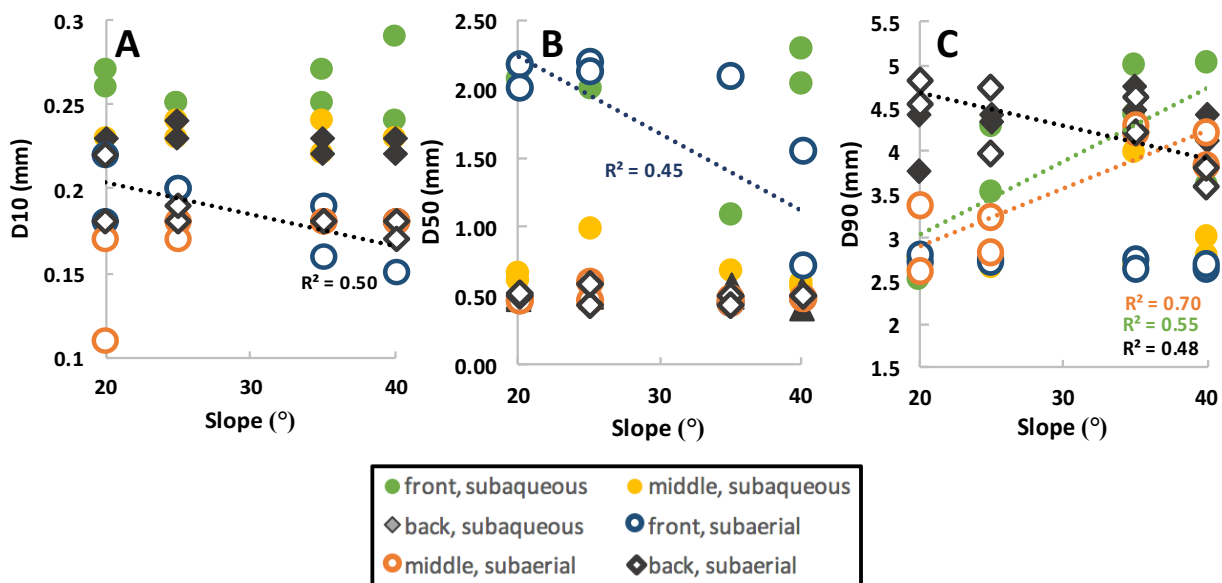
Figure 4.28. Grain size patterns expressed by the geometric percentiles for subaqueous and subaerial debris flow with slope variations A) D10, B) D50, C) D90 of slope variations.

4.4.4 Grain size sorting of debris flow mass

Sorting describes the distribution of grain size of sediments in sedimentary rocks or unconsolidated flow deposits. The focus of the current subsection is on the grain size sorting along subaqueous and subaerial debris flow deposits with varied mass, composition, and slope. Empirically fractions of the geometric percentiles, such as the D50 and D90 of front and middle, are used to determine the sorting of each flow deposit. Finally, a comparison between the varied flow deposits is discussed. Dividing the $D50_{front}$ with the $D50_{middle}$, and the $D90_{front}$ with the $D90_{middle}$, the grain size sorting is determined along the subaqueous and subaerial debris flow deposits with an increasing mass. Specifically, ratios of $D50_{front}/D50_{middle}$, and $D90_{front}/D90_{middle}$ which are close to 1 indicate that the medium and coarse grained size, respectively, are equally allocated along the deposits. Therefore, the sorting on these debris flow deposits is characterized by relatively well sorted, while ratios away from 1 define a relatively poorly sorted deposit.

$D50_{front}$ and $D50_{front}/D50_{middle}$ ratios for subaerial flow deposits with mass content higher than 8.0 kg do not exist due to very long runout distances. It is observed that for an increasing mass, ratios of ($D50_{front}/D50_{middle}$) in subaqueous and subaerial flow deposits is 2 to 4 times bigger than the coarse grained sorting ($D90_{front}/D90_{middle}$). Meaning that the medium grained size particles are not equal distributed along subaqueous and subaerial deposits and are described by relatively poorly sorted, explaining the fact that medium grained size are more concentrated in the front and finer in the middle of each deposit. However, coarse grained sorting ratios ($D90_{front}/D90_{middle}$) are close to 1 to all subaqueous and subaerial deposits, indicating the relatively well sorted and the similar distribution of the coarse grained particles along the middle and the front. Subaqueous debris flow deposits consisted of a coarser margins and finer interior (middle), while subaerial is characterized by a more

equal grain size distribution in the front and the middle deposits (gravel particles at the bottom covered by fine and coarse grained sand in the top due to kinematic sieving, see also fig.4.16. A-G). Figure 4.29, illustrates the medium ($D50_{front}$ /$D50_{middle}$) and coarse ($D90_{front}$ /$D90_{middle}$) grained size sorting along subaqueous and subaerial debris flow deposits with mass variations.
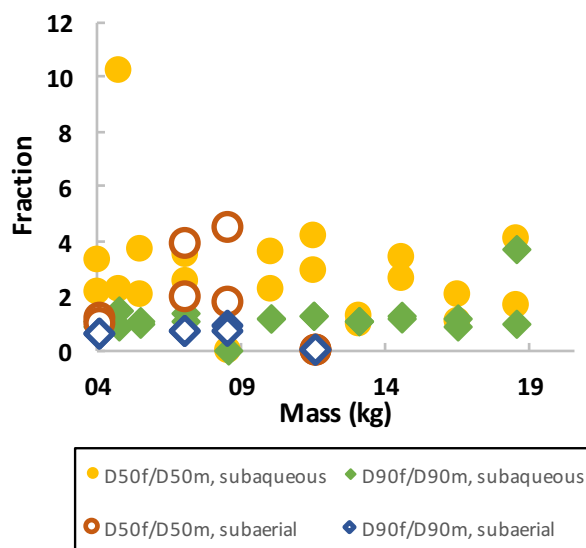

Figure 4.29. Grain size sorting along subaqueous and subaerial debris flow deposits.

4.4.5 Grain size sorting of debris flow composition

Subaerial debris flow deposits with water content higher than 50% do not exist due to very long run-out distances, thus a comparison with the subaqueous is not possible. Figure 4.30.A. illustrates the median and coarse ($D50_{front}$ /$D50_{middle}$ and $D90_{front}$ /$D90_{middle,}$ respectively) sorting of the subaqueous and subaerial debris flow deposits with water variations. $D50_{front}$ /$D50_{middle}$ ratios are 3 to 4 times higher than the $D90_{front}$ /$D90_{middle}$ in subaqueous flow deposits, explaining that medium grained particles are not equal concentrated along the middle and the front of the deposits. However, $D90_{front}$ /$D90_{middle}$ ratios of subaerial deposits are close to 1 and it is believed that the accumulation of the coarse grained particles is not affected by the water variations, describing the relatively well sorted character between the middle and the front. Coarse particles are mainly concentrated in the margins and the front, while the middle consisted of finer grained sand particles, leading to a marked difference in particle size between the deposits margins and interior of subaqueous debris flow deposits (see also fig.4.13. B-C).

Gravel variations rely on a relatively well to poorly sorted subaqueous and subaerial debris flow deposits. $D50_{front}$ /$D50_{middle}$ and $D90_{front}$ /$D90_{middle}$ ratios vary between relatively well and poorly sorted graded. Coarse particles are concentrated in the subaqueous deposit margins and fronts with an increase in gravel content, while a fine grained top layer relies upon the coarse gravel bed in the deposit middle (see also for subaqueous fig.4.13. E and F). However, the sorting between the middle and the front of the subaerial flow deposits is more similar, consisting of a coarse bed mixed with a fine grained sand top (see also fig.4.14. E and F). Optimum in relatively well sorted front and middle

---

of the deposits is observed in subaqueous and subaerial debris flow with gravel content equal to 52 and 64 %. However, grain size sorting in subaqueous and subaerial deposit front and middle with less gravel content, describe them as relatively poorly sorted.

Sorting can be only explained by debris flow with clay content between 0 and 11%, while for higher clay content was impossible to derive and analyse samples. This performed to the subaqueous debris flow where a big amount of clay was suspended due to turbidity current flow before the deposition, applying in different depositional conditions and, thus made easier the collection and analysis of the samples. However, in subaerial debris flow the conditions were different, imposing no clay suspension, and depositing in a more viscous way. Subaqueous debris flow with clay content less than 11% contain significant differences in grain size along the deposit, meaning that the gravel particles were accumulated in the front, while the interior was consisted by fine and coarse-grained sand (see fig.4.13.H). However, clay content larger than 11% leaded to a too viscous subaqueous and subaerial deposit, where distinct sorting was absent. The high viscosity of these flows may be the possible reason which causes this, where grain interactions are effectively constrained by highly viscous pore fluid.
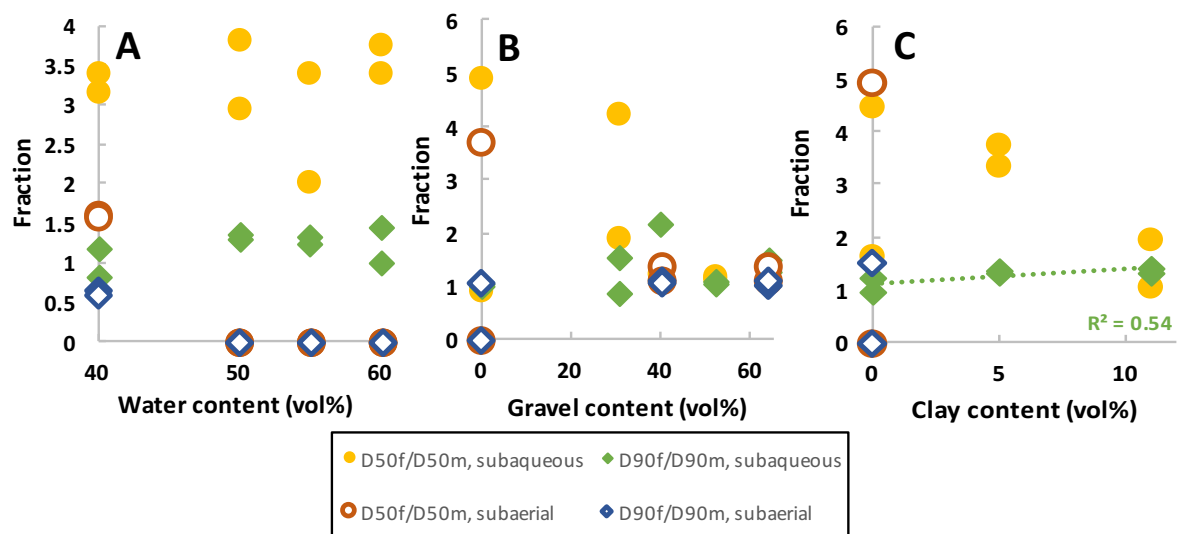

Figure 4.30 Grain size sorting of subaqueous and subaerial debris flow deposits with varied composition A) water, B) gravel, C) clay variations.

4.4.6 Grain size sorting of outflow channel slope

Grain size sorting varies along the subaqueous and subaerial debris flow deposit which varies from relatively well to poorly sorted. $D50_{front}$ /$D50_{middle}$ ratios are 3 to 4 times bigger than $D90_{front}$ /$D90_{middle}$ ratios indicating that the amount of medium grained particles is not uniform distributed along subaqueous and subaerial debris flow deposits. Relatively poorly sorted are classified the subaerial deposits with slope variations in terms of the medium grained particle size allocation. A well sorted coarse gravel bed at the bottom, consisted of a coarse to fine grained sand thin layer at the top of the subaerial debris flow deposits (see figure 4.19. A-D).

However, sorting in subaqueous debris flow deposits with slope variations define a slightly different trend. Specifically, sorting in subaqueous flow deposits indicates that coarse particles are mainly concentrated in the margins and the front, while the middle consisted of finer grained sand particles, leading to a significant difference in particle size between the deposits margins and interior of subaqueous debris flow deposits (see also fig.4.18. A-F). This is also correlated with the $D90_{front}$ /$D90_{middle}$ ratios which vary between 0.9 and 1.8 indicating the relatively well sorted character of the coarse particles at the bottom of the deposit front and middle (see also figure 4.18. A-F).
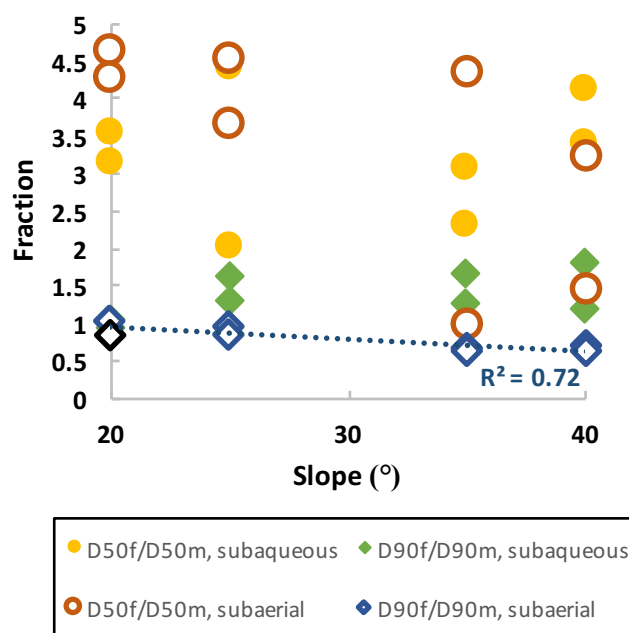

Figure 4.31. Grain size sorting of subaqueous and subaerial debris flow deposits with slope variations.

4.4.7 Summary of grain size pattern and sorting

A fixed range of grain size has been used to all experiments so there are not any marked differences in grain size sorting between the subaqueous and subaerial debris flow deposits. Additionally, it varies between moderately well to poorly sorted, along all deposits except for the very high clay content (>22%) where sorting was absent. Table 4.5 and 4.6 illustrates the average values of the geometric percentiles, D10, D50, and D90 derived from the front, middle, and back locations along both subaqueous and subaerial debris flow deposits, respectively. Subaqueous and subaerial debris flow deposits with mass variations are characterized in average by a fine-grained sand D10, a medium grained-sand D50, and a coarse-grained sand D90. Water-rich subaqueous and subaerial debris flows are described in average by a fine-grained sand D10, a medium-grained sand D50, and a coarse-grained sand D90 size in their deposits. Debris flow deposits with clay and outflow channel slope variations present similar average grain size distribution. Fine-grained sand characterizes the D10 size, medium-grained sand their median (D50), and coarse-grained sand their D90 size. The only thing that deviated, in terms of grain size distribution, and marked differences, is the subaerial experiments with gravel content. Their D10 is characterized by a fined-grained sand, coarse-grained sand describing the median size (D50), and coarse-grained sand the D90.

Coarse-grained sand and gravel particles are distributed in the margins and the front, while the interior was contained by fine and medium-grained sand in most of subaqueous experiments like the mass, water, and slope variations. In clay (>21%) rich subaqueous and subaerial flows grain size sorting was absent, due to high flow viscosity. Increasing gravel content caused a uniform accumulation of the coarse-grained sand, and gravel particles along the subaqueous and subaerial debris flow deposits.

	Mass	Water	Gravel	Clay (0-11%)	Slope
D10 (average)	0.21mm	0.22 mm	0.29 mm	0.20 mm	0.23 mm
D50 (average)	0.85 mm	0.90 mm	1.5 mm	0.93 mm	1.04 mm
D90 (average)	2.5 mm	2.24 mm	2.6 mm	2.4 mm	3.7 mm

Table 4.4: Subaqueous debris flow deposit average values of the geometric percentiles with varied debris flow parameters.

	Mass	Water	Gravel	Clay (0%)	Slope
D10 (average)	0.24 mm	0.18 mm	0.38 mm	0.17 mm	0.17 mm
D50 (average)	1.13 mm	0.96 mm	2.12 mm	1 mm	0.88 mm
D90 (average)	3.9 mm	3.9 mm	4.48 mm	3.8 mm	3.5 mm

4.5: Subaerial debris flow deposit average values of the geometric percentiles with varied debris flow parameters.

5. Discussion

Interpretations and comparison of the results will be based on literature (5.1, 5.2). Next, I will point out the influence of scaling (5.3). This chapter concludes with the recommendations for further research (5.4).

5.1 Effect of debris flow parameters on depositional mechanism, thickness and grain size sorting of subaqueous and subaerial deposits

Depositional mechanisms of debris flow are strongly affected by the varied debris parameters. According to several studies, a subaerial debris flow is deposited due to several processes, such as decay of excess pore fluid pressure (e.g., Terzaghi, 1956; Hutchinson, 1986), viscoplastic yield strength (Johnson, 1970; Coussot and Proust 1996), decrease of collision stresses (e.g., Lowe, 1976; Takahashi, 1978, 1991) and increasing grain contact friction and friction targeted at flow margins (Major, 1997, 2000; Major and Iverson, 1999). Only the hypothesis stated by Major and Iverson, (1999), is based on in-situ measurements from replicable, large-scale flume experiments, while the other hypotheses are unreliable, indicating that the exact mechanism that causes debris-flow deposition is still unknown.

What was tested during our small-scale experimental runs was a variation in several features, such as the mass, composition and the outflow channel slope of subaqueous and subaerial debris flow. Due to the fact that the pore and load pressure were not measured in the deposited area, there is only one record concerning the condition under which deposition occurs. The dominant force occurring under the subaerial deposition is gravity, while the effective gravity is reduced in water due to Archimedean buoyancy. This behaves as drag resistance in water, which is about one thousand times larger than in air (Blasio et al., 2006). Mohrig et al., (1998), Ilstad et al., (2004), and Blasio et al., (2006), stated that subaqueous debris flows are considered to be more mobile than the subaerial debris flows. Ilstad et al., (2004), also stated that fluid pressure at the front and in the interior of subaqueous debris flows has a strong influence on both mobility and depositional features.

Subaqueous debris flow deposition occurs under three different phases. Firstly, a dense debris flow is created at the bottom of the frictional bed slope, containing coarse-grained material and medium-grained sand, the latter of which is due to suspension. Due to high inertial forces between the coarse particles, their deposition occurs by sliding, whereas for medium-grained sand it occurs by inertia collisional forces and turbulence. Secondly, as the subaqueous debris flow moves within the bed slope in surges, the flow front exhibits a high vertical velocity component which may lead to the formation of turbidity currents (Blasio et al., 2006; Breien et al., 2007). Thirdly, when a subaqueous debris flow has clay content of ≥ 2%, suspension flow occurs on the top of the debris, where the clay is suspended due to the eroded material from the surface of the debris (Hamton, 1972) as a colloidal, and deposited later (after removing the water from the basin) at the margins of the tail and as a thin top layer body in most subaqueous debris flows (see also figure 4.8.A-I, figure 4.13.A-D and H-I, and figure 4.18.A-D). Figure 5.1 illustrates an example of the subaqueous experimental debris flow with clay content equal to 0.05 %. It is clear that at the top of the debris, significant suspension clay-rich flow occurs (figure. 5.1. A, B, C) during the motion of the debris flow, 0.4, 0.7, and 4.0 seconds after

the flow hits the water. Figure 5.1.D, shows the deposition of clay on the top and in the margins of the deposit. Additionally, the remobilization of the clay particles during the drainage of the water basin is depicted.
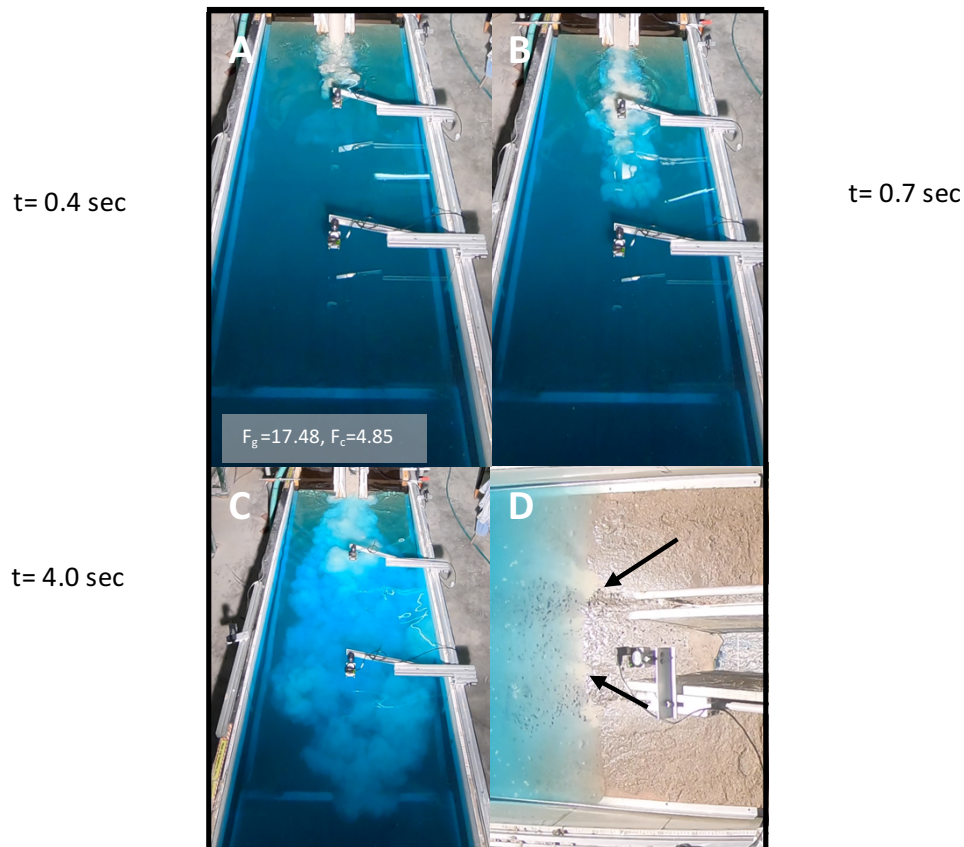
Figure 5.1. Subaqueous debris flow with clay content 0.05 %, A, B, C) Suspension flow due to clay, D) Deposition of clay on the top and the margins of the deposit, black arrows show the remobilization of clay during drainage of the basin.

Clay-rich debris flows (clay content 11-21%) may develop hydroplaning at the flow front (Mohrig et al., 1998). Mohrig et al., (1998), also stated that hydroplaning significantly enhances both the suspension of sediment and the resulting turbidity currents by increasing the velocities of the head of debris flows. In our small-scale subaqueous debris flow experiments hydroplaning is possible to occur, however there was not any underwater camera to record the moment when hydroplaning might have occurred. Therefore, I hypothesize that hydroplaning might occur in subaqueous debris flows with high clay content (11-21%), where they are considered to be more mobile than their subaerial counterparts.

In most subaqueous experimental runs the generation of turbidity currents via sediment erosion from the debris flows and suspension into the water column was possible to occur, however due to the small underwater length of the channel slope we cannot state with certainty that turbidity currents occured, indeed. Hampton (1972) and Mohrig et al., (1998) described that most of the

sediment constituting these turbidity currents is eroded from the fronts or heads of the debris flows. Turbidity currents were more possible to occur in our experimental subaqueous debris flow with water, clay, slope, and gravel (up to 40%) variations due to high sand enrichment, the water entrainment, and its ability to transport coarse and fine-grained sand (coarse and fine grained sand between 43.38-72.0 % and between 15.44-21.40%, respectively). When a sand-rich debris flow was released in water, they immediately started to decompose, the sand immediately subsided to the base of the flow and fine grained particles were ejected into the water column. The result was a three layered flow, with the subsiding layer near the bed, a fluidized sand layer in the middle and a turbidity current, composed of fine sediment on top of the deposit. This three layered subaqueous debris flow has been also observed in the studies of Brien et al., (2007) and Ilstad et al. (2004). Subaqueous experimental runs with mass and outflow channel slope variations were deposited in a similar trend describing the above discussed subaqueous deposit conditions.

Subaerial debris flow experiments (Iverson, 1997; Major, 1997; Major and Iverson, 1999; De Haas et al., 2015) indicate that deposition is a result of bed resistance along the flow perimeter, due to coarser material and high pore pressure dissipation. Indeed, our subaerial experiments were described, by a coarse grained to gravel deposit front, explaining that deposition is mainly affected by the frontal and marginal friction, forced by the accumulation of coarse particles and reduction of pore fluid pressure. This is also confirmed by Johnson et al. (2012) who stated that, as a debris flow accelerates down a channel, a flow front that is rich in coarse grains is formed by particle-size segregation. A saturated body consisting of finer grains follows the coarse-grained flow front. Momentum of the sediment deposits near the head of the flow is gradually decreased, resulting in sediments pushed aside by the sliding debris which forms lateral levees, providing a natural constraint for the flow, and forming elongated flow deposits. This is also observed in recent subaerial debris flow studies of Zhou et al., (2018). Increasing gravel content results in slightly steeper lateral levees, and the accumulation of the gravel and coarse particles at the front leads to a thicker subaerial deposit front than the body and the tail. All subaerial debris flows were deposited as elongated surges where, in the case of the viscous clay, multiple small surges were observed. One main channel constrained all the flow by being bordered by self-formed lateral coarse levees, leading to the depositional lobe, something that agrees with the studies of De Haas et al., (2015).

Subaqueous debris flows with mass and outflow channel slope variations result in thicker deposits than the subaerial debris flows. However, water, gravel and clay variations determine a thicker subaerial flow deposit. Specifically, when water, gravel and clay content increases, subaerial deposits become thicker, while subaqueous become thinner. This is due to the different deposition processes between the terrestrial and submarine environment. In the terrestrial environment the main force which concerns the depositional process is gravity combined with the change of inclination between the slope and the deposition plane. Due to the lack of buoyancy, the time of depositional processes can last less than the submarine environment. However, in the subaqueous environment the medium and fine-grained debris flow particles can float for more time before their deposition occurs. Consequently, an increase in debris flow mass or in channel slope will cause thicker subaqueous flow deposits.

Grain size distribution does not indicate obvious differences between subaqueous and subaerial debris flow deposits. In contrast, marked differences are observed in particle size between the front, the margins and the interior of both subaqueous and subaerial deposits. Due to the fixed range of grain size there are not any significant sorting differences between subaqueous and subaerial debris flows, varying between moderately well to poorly sorted. Subaqueous and subaerial debris flow deposits with mass, water, gravel (up to 31%), clay (up to 5%), and slope variations consisted of coarse grained margins and front, while the interior contained fine and medium grained sand. This is also in agreement with the recent studies of Iverson (1997), Iverson et al., (2010), Johnson et al., (2012), De Haas et al., (2015) and Zhou et al., (2018), where they also observed the accumulation of the coarse particles in the margins, while the interior was described by much finer particles. Additionally, Iverson (1997), also suggests that the accumulation of the coarse particles at the subaerial surge heads can occur in two ways: they can either travel to the head by self-transfer, or they can be integrated and retained if the flow obtains clast transportation. Middleton (1970), described that large clasts migrate and are retained due to kinematic sieving. De Haas et al., (2015), observed that in clay-rich (<21%) subaerial debris flows grain size sorting was absent due to high viscosity of these debris flows, wherein grain interactions are effectively buffered by a highly viscous pore fluid. This was also observed in our clay-rich experimental subaqueous and subaerial debris flow deposits, describing them as unsorted and too viscous for sorting to be formed.

5.2 Effect of debris flow parameters on the deposit runout distance and width

Trends in deposit runout distance and width of our small-scale subaqueous and subaerial experimental runs agree with other experimental and natural results. Runout distance has been interpreted by authors such as Prochaska et al., (2008), as the furthest extent of deposits being mapped as debris-flow deposits. Runout distance and deposit width are strongly dependent on flow velocity and composition (see also figures 4.23;4.24;4.25). Increasing mass of both subaqueous and subaerial experimental runs results in increased runout distance. Subaqueous and subaerial debris flow deposits rely on a positive relation with increasing mass (R^2=0.84 and R^2=0.82, respectively). Iverson, (1997) and De Haas et al., (2015), also observed that, with an increase of mass, subaerial debris flow deposits becomes longer. However, subaerial debris flow deposits, with increasing mass, are longer than the subaqueous, due to less frictional forces when going through air than in the ambient water, where the resistance force is higher. Consequently, the motion of the particles is less constrained in the air. A significant linear relation is also observed between the increasing mass and the deposit width, resulting in wider subaqueous and subaerial deposits (R^2=0.84 and R^2=0.82). However, subaqueous debris flow deposits are wider than the subaerial.

Water content variations and deposit runout distance of both subaqueous and subaerial debris flow are linearly related. In contrast, subaerial deposits exhibit longer runout distances than the subaqueous. The subaqueous deposit width is not affected by water variations. However, subaerial debris flows are longer and become significantly wider (R^2=0.94) with the increase of water.

This is in agreement with D'Agostino et al. (2010); De Haas et. al., (2015); Zhou et al., (2018), where they observed that subaerial runout distance becomes longer with the increase of water content. Increasing water content causes a decrease in frictional forces between the grains, thus longer runout distances occur. Correspondingly, Yin et al., (2017), observed that with higher water content subaqueous debris flow deposits become longer. Another case is the effect of gravel content on both subaqueous and subaerial debris flows. Subaerial deposit runout distance increases until the gravel content becomes 40%, and when the coarse-grained concentration exceeds that, runout distance is significant decreased due to a large accumulation of the coarse-grained and gravel particles in the flow front. This results in higher frontal frictional-collisional forces and shorter runout distances. This is in agreement with the small-scale experimental debris flows of De Haas et al., (2015), and with the large experimental debris flows at the USCS flume (Major and Iverson, 1999; Iverson et al., 2010; Johnson et al., 2012). Additionally, subaerial debris flow deposit width become shorter and narrower, due to the accumulation of coarse particles in the flow front and the margins. Specifically, deposit width becomes narrower with an increase of gravel content of more than 40% (from 0.021 to 0.017 m), and runout distance becomes shorter from 1.77 to 0.8 m. Subaqueous deposit runout distance increases until the gravel content becomes 40%, whereas larger gravel content leads to shorter runout distances and significant narrower widths. Subaqueous deposit width is affected more than the subaerial deposit width, by the increase of gravel larger than 40% (R^2=0.83). Subaqueous experimental debris flow deposits with gravel variations unfortunately do not exist in the literature and thus cannot be compared.

Runout distance and flow velocity decreased in both subaqueous and subaerial debris flow experiments with clay content higher than 21%, due to the increase in viscous forces. In our subaqueous and subaerial debris flow experiments I observed that for clay content less than 21%, runout distance and deposit width increased, while deposit thickness became thinner for the subaqueous and thicker for the subaerial flows. Mohrig et al., (1998), stated that in clay-rich subaqueous flows (>21%) the flow front is possible to exhibit higher velocity and changes in momentum, due to the thin film of trapped water between the impermeable clay pores. This might lead the flow front to accelerate away from the body to a completely detached point from the body, producing surges. Nevertheless, hydroplaning has been observed in studies of Mohring et al., (1998), Elverhoi et al., (2000), De Blasio et al., (2002), Harbitz et al., (2003), Ilstad et al., (2004); Brien et al., (2007), Yin et al., (2018). Although, due to lack of an underwater camera, we can not state with certainty that the flow front of our experimental clay-rich subaqueous debris flows exhibited hydroplaning. Therefore, only one observation exists in our small-scale experimental subaqueous debris flows which is possible to be caused by this process. Ilstad et al., (2004), observed and explained the resulting stretching which causes detachment of the material from the main flow body, creating an outrunner block that is then free to move independently from the main body. Figure 5.2 represents the only observation mentioned above. On that point, I hypothesize that the detached outrunner block might be caused by hydroplaning. Therefore, the presence of these specific outrunner blocks (the outrunners which are resulting only from the subaqueous debris flows with clay content between 10-21%), are lubricated by a thin water layer (might be trapped by the impermeable clay), reducing the basal shear stresses and increasing the runout distance of the blocks.
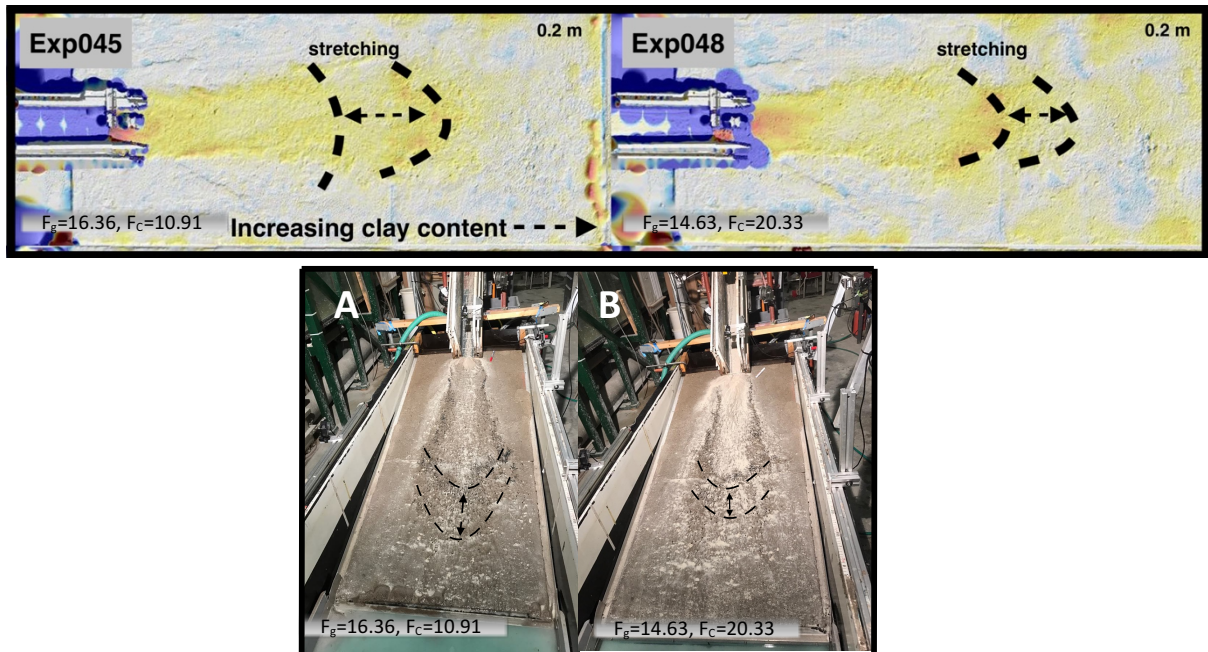
Figure 5.2. Subaqueous debris flow deposits with clay content Exp045) DEM photo-scans of 11%, and Exp048) 21%. A), B) Photos of the subaqueous debris flow deposits with clay 11%, and 21%, respectively. Dashed lines represent the flow body and the detached outrunners block. Arrows represent the resulting stretching which detaches the deposit front from the main deposit body.

Viscous clay flows had significantly reduced velocities due to viscous forces between the grains, which lead also to shorter both subaqueous and subaerial deposit runout distance and narrower width. Runout distances and width of subaerial and subaqueous flow deposits were decreased in a polynomial manner, reaching the highest velocities, runout distances and width. This was also observed in subaerial experimental debris flows with clay content (5-22 %) of De Haas et al., (2015). The increase in velocity of clay-rich subaerial debris flows was due to the lubricating effect of clay, resulting from the retained excess pore pressure (Haas et al., 2015).

Outflow channel slope variations greatly influenced the deposit runout distance and width. An increase in channel slope (20-35^0) caused an increase in subaqueous and subaerial runout distance due to the high gravitational energy. This is also in accordance with the studies of De Haas et al., (2015), where they also observed that an increase in outflow channel slope resulted in longer runout distances. A steeper slope (>35^0) results in higher gravitational potential energy and thus a higher vertical momentum component. Consequently, there would be greater total momentum loss after the steep transition between the channel slope and the outflow bed slope (from 40^0 to 10^0), since the vertical momentum component would be diminished due to the stronger collision of the debris with the outflow bled slope. Therefore, subaqueous and subaerial debris flow velocities and runout distances were decreased with a steeper slope. This is in agreement with the experimental subaerial debris flow of Zhou et al., (2018), where they also observed that with steeper slopes runout distance decreased.

In the majority of subaqueous debris flow deposits, outrunners have been observed few centimetres further than the flow front (see also fig. 5.3). Outrunners are individual particles or blocks in natural subaqueous flow deposits which can travel further than the flow front due to an abrupt delay of the flow front. De Blasio et al., (2006), stated that these pieces persist in their inertial motion and thus can travel further than the flow front. Ilstad et al., (2004), illustrated that a thin water layer or soft seabed sediments during the flow lubricates the outrunners. Due to this lubricating effect, the basal shear stresses are decreased and thus the runout length of the blocks is increased. A high volume of outrunners has been observed in subaqueous debris flows with mass, water, clay (up to 20%), and slope variations. However, experimental runs with gravel variations showed that the presence of outrunners is limited as the gravel content increased. Increase of gravel means that higher frictional flow front and marginal forces are applied during the flow, due to the large accumulation of the coarse particles in the flow front and margins. Therefore, as the lubricating effect was reduced, the volume and runout distance of outrunners was decreased as well. Outrunners have been worldwide observed in regions such as Nigeria (Nissen et al. 1999), Finneidfjord in Norway (Ilstad et al. 2004), and others.

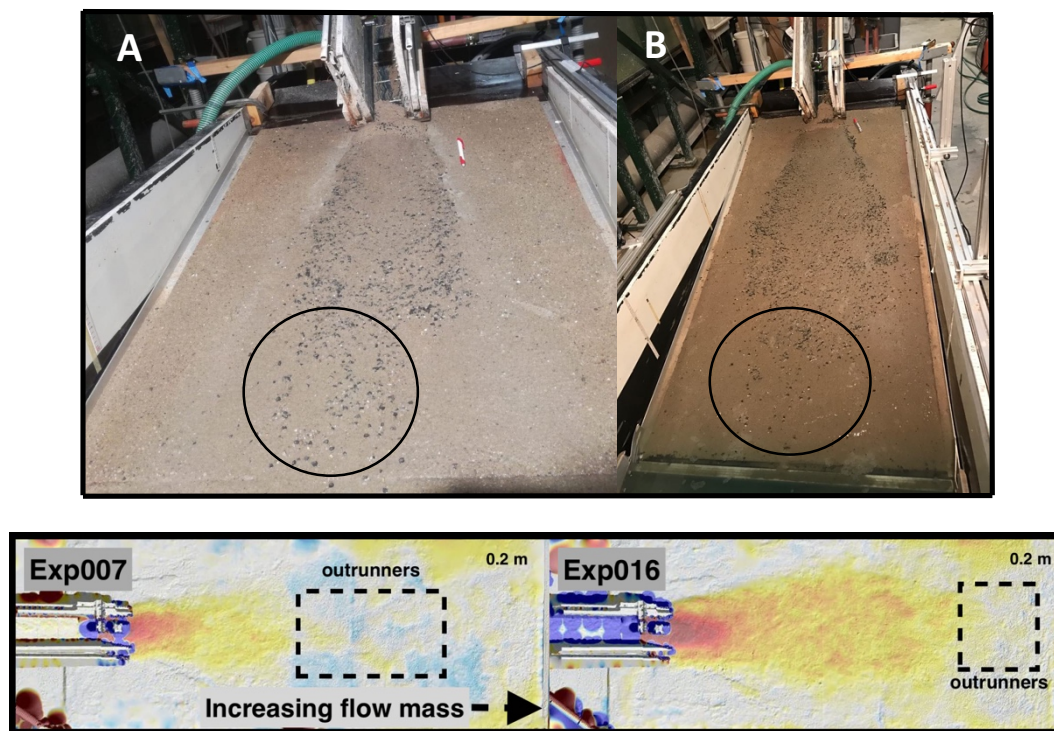*Figure 5.3: Subaqueous debris flow deposits. examples from experiments A) Exp007 (flow mass 6.5 kg) and, B) Exp016 (flow mass 12.5 kg). Cycles represent the outrunners. Exp007), Exp016) DEM photo-scans of the subaqueous debris flow with flow mass 6.5 and 12.5 kg, respectively.*

Table 5.1. Comparison between studies on the deposit runout distance and debris flow parameters.

Increase of → (this study)	Mass (3.5-18.0 kg)	Water (40-60 %)	Gravel (<40%)	Clay (< 21%)	Slope (20-35^0)
Subaerial runout distance (m)	Longer	Longer	Longer, while >40% of gravel leads to shorter runout distances	Longer, while >21% of clay leads to shorter runout distances	Longer, while a steeper slope (40^0) leads to shorter runout distances
Agree with:	Iverson, (1997); De Haas et al., (2015)	D'Agostino et al. (2010); De Haas et. al., (2015); Zhou et al., (2018).	De Haas et al., (2015); Major and Iverson, (1999); Iverson et al., (2010); Johnson et al., (2012)	De Haas et al., (2015)	Zhou et al., (2018)
Subaqueous runout distance (m)	Longer	Longer	Longer, while >40% of gravel leads to shorter runout distances	Longer, while >21% of clay leads to shorter runout distances	Longer, while a steeper slope leads to shorter runout distances
Agree with:	-	Yin et al., (2018)	-	-	-
Hydroplaning occurred	-	-	-	possible	-
Agree with:	-	-	-	Mohring et al., (1998), Elverhoi et al., (2000), De Blasio et al., (2002), Harbitz et al., (2003), Ilistad et al., (2004);Brien et al., (2007), Yin et al., (2017).	-
Volume of outrunner blocks	large	large	limited	large	large
Outrunners observed in studies of:		De Blasio et al., (2006);	and Ilistad et al., (2004)		

5.3 Consideration of scaling

Dimensional analysis was applied to the current study to compare the small-scale experimental results with the large-scale experiments of USGS Flume (Iverson, 1997) and natural debris flows. Our small-scale subaqueous and subaerial debris flow experiments indicated that debris flow behaviour, deposits, and grain size sorting coincide with observations of the natural debris flows. A coarse grained flow front, accompanied by a fine dilute grained interior and constrained by the formation of lateral coarse levees, was observed in our small-scale experiments. This is a typical characteristic of natural debris flow and is also in accordance with the earlier research of large-scale subaerial debris flow experiments of Iverson et al., (1997), Johnson et all., (2012), and small-scale subaerial experimental debris flow of De Haas et al., (2015), and Zhou et al., (2018). Subaqueous and subaerial deposit runout distance, width, and thickness greatly depend on composition, initial mass and outflow channel slope. This is in agreement at least with what has been observed in subaerial natural debris flows in relation to mass and slope variations (Rickenmann 1999, Rickenmann 2005), in experimental subaerial debris flow deposits with volume, composition, and slope variations of De Haas et a., (2015), and in experimental debris flow with composition and slope variations of Zhou et al., (2018).

Additionally, an indication based on the relatively good formation of subaerial grain size sorting showed that processes such as kinematic sieving, squeeze expulsion and preferential transport to the flow front are interrelated with the way the natural debris are formed, stated clearly by Vallance and Savage, (2000), Johnson et al., (2012). Experimental observations of subaqueous debris flow deposits of De Blasio et al., (2006), have shown that depositional mechanisms, flow behaviour, and deposit runout distance are greatly controlled by composition. Additionally, Ilstad et al., (2004), have also proved that flow behaviour, velocity, and deposition depend on composition.

It is observed that the physical parameters describing the debris flow in this study are in the limits of the physical parameters which were used in the large-scale USGS Flume, and of debris flows in nature (Iverson, 1997). Proportionally, the (non)dimensionless numbers calculated in this study are also comparable to natural debris flows, however they differ in striking ways. Bagnold and Savage numbers are higher than the large-scale USGS flume, indicating that the ratio of the collisional to viscous and of collisional to frictional forces would be higher in our small-scale experiments. Indeed, by performing experiments in a small-scale experimental setup the impact of flow viscosity and inertia forces is large, while the pore pressure is small. Additionally, the effect of particle collision is larger than the pore fluid viscosity, resulting in a large grain Reynold number. The ratio of friction to viscous forces (friction number), as well the solid to fluid inertia (mass number), the tendency for pore fluid pressure to buffer grain interactions (Darcy number), and the influence of the viscous effects relative to flow size (Reynold number) are in general within the range of the exact values in natural debris flows. Our small-scale experimental results prove that they can be compared to the scale of a natural debris flow. The following table (table 5.2) summarizes the above discussed.

Parameter	Symbol (Unit)	This study Debris flow	USGS Flume Debris flow	Natural debris flow
debris flow thickness	$H(m)$	0.005-0.04	0.1	0.1-10
typical grain diameter	$\delta(m)$	0.0003-0.004	0.001	$10^{-5} - 10$
flow shear rate	$\gamma(1/s)$	44.5-298.85	100	$1-100$
fluid density	$\rho_f(kg/m^3)$	1000	1100	1000–1200
solid density	$\rho_s(kg/m^3)$	2650-3400	2700	2500–3000
flow velocity	$u(m/s)$	1-3.75	10	0.1–20
solid volume fraction	$v_s(-)$	0.4-0.6	0.6	0.4–0.8
fluid volume fraction	$V_f(-)$	0.4-0.6	0.4	0.2–0.6
fluid viscosity	$\mu(Pa\,s)$	$0.001–0.0035^{b}$	0.001	0.001–0.1
Internal friction angle	$\phi(^{0})$	42^{a}	40	$25-45$
Hydraulic permeability	$k(m^2)$	$1.1*10^{-16}-2.1*10^{13b}$	10^{-11}	$10^{-13} - 10^{-9}$
Savage number	$Sv(-)$	$8.1*10^{-5}-1.5$	0.2	$10-7–100^{a,e,f}$
Bagnold number	Bn	$7.07-1.9*10^{4}$	400	$10^{0}-10^{8\,a,e}$
Friction number	F_n	67-5320	$2*10^{3}$	$10^{0}-10^{5\,a,f}$
Mass number	M_n	1.7-5.1	4	$1–10^{f}$
Darcy number	D_n	$1.3*10^{4}-1.5*10^{8}$	600	$10^{4}-10^{8}$
grain Reynold number	Re_g	1.1-2689	100	$0.01–2^{c,e}$
Reynold number	Re	$1.6*10^{4}-5.9*10^{5}$	$3*10^{3}$	$10^{5}-10^{7\,d,e}$

Table 5.2: Comparison of the (non)dimensional current study with the USGS flume (Iverson, 1997), and the natural debris flow. The header indicates the source where the values have been taken or calculated from. [a)] Iverson, (1997), [b)] Haas et al., (2015), [c)] Major, (2000), [e)] Iverson and Deligner, (2001), [f)] Zhou and Ng (2010).

5.5 Recommendations for further research

To begin with, alterations and corrections of the experimental setup are suggested. The channel bed and sidewalls of the debris flow flume were covered by sandpaper for identically natural bed roughness. For future experimental runs, it would be desirable to replace the sandpaper with a coarser one for more realistic representation of the debris flow channel behavior. Additionally, for the subaqueous experimental runs, it would be better if an outflow channel slope was located partly underwater, together with an underwater video camera. In that way, the occurrence or not of turbidity currents would be better visualized and analyzed. Another underwater video camera at the bottom of the outflow bed would help to improve the analysis and observe if hydroplaning was present or absent.

Next, subaqueous debris flows are more difficult to be observed in nature; thus, more future experimental research is needed. Experimental runs of Mohrig et al., (1998), Elverhoi et al., (2000), Ilstad et al., (2004), De Blasio et al., (2002), (2006), Yin and Rui, (2018), analyzed the subaqueous debris flow behavior and deposits. The materials which they used were mainly sand, clay, and mud, while the solid coarse fraction was absent. Considering that the relation between debris flow behavior and composition is strong, it would be therefore recommended to analyze the relation between low-medium-high solid fraction and improve on that, for future runout distance predictions on physical debris flow events (dependent on the location of the hazard area).

The practical impact of a debris flow, either as subaerial or as subaqueous, is great, as significant hazards often occur not only due to the flow, but also due to the hazards which trigger as secondary phenomena. Continuous monitoring of the earth displacement is desired in areas prone either to subaqueous or subaerial debris flows. Furthermore, a well recognized debris-flow hazard and risk assessment in areas where such hazards and risks are highest, is desired.

6. Conclusions

When a subaerial debris flow moving downslope hits a water reservoir, such as a lake or sea, tremendous waves are generated, together with a formation of a subaqueous debris flow. Subaqueous and subaerial debris flows are dangerous events that can cause major casualties and can trigger other secondary hazard phenomena. After the hazard event, the deposition starts either in the terrestrial or the submarine environments. This master thesis project is focused on the effect of debris flow mass, composition, and slope variations on the deposits, and the comparison of the debris flow dimensions between the subaqueous and subaerial debris flow deposits. I performed 99 experiments (60 subaqueous and 33 subaerial) in total, with variations in mass (3.5-18.0 kg), water (40-60%), gravel (0-64%), clay (0-29%), and slope angle (20-40^0). A summary of the conclusions and results of the experimental study is presented below:

- ❖ The strongest correlation is observed between subaerial debris flow momentum, average velocity and weight and the mass variations. Momentum is also affected by the subaerial gravel and the subaqueous clay due to the strong frictional forces and viscous forces, respectively, which occur between the particles. This also highlights the connection between the velocity and density. The major impact on debris flow thickness seems to concern the subaerial water content and the subaqueous mass, which provide a thicker flow as both are increased. Average flow velocity is controlled by the subaqueous water and clay and by the subaerial mass.

- ❖ Subaerial debris flows are longer than the subaqueous due to different dominant forces occurring under depositional processes in terrestrial and submarine environments. Runout distance is best correlated with the subaqueous mass and clay variations and with the subaerial mass and gravel variations. High gravel and clay content reduce the runout distance due to high frictional and viscous forces between the gravel and clay particles, respectively. Large accumulation of coarse particles in the front and the margins of the subaerial and subaqueous debris flow deposits cause the frontal and lateral friction to increase and thus higher resistance at the flow front. Increasing water content results in a linear relation with the subaqueous and subaerial deposit runout distance. Outflow slope variations (20-35^0) cause an increase in runout distance. In contrast, a steeper slope causes a greater total momentum loss after the steep transition between the channel slope and the outflow bed slope (10^0), and thus higher collisional particle forces and shorter runout distances.

- ❖ Subaqueous debris flow deposits are significantly wider than the subaerial. Subaqueous and subaerial deposit width has a linear relation with increasing mass. Water content affects mainly the subaerial debris flow deposits by making them wider. Gravel content variations affect mainly the subaqueous deposit width which becomes significantly narrower, while the width of the subaerial debris flow deposits are not affected by the gravel variations. Deposit width of both subaqueous and subaerial debris flows with increasing clay content become wider due to the lubricating effect of clay, until the clay content becomes 21%, when with any further increase it becomes narrower for both deposits due to the increase of viscous forces.

- ❖ Deposit thickness is described only by the subaqueous clay and subaerial gravel. Subaerial debris flow with clay variations becomes thicker, while subaqueous becomes thinner. Increasing gravel content also makes the subaerial deposit thicker, while the subaqueous are not affected by gravel variations.
- ❖ The relation between flow velocity and runout distance has an optimum in subaerial debris flow with water variation, while in subaqueous the optimum exists with clay content. The correlation between subaerial debris flow velocity and runout distance with mass and gravel variations is important. Flow velocity plotting against the deposit width seems to be affected by subaqueous debris flow deposits with clay and slope variations, whereas the subaerial flow deposits are controlled by the gravel variations.
- ❖ By using a specific type of grain size on all experiments, marked differences in grain size sorting between the subaqueous and subaerial debris flow deposits are not observed, while they vary between moderately well to poorly sorted, along all deposits except for very high clay content (>22%), where sorting was absent. Coarse-grained sand and gravel particles are distributed in the margins and the front, while the interior contains fine and medium-grained sand in most subaqueous and subaerial experiments with mass, water, and slope variations. In clay-rich (>21%) subaqueous and subaerial flows grain size sorting was absent due to high flow viscosity. High gravel content results in a uniform accumulation of coarse-grained sand and gravel particles along the subaqueous and subaerial debris flow deposits.
- ❖ Performing experiments in a small-scale setup leads to high impact of flow viscosity and inertia forces, as well as lower pore pressure. However, a small-scale experimental setup gives us the chance to repeat experimental runs efficiently; thus, a better interpretation of the results can exist. Deposit runout distance, width, and thickness, have been influenced by the basal bed and flow front friction.

REFERENCES

Anders Elverhøi, Carl B. Harbitz, Panagiotis Dimakis, David Mohrig, Jeff Marr and Gary Parker, (2000). On the dynamics of subaqueous debris flows Source: Oceanography, Vol. 13, No. 3, SPECIAL ISSUE: Ocean Biogeographic Information System (2000), pp. 109-117

Ahnert, F. (1970). Functional relationships between denudation, relief, and uplift in large, mid-latitude drainage basins. *American Journal of Science*, *268*(3), 243-263.

Ataie-Ashtiani B and Shobeyri G (2008) Numerical simulation of landslide impulsive waves by incompressible smoothed particle hydrodynamics. *Int. J. Num. Meth.*, 56, 209–232

Bagnold, R. A. (1954), Experiments on a gravity-free dispersion of large solid spheres in a Newtonian fluid under

Beaty, C. B. (1990). Anatomy of a White Mountains debris-flow—the making of an alluvial fan. *Alluvial Fans: A Field Approach. Wiley, New York*, 69-89.

Blair, T. C., & McPherson, J. G. (2009). Processes and forms of alluvial fans. In *Geomorphology of Desert Environments* (pp. 413-467). Springer Netherlands.

Boukpeti, N., D. J. White, M. F. Randolph, and H. E. Low. 2012. Strength of fine-grained soils at the solid–fluid transition. *Geotechnique* 62 (3):213–26.

Carmine Fallico, (2014). *Research Article* Reconsideration at Field Scale of the Relationship between Hydraulic Conductivity and Porosity: The Case of a Sandy Aquifer in South Italy. Hindawi Publishing Corporation Scientific World Journal Volume 2014, Article ID 537387, 15 pages http://dx.doi.org/10.1155/2014/537387

Chen, C. L. (1988), Generalized viscoplastic modelling of debris flow, J. Hydraul. Res., 114(3), 237–258.

Costa, J. E., and Williams, G.P. (1984). Debris flow dynamics (videotape). Geol. Surv. Prof. Pap. (U.S.)677, 1-75

Costa, J. E. (1988), Rheologic, geomorphic, and sedimentologic differentiation of water flood, hyperconcetrated flows, and debris flows, in *Flood Geomorphology*, chap. Rheologic, geomorphic, and sedimentologic differentiation of water floods, hyperconcentrated flows, and debris flows, pp. 113–122, John Wiley, New York.

Coussot, P., D. Laigle, M. Arattano, A. Deganutti, and L. Marchi (1998), Direct determination of rheological characteristics of debris flow, *J. Hydraul. Eng.*, *124*(8), 865–868.

Cruden, D.M. and Varnes, D.J. (1996) Landslide types and processes. In: A.K. Truner and R.L. Schuster (eds), Landslides Investigation and Mitigation (Special Report 247, pp. 36-75). Transportation Research Board, US National Research Council, Washington, DC.

David Mohring, Kelin X. Whipple, Midhat Hondzo, Chris Ellis, Gary Parker, (1998). Hydroplaning of Subaqeous debris flow. GSA Bulletin; March 1998; v. 110; no. 3; p. 387–394; 5 figures; 2 tables. Present address: Exxon Production Research Company

D'Agostino, V., Cesca, M., & Marchi, L. (2010). Field and laboratory investigations of runout distances of debris flows in the Dolomites (Eastern Italian Alps). *Geomorphology*, *115*(3), 294-304

Davies, T.R.H. (1986) Large debris flows: A macroviscous phenomena. *Acta Mechanica*, **63.**161-178

De Blasio FV, Engvik L, Harbitz CB and Elverhøi A (2004a) Hydroplaning and submarine debris flows. J. Geophys. Res., 109, C01002, doi:10.1029/2002JC001714

De Haas, T., L. Braat, J. R. F. W. Leuven, I. R. Lokhorst, and M. G. Kleinhans (2015), Effects of debris flow composition on runout, depositional mechanisms, and deposit morphology in laboratory experiments, *J. Geo- phys. Res. Earth Surf.*, *120*, 1949–1972, doi:10.1002/2015JF003525

Dowling, C. A., & Santi, P. M. (2014). Debris flows and their toll on human life: a global analysis of debris-flow fatalities from 1950 to 2011. *Natural hazards*, *71*(1), 203-227.

Dietrich, J.H. (1988) Growth and persistence of Hawaiian rift zones. Journal of *Geophysical Research*, **93**, 4258-4270.

Embley, R. W. (1976), New evidence for occurrence of debris flow deposits in the deep sea, Geology, 4, 371–374.

Fabio V. De Blasio,Lars Engvik Carl B. Harbitz and Anders Elverhøi, (2004). Hydroplaning and submarine debris flows. Journal of Geophysical research, VOL. 109, C01002, doi:10.1029/2002JC001714, 2004

Folk RL, Ward WC. 1957. Brazos River bar: a study in the significance of grain size parameters. *Journal of Sedimentary Petrology* **27**: 3–26.

Friedman GM, Sanders JE. 1978. *Principles of Sedimentology*. Wiley: New York.

Fritz, H. M., F. Mohammed, and J. Yoo (2009), Lituya bay landslide impact generated mega-tsunami 50th anniversary, Pure Appl. Geophys., 166, 153–175, doi:10.1007/s00024-008-0435-4.

George Koukis & Nikolaos. St. Sampatakakis, (2001), Technical Geology. (Book). ISBN: 960-7530-09-8

Gray, J., and B. Kokelaar (2010), Large particle segregation, transport and accumulation in granular free-surface flows, *J. Fluid Mech.*, *652*, 105 – 137.

Hammack, J.L., 1973. A note on tsunamis: their generation and propagation in an ocean of uniform depth. J. Fluid Mechanics 60 (4), 769–799.

Hampton, M. A. (1972), The role of subaqueous debris flow in generating turbidity currents, J. Sediment. Petrol., 42, 775–793.

H. BREIEN, M. PAGLIARDI, F.V. DE BLASIO, D. ISSLER., A. ELVERHØI. (2007). EXPERIMENTAL STUDIES OF SUBAQUEOUS VS. SUBAERIAL DEBRIS FLOWS – VELOCITY CHARACTERISTICS AS A FUNCTION OF THE AMBIENT FLUID. Department of Geosciences/International Centre for Geohazards (ICG), University of Oslo,Norway, Department of Hydraulic and Environmental engineering, University of Pavia, Italy.

Hooke, R. L. (1967). Processes on arid-region alluvial fans. *The Journal of Geology*, *75*(4), 438-460.

Hürlimann, M., B. W. McArdell, and C. Rickli (2015), Field and laboratory analysis of the runout characteristics of hillslope debris flows in Switzerland, *Geomorphology*, *232*, 20–32

Hungr, O. (1995), A model for the runout analysis of rapid flow slides, debris flows, and avalanches, Can. Geotechn. J., 32, 610–623.

Hungr, O., Evans, S.G., Bovis, M., and Hutchinson, J.N. (2001) Review of the classification of Landslides of the flow type. Environmental and Engineering Geoscience, VII,221-238.

Hutter, K., and L. Schneider (2010b), Important aspects in the formulation of solid-fluid debris-flow models. Part II. Constitutive modelling, Contin- uum Mech. Thermodyn., 22, 391–411.

Iverson, R. M. (1997), The physics of debris flows, *Rev. Geophys.*, *35*(3), 245–296.

Iverson, R. M., and R. P. Denlinger (2001), Flow of variably fluidized granular masses across three-dimensional terrain: 1. Coulomb mixture theory, J. Geophys. Res., 106(B1), 537–552.

Iverson, R. M., M. Logan, R. G. LaHusen, and M. Berti (2010), The perfect debris flow? Aggregated results from 28 large-scale experiments, *J. Geophys. Res.*, *115*, F03005, doi:10.1029/2009JF001514

Jakob, M., Hungr, O., & Jakob, D. M. (2005). Debris-flow hazards and related phenomena (Vol. 739). Berlin: Springer

Jakob, M., Stein, D., & Ulmi, M. (2012). Vulnerability of buildings to debris flow impact. *Natural Hazards*, *60*(2), 241-261.

Jeevan KAFLE, Puskar R. POKHREL, Khim B. KHATTRI, Parameshwari KATTEL, Bhadra Man TULADHAR, Shiva P. PUDASAINI, (2016). Landslide-generated tsunami and particle transport in mountain lakes and reservoirs. Annals of Glaciology., 57(71) 2016 doi: 10.3189/2016AoG71A034

Johnson, A. M. (1970), *Physical Processes in Geology: A Method for Interpretation of Natural Phenomena—Intrusions in Igneous Rocks, Fractures, and Folds, Flow of Debris and Ice*, Freeman, Cooper, San Francisco, Calif.

Jørstad, F. (1968), Waves generated by landslides in Norwegian fjords and lakes, Norw. Geotech. Inst. Publ., 79, 13–32.

Johnson, C., B. Kokelaar, R. Iverson, M. Logan, R. LaHusen, and J. Gray (2012), Grain-size segregation and levee formation in geophysical mass flows, *J. Geophys. Res.*, *117*, F01032, doi:10.1029/2011JF002185.

Krumbein WC. 1938. Size frequency distribution of sediments and the normal phi curve. *Journal of Sedimentary Petrology* **8**: 84–90.

Locat , J., Gardner, J.V., Lee, H., Mayer, L., Hughes-Clarke, J.E., and Kammerer, E. (1999), Using multibeam surveys for subaqeous landslide investigation. In: N-Yagi. (ed.), Slope Stability Engineering (pp.127-134). A.A Balkema. Rotterdam.

Locat, J.and Mienert, J.(2003) Submarine Mass Movements and their Consequences (Kluwer Advances in Natural and Technological Hazards Research No. 19, 540 pp.) Kluwer Academic, Boston.

Lowe, D. R. (1976), Grain flow and grain flow deposits, *J. Sediment. Res.*, *46*(1), 188–199

Masson, D., C. Harbitz, R. Wynn, G. Pedersen, and F. Lшvholt. 2006. Submarine landslides: Processes, triggers and hazard prediction. *Philosophical Transactions of the Royal Society A: Mathematical, Physical and Engineering Sciences* 364:2009–39.

Marchi, L., Arattano, M., & Deganutti, A. M. (2002). Ten years of debris-flow monitoring in the Moscardo Torrent (Italian Alps). *Geomorphology*, *46*(1), 1-17.

Major, J. J. (1997), Depositional processes in large-scale debris-flow experiments, *J. Geol.*, *105*(3), 345–366.

Major, J. J., and R. M. Iverson (1999), Debris-flow deposition: Effects of pore-fluid pressure and friction concentrated at flow margins, *Geol. Soc. Am. Bull.*, *111*(10), 1424–1434.

Major, J. J. (2000), Gravity-driven consolidation of granular slurries—Implications for debris-flow deposition and deposit characteristics, *J. Sediment. Res.*, *70*(1), 64–83.

McCammon RB. 1962. Efficiencies of percentile measures for describing the mean size and sorting of sedimentary particles. *Journal of Geology* **70**: 453–465.

McManus J. 1988. Grain size determination and interpretation. In *Techniques in Sedimentology*, Tucker M (ed.).

Blackwell: Oxford; 63–85.

McCoy, S. W., Kean, J. W., Coe, J. A., Staley, D. M., Wasklewicz, T. A., & Tucker, G. E. (2010). Evolution of a natural debris flow: In situ measurements of flow dynamics, video imagery, and terrestrial laser scanning. *Geology*, *38*(8), 735-738.

McAdoo, B.G., Pratson L.F., and Orange, D.L., (2000) Submarine landslide geomorphology,US continental slope. *Marine Geology*, **169,** 103-136.

Mei Yin, Yi Rui & Yanyi Xue., (2017)., Centrifuge study on the runout distance of submarine debris flows.MARINE GEORESOURCES & GEOTECHNOLOGY https://doi.org/10.1080/1064119X.2017.1411407

Mohrig, D., A. Elverhoi, and G. Parker, (1999): Experiments on the relative mobility of muddy subaqueous and subaerial debris flows, and their capaci- ty to remobilize antecedent deposits. Marine Geologu 154, 117-129

Mienert, J and Weaner, P. (2003), *European Margin Sediment Dynamics* (309 pp.) Springer- Velag, New York

Mohrig, D., A. Elverhoi, and G. Parker,. 1999: Experiments on the relative mobility of muddy subaqueous and subaerial debris flows, and their capaci- ty to remobilize antecedent deposits. Marine Geologu 154, 117-129.

Müller, L. (1964), The rock slide in the Vajont Valley, Rock Mech. Eng. Geol., 2, 148–212.

Norem, H., Locat, J., and Schieldrop, B. (1990) An approach to the physics and the modelling of subaqueous landslides, *Marine Geotechnology*, **9**, 91-111.

O'Brien, J. S., P. J. Julien, and W. T. Fullerton (1993), Two-dimensional water flood and mudflow simulation, J. Hyd. Eng., 119(2), 244–261.

Pederson, C. A., Santi, P. M., & Pyles, D. R. (2015). Relating the compensational stacking of debris-flow fans to characteristics of their underlying stratigraphy: Implications for geologic hazard assessment and mitigation. *Geomorphology*, *248*, 47-56.

Phillips, C. J., and Davies, T. R. H., 1991, Determining rheologic parameters of debris flow material: Geomorphology, v. 4, p. 101–110.

Pierson, T. C. (1984), Why debris flows stop, *GSA Abstracts with Programs*, *16*, 623.

Pudasaini SP, Kattel P, Kafle J, Pokhrel PR and Khattri KB (2014) Two-phase and three-dimensional simulations of complex fluid– sediment transport down a slope and impacting water bodies. *Geophys. Res. Abstr.*, 16, EGU2014-5084

Pudasaini SP and Hutter K (2007) *Avalanche dynamics: dynamics of rapid flows of dense granular avalanches*. Springer, Berlin and New York.

Pudasaini, S. P., Y. Wang, and K. Hutter (2005), Modelling debris flows down general channels, Nat. Hazards Earth Syst. Sci., 5, 799–819.

Rickenmann, D. (1999), Empirical relationships for debris flows, *Nat. Hazards*, *19*(1), 47–77.

Savage, S. B., and K. Hutter (1989), The motion of a finite mass of granular material down a rough incline, J. Fluid Mech., 199, 177–215.

Savage, W., & Baum, R. (2005). Instability of steep slopes. Debris-flow hazards and related phenomena, 53-79.

Schwab, W.C., Lee, H.J., Twichell, D.C., Locat, J., Nelson, H.C., McArthur, M., and Kenyon, N.H. (1996) Sediment mass-flow processes on a depositional lobe, outer Misissippi Fan Journal of *Sedimentary Research* **66,**916-927.

Silva, A.J., Baxter, C.D.P., LaRosa, P.T., and Bryant, W.R. (2004) Investigation of mass wasting on the continental slope and rise. *Marine Geology*, **203**, 355-366.

SIMON J. BLOTT AND KENNETH PYE, (2001), GRADISTAT: A GRAIN SIZE DISTRIBUTION AND STATISTICS PACKAGE FOR THE ANALYSIS OF UNCONSOLIDATED SEDIMENTS. *Earth Surface Processes and Landforms   Earth Surf. Process. Landforms* **26**, 1237–1248 (2001) **DOI**: 10.1002/esp.261

Shanmugam, G., 1997: Deepwater exploration; concep- tual models and their uncertainties. Bulletin - Houston Geological Society, 39; .

Shieh, C. L., Chen, Y. S., Tsai, Y. J., & Wu, J. H. (2009). Variability in rainfall threshold for debris flow after the Chi-Chi earthquake in central Taiwan, China.*International Journal of Sediment Research*, *24*(2), 177-188

Shiva P. Pudasaini, (2011). *A general two-phase debris flow model*. JOURNAL OF GEOPHYSICAL RESEARCH, VOL. 117, F03010, doi:10.1029/2011JF002186, 2012

Shiva P. Pudasaini., (2014). Dynamics of submarine debris flow and tsunami., Acta Mech 225, 2423–2434 (2014) DOI 10.1007/s00707-014-1126-0

Stefano Crema, (2010). Hydrological control on triggering and magnitude of debris flows in Alpine catchments. Sede Amministrativa: Universita` degli Studi di Padova Dipartimento TERRITORIO E SISTEMI AGRO-FORESTALI

Suwa, H. I. R. O. S. H. I., Okano, K. A. Z. U. Y. U. K. I., & Kanno, T. A. D. A. H. I. R. O. (2011). Forty years of debris flow monitoring at Kamikamihorizawa Creek, Mount Yakedake, Japan. In *5th international conference on debris-flow hazards mitigation: mechanics, prediction and assessment. Casa Editrice UniversitaLa Sapienza, Roma* (pp. 605-613).

Takahashi, T. (1978), Mechanical aspects of debris flow, *J. Hydraul. Div.*, *104*, 1153–1169. Takahashi, T. (1991), *Debris Flow*, Balkema, Rotterdam, Netherlands.

Takahashi, T. (2001), Debris flow (IAHR Monograph, 165 pp.). A.A. Balkema, Rotterdam.

Takahashi, T. (2007), Debris Flow: Mechanics, Prediction and Counter- measures, Taylor and Francis, New York.

Takahashi, T. (2014). Debris flow: mechanics, prediction and countermeasures. CRC press.

Terzaghi, K. (1956), Varieties of submarine slope failures, in Proceedings of Eighth Texas Conference on Soil Mechanics and Foundation Engineering: Austin, University of Texas, Bureau of Engineering Research, Spec. Publ. 29, Harvard Univ., Cambridge, Mass., 14–15 Sept.

Trask PD. 1932. *Origin and Environment of Source Sediments of Petroleum*. Gulf Publishing Company: Houston.

Trygve Ilstada, Jeffrey G. Marrb, Anders Elverhbia, Carl B. Harbitzc, (2004). Laboratory studies of subaqueous debris flows by measurements of pore-fluid pressure and total stress. Marine Geology 213 (2004) 403–414

Young, A.G., Bryant, W.R., Slowey N.C., Brand, J.R.,and Gartner, S., (2003), Age dating of past slope failures of the Sigsbee Escarpment within Atlantis and Mad Dog Developments. *Proceedings of the Osshore Technology Conference* (CD-ROM).

Varnes, D.J. (1978) Slope movement types and processes. In: R.J. Schuster and R.I. Krizek (eds), Landslides, Analysis and Control (Special Report 176, p.11-33). Transportation Research Board, National Academy of Sciences, Washington, DC.

Vallance, J. W., and S. B. Savage (2000), Particle segregation in granular flows down chutes, in *IUTAM Symposium on Segregation in Granular Flows*, pp. 31–51, Springer, Netherlands.

Van Asch, T. (2013). *Mountain risks: from prediction to management and governance*. J. Corominas, S. Greiving, J. P. Malet, & S. Sterlacchini (Eds.). Springer-Verlag.

Van Steijn, H., and J. Coutard (1989), Laboratory experiments with small debris flows: Physical properties related to sedimentary characteristics, *Earth Surf. Processes Landforms*, *14*(6), 587–596.

Wiegel, R.L., 1955. Laboratory studies of gravity waves generated by the movement of a submerged body. Trans. Am. Geophys. Union 36, 759–774.

Wohl, E. E., & Pearthree, P. P. (1991). Debris flows as geomorphic agents in the Huachuca Mountains of southeastern Arizona. *Geomorphology*, *4*(3-4), 273-292.

Zahibo, N., E. Pelinovsky, T. Talipova, and I. Nikolkina (2010), Savage- Hutter model for avalanche dynamics in inclined channels: Analytical solutions, J. Geophys. Res., 115, B03402, doi:10.1029/2009JB006515.

Zhou, G. G., and C. W. Ng (2010), Dimensional analysis of natural debris flows, *Can. Geotech. J.*, *47*(7), 719–729.

APPENDIX

A1.E Supplementary excel files
- ❖ A1.E1:E1_experimental runs
- ❖ A1.E2:E2_debris flow characteristics
- ❖ A1.E3:E3_debris flow deposit dimensions
- ❖ A1.E4:E4_geometric percentiles and grain size sorting
- ❖ A1.E5.E5_sieving analysis of subaqueous debris flow deposits
- ❖ A1.E6.E6_sieving analysis of subaerial debris flow deposits

A2.E Supplementary DEM photo-scans
- ❖ A2.E.1.E.1_Subaqueous debris flow deposits
- ❖ A2.E.2.E.2_Subaerial debris flow deposits

❖ **Summary of subaqueous debris flow characteristics**

	Mass	Water content	Gravel content	Clay content	Slope
Thickness (outlet)	0.89	0.57	-	0.65*	0.76*
Weight	0.68	-	-	0.80	0.53
Velocity (average)	0.49	0.87	0.67*	0.94*	0.71
Momentum	0.92	0.70	0.68	0.95*	0.45

Table 0.1. R^2 values of subaqueous debris flow parameters and the equivalent thickness, weight, velocity, and momentum. * indicates polynomial regression, no values indicate unimportant relation. colors indicate the strength of the relation, the darker the color the higher strength.

❖ **Subaerial debris flow characteristics**

	Mass	Water content	Gravel content	Clay content	Slope
Thickness (outlet)	0.83	0.90	0.55*	0.84*	0.81
Weight	0.87	-	-	0.96*	0.94*
Velocity (average)	0.89	0.70	0.37	-	0.63
Momentum	0.99	0.69	0.95	-	0.74*

Table 0.2. R^2 values of subaerial debris flow parameters and the equivalent thickness, weight, velocity, and momentum. * indicates polynomial regression, no values indicate unimportant relation. colors indicate the strength of the relation, the darker the color the higher strength.

❖ **Summary of subaqueous and subaerial debris flow deposit dimensions**

	Mass	Water	Gravel	Clay	Slope
Deposit run-out distance	0.84	0.61	0.27*	0.91*	0.39
Deposit width	0.87	-	0.84	0.92*	0.37
Deposit thickness	-	-	-	0.70	
Velocity-run-out distance	0.68	0.55	0.63	0.76	-
Velocity- width	0.55**	0.22	0.37	0.78	0.74*

Table 0.3: R^2 values (linear regression) of subaqueous debris flow deposits dimensions with varied mass, composition, and slope . *) indicates polynomial relation, **) indicates exponential relation, colors indicate the strength of the relation, the darker the color the higher strength.

	Mass	Water	Gravel	Clay	Slope
Deposit run-out distance	0.82	0.75	0.83*	0.62*	0.30
Deposit width	0.80	0.93	0.23*	0.83*	0.38
Deposit thickness	0.44		0.83	0.64	
Velocity-run-out distance	0.70	0.92	0.67		0.40
Velocity- width	0.64	0.62	0.75	-	0.46*

Table 0.4: R^2 values (linear regression) of subaerial debris flow deposits dimensions with varied mass, composition, and slope . *) indicates polynomial relation, the darker the color the higher strength

❖ **Average values of geometric percentiles**

	Mass	Water	Gravel	Clay (0-11%)	Slope
D10 (average)	0.21mm	0.22 mm	0.29 mm	0.20 mm	0.23 mm
D50(average)	0.85 mm	0.90 mm	1.5 mm	0.93 mm	1.04 mm
D90(average)	2.5 mm	2.24 mm	2.6 mm	2.4 mm	3.7 mm

Table 5: Subaqueous debris flow deposit average values of the geometric percentiles with varied debris flow parameters.

	Mass	Water	Gravel	Clay (0%)	Slope
D10 (average)	0.24 mm	0.18 mm	0.38 mm	0.17 mm	0.17 mm
D50(average)	1.13 mm	0.96 mm	2.12 mm	1 mm	0.88 mm
D90(average)	3.9 mm	3.9 mm	4.48 mm	3.8 mm	3.5 mm

Table 6: Subaerial debris flow deposit average values of the geometric percentiles with varied debris flow parameters.

.

Statement of originality of the MSc thesis

I declare that:

1. this is an original report, which is entirely my own work,

2. where I have made use of the ideas of other writers, I have acknowledged the source in all instances,

3. where I have used any diagram or visuals I have acknowledged the source in all instances,

4. this report has not and will not be submitted elsewhere for academic assessment in any other academic course.

Student data:

Name: *Nicoleta Santa*

Registration number: *6182984*

Date: *April, 2019*

Signature: